Towards the Intensification of Convective Rain Events with Rising Temperatures in Germany

Dissertation
zur Erlangung des Doktorgrades
der Naturwissenschaften

vorgelegt beim Fachbereich 11 Geowissenschaften/Geographie
der Johann Wolfgang Goethe-Universität
in Frankfurt am Main

von
Christopher Purr

aus Suhl

Frankfurt am Main, 2022
(D30)

vom Fachbereich 11 Geowissenschaften/Geographie der
Johann Wolfgang Goethe-Universität als Dissertation angenommen.

Dekan:

Prof. Dr. Jürgen Runge

Gutacher:

Prof. Dr. Bodo Ahrens

Prof. Dr. Heinke Schlünzen

Datum der Disputation:

Abstract

Extreme convective precipitation events are among the most severe hazards in central Europe and are expected to intensify under global warming. However, the degree of intensification and the underlying processes are still uncertain. In this thesis, recent advances in continuous, radar-based precipitation monitoring and convection-permitting climate modeling are used to investigate Lagrangian properties of convective rain cells such as precipitation intensity, cell area, and precipitation sum and their relationship to large-scale, environmental conditions.

Firstly, convective precipitation objects are tracked in a gauge-adjusted radar-data set and the properties of these cells are related to large-scale environmental variables to investigate the observed super-Clausius-Clapeyron (CC) scaling of convective extreme precipitation. The Lagrangian precipitation sum of convective cells increases with dew point temperature at rates well above the CC-rate with increasing rates for higher dew point temperatures. These varying, high rates are caused by a covarying increase of CAPE with dew point temperature as well as the effect of high vertical wind shear causing an increase in cell area and thus precipitation sum. At the same time, cells move faster at high vertical wind shear so that Eulerian scaling rates are lower than Lagrangian but still above the CC-rate. The results show that wind shear and static instability need to be taken into account when transferring precipitation scaling under current climate conditions to future conditions. Secondly, the representation of convective cell properties in the convection-permitting climate model COSMO-CLM is evaluated. The model can simulate the observed frequency distributions of cell properties such as lifetime, area, mean and maximum intensity, and precipitation sum. The increase of area and intensity with lifetime is also well captured despite an underestimation of the intensity of the most severe cells. Furthermore, the model can represent the temperature scaling of intensity, area, and precipitation sum but fails to simulate the observed increase of lifetime. Thus, the model is suitable to study climatologies of convective storms in Germany. Thirdly, two COSMO-CLM projections at the end of the century under emission scenario RCP8.5 were investigated. While the number of convective cells and their lifetime remain approximately constant compared to present conditions, intensity and area increase strongly. The relative increase of intensity and area is largest for the highest percentiles meaning that extreme events intensify the most. The characteristic afternoon maximum of convective precipitation is damped, and shifted to later times of day which leads to an increase of nighttime precipitation in the future. Scaling rates of cell properties with dew point temperature are nearly identical in present and future in the simulation driven by the EC-Earth model which means that the upper limit of cell properties like intensity, area, and precipitation sum could be predicted from near-surface dew point temperature. However, this result

could not be reproduced by the simulation driven by MIROC5 and needs further investigation.

Kurzzusammenfassung

Konvektive Starkregenereignisse gehören zu den verheerendsten Naturkatastrophen in Mitteleuropa und werden im Zuge des anthropogenen Klimawandels voraussichtlich an Intensität zunehmen. Die Höhe dieser Zunahme und die zugrundeliegenden physikalischen Prozesse sind allerdings noch sehr unsicher. Durch technischen Fortschritt stehen mittlerweile Fernerkundungstechniken zur Verfügung, die eine kontinuierliche Beobachtung konvektiver Stürme erlauben. Außerdem können Klimasimulationen seit einigen Jahren hochreichende Konvektion direkt simulieren. Auf Basis eines Zellverfolgungsalgorithmus wurden in dieser Arbeit sowohl beobachtungs- als auch modellbasierte Klimatologien von Eigenschaften konvektiver Zellen für Gegenwart und Zukunft analysiert.

Mithilfe eines an ortsfeste Niederschlagsmessungen angeeichten Radardatensatzes wurde untersucht, wie großskalige atmosphärische Variablen die Eigenschaften konvektiver Stürme beeinflussen und welche Prozesse für das beobachtete super-Clausius-Clapeyron (CC) Scaling von konvektiven Niederschlägen verantwortlich sein könnten. Die Niederschlagssumme konvektiver Zellen steigt mit der Taupunkttemperatur weit über der CC-Rate an, wobei der Anstieg mit steigender Taupunkttemperatur zunimmt. Dieser starke Anstieg wird durch eine Zunahme von CAPE mit der Taupunkttemperatur verursacht, sowie durch den Effekt, dass vertikale Windscherung die Fläche der konvektiven Zellen und somit auch die Niederschlagssumme erhöht. Gleichzeitig sorgt hohe vertikale Windscherung dafür, dass die konvektiven Zellen sich schneller verlagern, sodass die ortsfesten Skalierungsraten unter denen der mitbewegten Niederschlagssumme, aber immer noch über der CC-Rate liegen. Diese Ergebnisse zeigen, dass das gegenwärtige Scaling nicht ohne Weiteres in die Zukunft übertragen werden kann, sondern Windscherung und die atmosphärische Schichtung berücksichtigt werden müssen.

Es wurde evaluiert, inwieweit das regionale Klimamodell COSMO-CLM die Eigenschaften konvektiver Zellen abbilden kann. Hierzu wurden Simulationen, die mit Reanalysen angetrieben wurden, mit Beobachtungsdaten verglichen. Das Modell kann sowohl die beobachteten Häufigkeitsverteilungen der Zelleigenschaften ‚Lebensdauer', ‚mittlere und maximale Intensität', ‚Fläche' und ‚Niederschlagssumme' gut wiedergeben, als auch den Anstieg von Intensität und Fläche mit der Lebensdauer. Allerdings wird die Intensität und Fläche der extremsten Zellen unterschätzt. Des Weiteren kann die Simulation den Anstieg der hohen Perzentile von Intensität, Fläche und Niederschlagssumme mit der Temperatur wiedergeben, aber nicht den Anstieg der Lebensdauer. Somit ist das Model geeignet, die Klimatologien konvektiver Stürme in Deutschland zu untersuchen.

Für die Zukunft (2071-2100) wurden zwei COSMO-CLM Simulationen, angetrieben von verschiedenen Globalmodellen unter dem repräsentativen Konzentrationspfad RCP8.5, untersucht. Die Intensität und Fläche der konvektiven Zellen steigt im Vergleich zur Gegenwart (1976-2005) in beiden Simulationen stark an, wohingegen Anzahl und Lebens-

zeit der Zellen gleich bleiben. Der relative Anstieg von Intensität und Fläche ist am größten für die hohen Perzentile, was bedeutet, dass sich extreme konvektive Ereignisse am stärksten intensivieren. Der typische Tagesgang des konvektiven Niederschlags ist in der Zukunft gedämpft. Während am Nachmittag weniger konvektiver Niederschlag fällt, nimmt er in der Nacht zu. Die Skalierungsraten der Zelleigenschaften mit dem Taupunkt sind in Gegenwart und Zukunft in der Simulation, die vom EC-Earth Modell angetrieben wird, nahezu identisch. Das bedeutet, dass die bodennahe Taupunkttemperatur einen guten Prädiktor für die Obergrenze von Intensität, Fläche, und Niederschlagssumme konvektiver Zellen darstellt. Dieses Ergebnis konnte allerdings nicht für die zweite, von MIROC5 angetriebene Simulation reproduziert werden, und bedarf daher weiterer Untersuchung.

Contents

List of Contributing Peer-Reviewed Publications

- Christopher Purr, Erwan Brisson, and Bodo Ahrens: *Convective Shower Characteristics Simulated with the Convection-Permitting Climate Model COSMO-CLM*, Atmosphere (2019, 10, 810; doi:10.3390/atmos10120810).
- Christopher Purr, Erwan Brisson, and Bodo Ahrens: *Convective rain cell characteristics and scaling in climate projections for Germany,* International Journal of Climatology (2021, 1-12; doi: 10.1002/joc.7012).
- Christopher Purr, Erwan Brisson, K. Heinke Schlünzen, and Bodo Ahrens: *Convective rain cell properties and the resulting precipitation scaling in a warm temperate climate*, Submitted to Quarterly Journal of the Royal Meteorological Society.

List of Figures

List of Tables

1. Introduction – Deep Convection in Climate Change

Extreme convective precipitation is among the most severe natural hazards. Several severe convective precipitation events occurred in Germany in recent years, most notably in 2016 (Piper et al. 2016) and 2021[1], which increased public interest in this phenomenon and the question of how much such events will intensify under anthropogenic climate change.

Theoretical considerations, complex climate models, and observations agree that the hydrological cycle and, with it, extreme precipitation in large parts of the world will intensify in a warming climate (Trenberth et al. 2003, Fischer & Knutti 2016). As a first approximation, using the atmosphere's water holding capacity to deduce changes in extreme convective precipitation has been intensely discussed in recent years (Lenderink and van Meijgaard 2008, Zhang et al. 2017). The water holding capacity of air is described by the Clausius-Clapeyron (CC) equation which states that the water holding capacity increases exponentially by approximately 7 %/K.

However, multiple effects can cause deviations from this rate. Firstly, assuming an increase according to the CC-rate implies that the relative humidity remains constant in a climatological sense. This assumption can be invalidated if changes in the general circulation cause changes in the relative humidity in a particular region. Typically, scaling curves of extreme precipitation with temperature peak at a certain temperature (Drobinski et al. 2016). Above this temperature, precipitation is limited by decreasing moisture availability. This temperature increases in the future, which implies that present scaling curves cannot be used to predict precipitation extremes in the future (Prein et al. 2017a). To circumvent this problem, low-level moisture as measured by dew point temperature has been suggested as a covariate for precipitation scaling (Lenderink et al. 2011).

As a further complication for both temperature and dew-point temperature scaling, subdaily precipitation extremes have been shown to increase at rates above the CC-rate in certain regions, for example, Germany. Here, Berg et al. (2013) found scaling rates of convective precipitation at twice the CC-rate. Various hypotheses about the cause of this

[1] Hydro-klimatologische Einordnung der Stark- und Dauerniederschläge in Teilen Deutschlands im Zusammenhang mit dem Tiefdruckgebiet „Bernd“ vom 12. bis 19. Juli 2021. https://www.dwd.de/DE/leistungen/besondereereignisse/niederschlag/20210721_bericht_starkniederschlaege_tief_bernd.pdf?__blob=publicationFile&v=6. Letzter Zugriff: 21.11.2021

effect are discussed in the literature which do not necessarily exclude each other. Firstly, precipitation extremes are caused by convective precipitation to a larger degree at higher temperatures. Secondly, the dynamics of convective storms might change with increasing temperature (Trenberth 1999). This hypothesis states that higher temperatures lead to more available moisture at cloud base. More moisture increases latent heating in the updraft of convective storms, invigorating the updraft. A stronger updraft can source moisture from a larger area in the boundary layer. In addition to this positive feedback in convective updrafts, the degree of convective organization and its temperature dependence has been discussed (Moseley et al. 2016, Haerter et al. 2017, Lochbihler et al. 2019).

These uncertainties in the effect of global warming and associated regional changes on convective precipitation motivated this work. The goal is to investigate the dependence of convective storms on large-scale variables, especially temperature and dew point temperature, and other well-known ingredients for convection such as vertical instability and wind shear in observational data and convection-permitting climate simulations.

Historically, two facts have complicated the investigation of convective storms. Firstly, their small spatial (ca. 10 km) and temporal (ca. 1 h) scales have prevented continuous observations until a few years ago. The progress of weather radars has eliminated this obstacle making it possible to observe convective storms continuously in time and space (Lengfeld et al. 2020). Secondly, their non-linear behavior requires non-hydrostatic atmosphere models with a complex representation of microphysics. For a couple of years now, convection-permitting climate models (CPMs), which are characterized by a fine grid spacing (< 4 km), have been used to simulate convective storms explicitly instead of parameterizing convection (see Prein et al. 2015 for a review). Their main advantage is a better representation of the diurnal cycle of precipitation and extreme precipitation intensities on short time scales compared to models that parameterize convection. For evaluating CPMs, most studies use rain gauge data or gridded precipitation data sets based on gauge data as observations, which can lead to an underestimation of storm frequency and storm peak intensity (Schroeer et al. 2018a). In contrast, using radar data allows for evaluating the space-time dynamics of convective cells but has been done very rarely so far (Brisson et al. 2017, Prein et al. 2020). To the authors' knowledge, sub-hourly precipitation output from continuous CPM simulations has not been evaluated yet.

As mentioned above, extrapolating precipitation scaling rates at the regional scale to the future is questionable because of potential changes in the large-scale circulation. This is especially true for Germany because of its mid-latitude location and the influence of vary-

ing synoptic situations on precipitation statistics. As general circulation models differ considerably in their representation of atmospheric dynamics (Shepherd 2014), large ensembles are necessary to assess the robustness and significance of change signals in mean and extreme precipitation. As large ensembles of CPM simulations are computationally demanding and not yet available, this thesis assesses the plausibility and reliability of simulations in another way by understanding the processes that lead to changes in convective cell properties[2]. Therefore, CPM simulations forced by a historical and a future, high-emission scenario were used to compare convective cell properties and their relationship to the large-scale environment. Additionally, this approach can potentially be used as a statistical model to calculate changes in convective cell properties from environmental variables of coarse-grid models (e.g., Seeley and Romps 2015, Púčik et al. 2017).
Using the tools described above, this thesis aims at answering the following research questions:

1) Process Understanding

a. What is the effect of large-scale environmental variables on convective cell properties and the dew point temperature scaling of these properties?
b. To what extent does higher cell velocity offset the higher organization of convective cells in high-shear environments with respect to precipitation at fixed location?

To answer these questions, the influence of environmental variables (CAPE, wind shear, and dew point temperature) on convective cell properties based on radar observations on a climatological time scale was investigated. Specifically convective rain cells were tracked in 5-min radar data and connected to environmental variables from reanalysis data. The results are presented in more detail in paper 1 (Appendix A).

[2] The terms “cell properties” and “cell characteristics” are used synonymously in this thesis.

2) Evaluation of the Convection-Permitting Climate Model COSMO-CLM

a. How well can a convection-permitting climate model represent the properties of convective cells?
b. Can the model reproduce the temperature scaling of cell properties?

These questions were tackled by tracking convective cells in 5-min precipitation model output and comparing the cell properties to the radar results. The results are presented in more detail in paper 2 (Appendix B). In addition, another hindcast simulation was evaluated to test the influence of different driving reanalysis data (Appendix D).

3) Future Changes in Convective Cells

a. How will convective cells change in the future?
b. Is the scaling behavior of Lagrangian cell properties similar in present and future conditions?

Changes in convective cell properties were investigated in a convection-permitting climate model under a strong emission scenario (RCP8.5). The results are presented in more detail in paper 3 (Appendix C). The reliability of the results was assessed by analyzing another convection-permitting simulation that uses the same RCM with a larger domain driven by a different general circulation model (GCM). This analysis can be found in Appendix E.

2. Theoretical Background

2.1. Convective Storms in Mid-Latitudes

Parcel Theory

The term *convection* generally refers to a mode of heat transfer in a fluid. In meteorology, convection denotes the thermally direct circulation caused by an unstable vertical distribution of mass. The stability of a column of air is typically investigated using *parcel theory*. This concept rests on several simplifications. It does not consider: (i) dynamic vertical pressure perturbations, (ii) mixing of updraft air with ambient environmental air (entrainment), and (iii) the weight of condensed water (hydrometeor loading) rising in the updraft parcel. We briefly revisit *parcel theory* in the following.
As a first step, we define the *buoyancy* force. The starting point is the vertical equation of motion in hydrostatic balance, neglecting viscosity and the Coriolis force:

$$\frac{dw}{dt} = -\frac{1}{\rho}\frac{\partial p}{\partial z} + g \tag{1}$$

where w is the vertical velocity, ρ is the air density, p is the pressure, and g is the gravitational acceleration. Buoyancy is caused by density variations in the atmospheric column, which in turn cause an unbalanced pressure gradient. By introducing a horizontally homogeneous base state in hydrostatic balance (indicated by overbars), which is defined as

$$0 = -\frac{\partial \bar{p}}{\partial z} - \bar{\rho} g \tag{2}$$

and substracting it from (1) we obtain the following equation:

$$\frac{dw}{dt} = -\frac{1}{\rho}\frac{\partial p'}{dz} - \frac{\rho'}{\rho} g = -\frac{1}{\rho}\frac{\partial p'}{dz} + B \tag{3}$$

where B is the buoyancy force and the primed variables denote deviations from the base state. Using the equation of state and neglecting products of perturbations, the buoyancy can be rewritten as

$$B = \frac{\rho'}{\bar{\rho}} g \approx \left(\frac{p'}{\bar{p}} - \frac{T_v'}{\overline{T_v}} \right) g \approx - \frac{T_v'}{\overline{T_v}} g \tag{4}$$

where T_v is the virtual temperature and it has been used that $\left| \frac{p'}{\bar{p}} \right| \ll \left| \frac{T_v'}{\overline{T_v}} \right|$. To investigate the buoyancy of an air parcel in an updraft, it is customary to calculate its buoyancy using the parcel's virtual temperature T_{v_p} and the virtual temperature of the environment $T_{v_{env}}$ so that:

$$B = g(\frac{T_{v_p} - T_{v_{env}}}{T_{v_{env}}}) \tag{5}$$

Static stability of an air column can be assessed by displacing an air parcel, which has the same temperature as its environment, i.e. $\bar{T} = T = T_0$ in the vertical:

$$\frac{d^2 \Delta z}{dt^2} = g \frac{T - \bar{T}}{\bar{T}} \tag{6}$$

where Δz denotes the distance of the vertical displacement. The temperature of the parcel at the new position can be expressed via the moist adiabatic lapse rate Γ_m or the dry adiabatic lapse rate Γ_d. The environmental lapse rate is $\gamma = d\bar{T}/dz$. Using a first-order Taylor-Approximation for the temperature at the new position this leads to:

$$\frac{d^2 \Delta z}{dt^2} + \frac{g}{T_0} (\Gamma_p - \gamma) \Delta z = 0 \tag{7}$$

The solution to this second order ordinary differential equation is real for $\gamma > \Gamma_p$, which means the stratification is *unstable* and Δz increases with time. In contrast, the solution is imaginary for $\gamma < \Gamma_p$, which means the stratification is *stable* and the parcel oscillates about its initial place. A further distinction can be made between saturated and unsaturat-

ed displacements. The term "absolutely unstable," refers to the situation when $\gamma > \Gamma_d$ and "absolutely stable" means $\gamma < \Gamma_m$. When $\Gamma_m > \gamma > \Gamma_d$, the atmosphere is "conditionally unstable" (stable with respect to unsaturated vertical displacements, unstable with respect to saturated vertical displacements).

A useful and widely adopted measure for the strength of convective updrafts is convective available potential energy (CAPE). CAPE is defined as

$$CAPE = \int_{LFC}^{EL} B\, dz \tag{8}$$

Where LFC denotes the *Level of Free Convection* and EL denotes the *Equilibrium Level*. CAPE can be used to estimate the maximum updraft speed in the following way. We assume that acceleration in the vertical is caused by buoyancy only:

$$\frac{dw}{dt} = B \tag{9}$$

Multiplying both sides by $w \equiv dz/dt$ yields:

$$w\frac{dw}{dt} = B\frac{dz}{dt} = \frac{d}{dt}\left(\frac{w^2}{2}\right) \tag{10}$$

Thus:

$$dw^2 = 2Bdz \tag{11}$$

Integrating (11) from the LFC to the EL (assuming that *w=0* at the LFC and *w(EL)=max(w)*) yields:

$$\int_{LFC}^{EL} dw^2 = 2\int_{LFC}^{EL} Bdz \tag{12}$$

$$w_{EL}^2 - w_{LFC}^2 = 2 \int_{LFC}^{EL} B dz = w_{max}^2 \tag{13}$$

$$w_{max} = \sqrt{2CAPE} \tag{14}$$

This equation sets an upper limit for maximum updraft velocity. In reality, updraft velocity is reduced by entrainment and hydrometeor loading to varying degrees.

Initiation and organization of convective storms

Convective storms can occur when sufficient instability is present and potentially buoyant air is lifted to its level of free convection. Convective storms can be organized in a variety of ways. Although the processes which determine the severity and form of a convective storm are very complex, the environmental conditions which determine the strength and shape of a convective storm to a large degree can be summarized into three categories: (1) low-level (boundary layer) moisture, (2) vertical instability, and (3) vertical wind shear (see e.g., Weismann and Klemp, 1982 or Rasmussen and Blanchard, 1998). These conditions are a necessary but insufficient condition for convective storms. Additionally, a trigger mechanism has to be present to initiate deep convection. These trigger mechanisms typically are mesoscale air mass boundaries, orographic processes, or differential land surface heating. These result in horizontal density gradients that facilitate the depletion of vertical instability.

As mentioned above, CAPE is useful for predicting the intensity of convection but is mainly related to updraft strength and not directly to precipitation intensity. Precipitation intensity in convective storms can be influenced by various processes, like entrainment rates differing between storm types and evaporation below cloud base. Precipitation efficiency, the ratio of total precipitation of a convective cloud to the moisture inflow at cloud base has been shown to be strongly influenced by vertical wind shear (Weisman & Klemp 1982, Market & Allen 2003, Chen et al. 2015).

Wind shear determines the organization of convective storms via various processes. Firstly, it increases the organization of convective storms by separating the updraft from the downdraft (= precipitation) region. Furthermore, it can facilitate the development of supercells by tilting horizontal vortices into the vertical and thus creating a rotating up-

draft. The spectrum of convective storms ranges from unorganized, single convective cells at low wind shear via multicells, characterized by the repeated development of new cells in the vicinity of old ones at intermediate wind shear to supercells and mesoscale convective systems at high wind shear (Houze 2014). Figure 1 shows a schematic of the spectrum of convective storms.

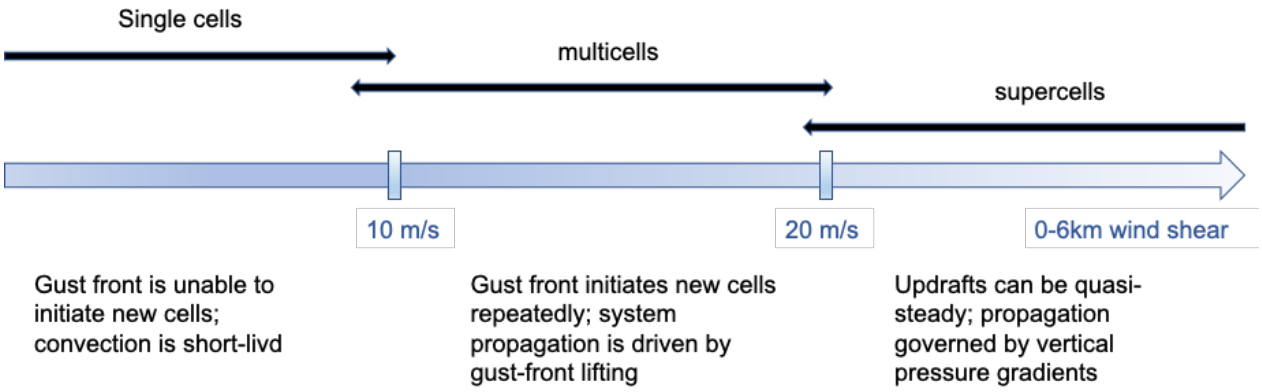

Figure 1: Spectrum of storm types as a function of wind shear. Adapted from Markowski and Richardson 2010, p. 206.

2.2. Deep Convection in Convection-Permitting Climate Models

Convection-permitting climate models (CPMs) are regional climate models (RCMs) that can simulate deep convection explicitly instead of parameterizing it. The grid spacing below which the main features of deep convection can be explicitly resolved is commonly estimated at ~ 4 km (Prein et al., 2015; Weisman et al., 1997), although it has been argued that explicit representation of deep convection is beneficial above 4 km in some respects (Vergara-Temprado et al. 2020). The lower boundary of spatial resolution is typically set at 1 km, below which Large-Eddy-Simulations (LES) are advantageous to resolve parts of the turbulence spectrum. Most studies using CPMs use a 1-way dynamical downscaling approach where the simulation is driven by lateral boundary data from global climate models or reanalyses (Laprise et al. 2008). The maximum step in resolution of 12 identified for coarser RCMs also applies for CPMs, although larger steps are possible when using a larger spin-up zone (Berthou et al. 2020). This factor of 12 typically makes a two-step approach feasible to get from the typical GCM-resolution of 75 km to CPM-resolution (Brisson et al. 2016). The majority of modeling centers (28 out of 30) participating in a current coordinated experiment of convection-permitting experiments (FPS-Convection CORDEX, Coppola et al. 2020) adopt such a two-way nesting approach (Lu-

cas-Picher et al. 2021). Switching off the parameterization of deep convection requires changes in other parametrizations such as microphysics, radiation, and turbulence. Because not all convective clouds can be resolved at kilometer-scale resolution, it may be necessary to parameterize shallow convection depending on the model setup (Chow et al. 2019). For the microphysics parameterization, it has been shown that adding dense hydrometeors, like graupel, to the parameterization leads to more intense and more realistic convective precipitation (Brisson et al. 2016). Using a two-moment microphysics scheme can lead to improvements in areas with steep orography but not necessarily in other regions (Orr et al., 2017; Van Weverberg et al., 2014).

The main benefit of convection-permitting models is a better representation of precipitation statistics, especially of the diurnal cycle of precipitation and extreme precipitation. Nevertheless, they can also improve the representation of other variables, such as temperature or cloud cover. Furthermore, they have the potential to improve the representation of other hazards associated with deep convection, like lightning (Brisson et al. 2021) and hail.

As CPM simulations are computationally expensive, the number of studies covering large, continental-scale domains and time periods of decades is still limited. An overview of recent CPM studies can be found in Lucas-Picher et al. (2021). For Germany, Knist et al. (2018) conducted a CPM study using the WRF model, which showed a decrease in mean precipitation and an increase in extreme hourly precipitation. In this study, the temperature scaling of hourly precipitation extremes exceeds the C-C-rate. Varying scaling rates have been reported for different areas in Europe (Lucas-Picher et al., 2021).

2.3. Precipitation Scaling with Temperature and Moisture

This section begins by reviewing the use of the Clausius-Clapeyron equation to estimate the response of extreme precipitation to climate change. Afterward, methods to calculate precipitation scaling with temperature and moisture are discussed.

The Clausius-Clapeyron equation describes the dependency of the saturation water vapor pressure on temperature and is commonly used as a starting point when discussing changes in extreme precipitation with climate change. It is frequently approximated by the Magnus formula:

$$e_S(T) = 6.1094 * e^{\frac{17.625T}{T+243.04}} \quad (15)$$

where e_S denotes the saturation vapor pressure, and T denotes the temperature in °C. Although the exponent varies with temperature, this formula is often approximated as an exponential function with a fractional increase of ca. 7 %/K for typical tropospheric temperatures.

From the increase of saturation vapor pressure with temperature, it follows that atmospheric water vapor content will increase with temperature approximately at the CC-rate globally as climate models agree on an approximately constant relative humidity (O'Gorman and Muller 2010). However, this increase may vary regionally and is expected to be lower over land areas (Byrne and O'Gorman, 2018).

Theoretical considerations alone are not sufficient to estimate changes in mean and extreme precipitation with climate change as complex feedback processes are involved in precipitation formation, and changes in the transport of moisture and large-scale stratification play an important role. Global mean precipitation is governed by energetic constraints meaning that the intensification of the hydrological cycle is lower than expected from water availability alone because the increase in global precipitation is offset by an increase in net radiative cooling (Allen and Ingram 2002). Global climate models agree on an increase of 1-3 %/K in mean global precipitation (Collins et al. 2013).

In contrast, extreme precipitation usually occurs when all available moisture in a precipitating system has precipitated out. Thus, it is assumed that precipitation extremes are largely constrained by moisture availability. Early climate models already predicted an increase in extreme daily precipitation on a global scale (e.g. Noda & Tokioka 1989 or Gordon et al. 1992). These findings have been largely confirmed by newer models (Kotlarski et al. 2014) and observations (Donat et al. 2016) on continental scales. As an example, Fischer & Knutti (2016) compared daily precipitation extremes in Europe from two datasets to the expected increase by the Clausius-Clapeyron equation and found them to be in good agreement (Figure 2b). On the local scale, insignificant or even decreasing trends in extreme precipitation can occur caused by the large internal variability of precipitation or local changes in moisture availability or atmospheric circulation (Groisman et al. 2005).

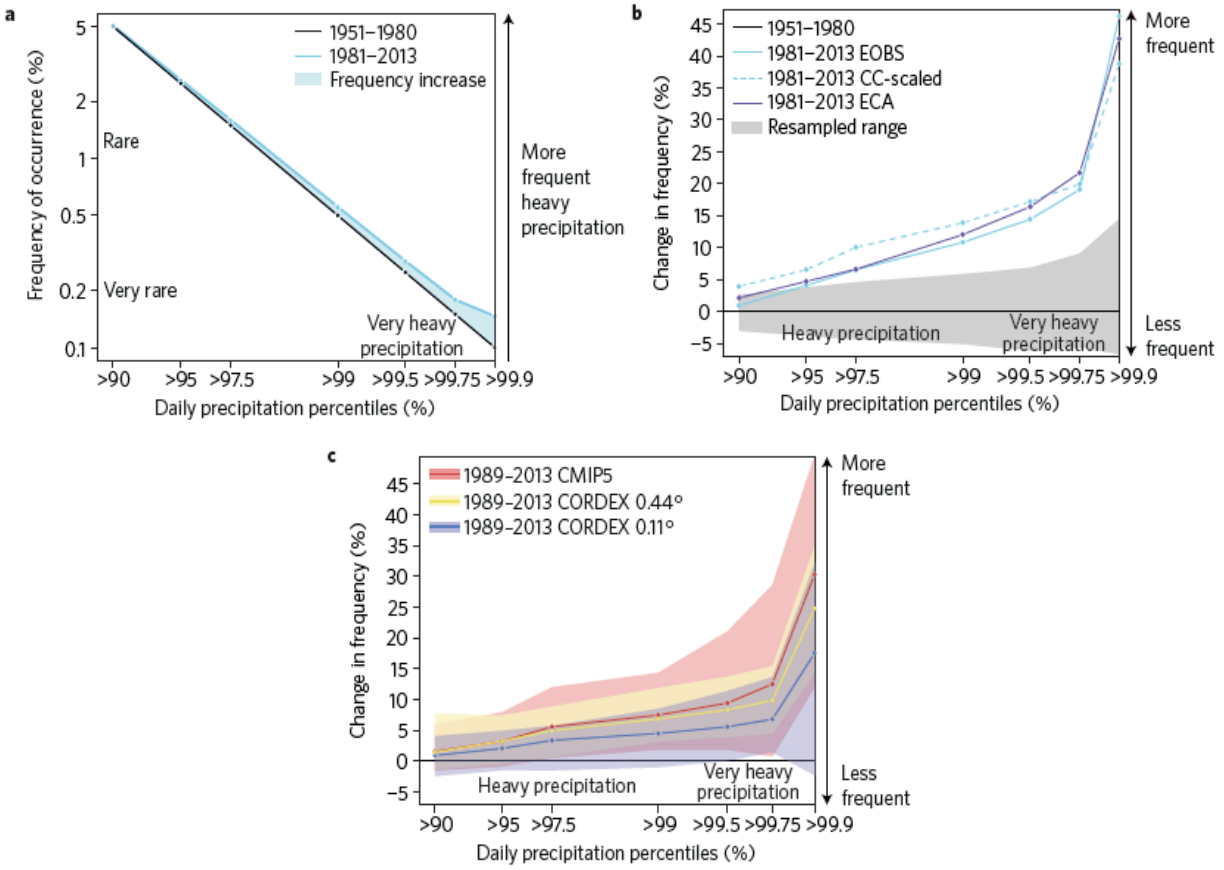

*Figure 2: Increase in daily precipitation extremes **a**, Observed frequency of occurrence of heavy precipitation in Europe in the periods 1951–1980 (black) and 1981–2013 (light blue solid) according to the EOBS gridded observation data set. **b**, Ratio of observed daily precipitation frequency in 1981–2013 versus 1951–1980 according to the EOBS gridded observation data set (light blue solid) and the ECA station series (violet solid). Light blue dashed lines show changes for 1981–2013 as expected from Clausius–Clapeyron (CC) scaling due to the regional mean warming of 0.75 °C between the two periods. **c**, Same as **b** but for CMIP5 models (red), EURO-CORDEX models run at 0.44° resolution (yellow) and 0.11° resolution (blue). Models are masked by the observational data set. Shading denotes minimum– maximum ranges across all models in the ensembles, but note that no model follows the upper or lower bound of the shading for all percentiles. Reprinted by permission from Springer Nature: Fischer, E., Knutti, R. Observed heavy precipitation increase confirms theory and early models. Nature Clim Change 6, 986–991©2016.*

As mentioned in the introduction, sub-daily precipitation extremes have been found to increase at rates higher than the CC-rate under current climate conditions. These sub-daily precipitation extremes are caused by convective precipitation. Multiple hypothesis have been suggested to explain this behavior, such as a shift from stratiform to convective precipitation for higher temperatures, a positive feedback-loop between moisture supply at cloud base, latent heating in the updraft, and updraft strength, and increased organization (see Fowler et al. 2021 for a review).

Distinguishing between dynamical and thermodynamical processes contributing to precipitation can help to understand changes in extreme precipitation conceptually. O'Gorman et al. (2015) use the following equation to describe the precipitation rate in an extreme event:

$$P = -\varepsilon\{\omega(p) * S((T,p)\} \tag{16}$$

Where ε denotes precipitation efficiency, $\omega(p)$ is vertical velocity in pressure coordinates, $S((T,p) = \frac{dq_s}{dp|_{\theta_e^*}}$ is the derivative of saturation specific humidity q_s with respect to pressure taken at constant saturation equivalent potential temperature θ_e^* (meaning the derivative along a moist adiabat), and the brackets {} denote the mass weighted integral over the troposphere. Thus, ω represents the dynamical contribution, and S represents the thermodynamical contribution to precipitation intensification. The authors call ε the microphysical contribution as it can be influenced for example by aerosol concentrations. However, in the case of convective precipitation, ε can also be influenced by vertical wind shear as stated before and could thus be considered a dynamical contribution.
Although the increase of the thermodynamic contribution S with warming is influenced by changes in the moist adiabatic lapse rate, the authors argue that it can be shown to scale with near surface humidity at 6-7 %/K. For stratiform precipitation, the authors argue that the contribution of the dynamical component is negligible for extratropical regions by analyzing the quasi-geostrophic omega equation. This line of reasoning would explain the observed and projected consistent increase of daily precipitation extremes at about 7 %/K. In contrast, the dynamic contribution ω might change for convective precipitation due to the aforementioned positive feedback-loop or changes in convective storm-type and thus organization.

Methods to quantify extreme precipitation "scaling"

The term "scaling", when referring to the dependence of extreme precipitation on temperature, was first used in the literature in 2008 by Lenderink & van Meijgaard (2008). They investigated the dependence (or "scaling") of extreme precipitation on day-to-day temperature variability by binning hourly precipitation into temperature classes and computing high (e.g. 99th) percentiles for each bin. Since then, this procedure has been widely adopt-

ed and is often called *binning scaling* or *apparent scaling* (Zhang et al. 2017). Statistically, these *scaling curves* can be seen as the highest percentiles of precipitation distributions conditioned on daily temperature.

In contrast to *binning scaling*, *trend scaling* refers to the ratio of long-term absolute changes in extreme precipitation and mean temperature (Zhang et al., 2017). To calculate trend scaling, the highest percentiles of precipitation from two full climate periods are empirically computed and the ratio is divided by the mean temperature change signal between these periods. This approach was used, for example, by Fischer & Knutti (2016) to compute the changes in extreme daily precipitation described previously.

Commonly, the term *scaling* is used to describe scale invariance, i.e., a property of power laws where "a relative change in one quantity gives rise to a proportional relative change in the other quantity, independent of the initial size of those quantities"[3]. As convective precipitation has been shown to increase at varying rates across the temperature or dew point temperature range, using the term *scaling* is questionable in this context. In general, whenever the term *scaling* is used in the literature related to the intensification of precipitation with temperature, it should be interpreted as "consistent exponential increase".

Binning scaling can be seen as a substitute for *trend scaling* used because of the limited observations of hourly precipitation and has a number of limitations. As *binning scaling* is related to daily temperature variability it includes varying synoptic conditions, times of day, and seasons. Therefore, it is hard to distinguish between thermodynamic and dynamic effects based on the *binning scaling* of precipitation at a fixed location. Furthermore, the temperature scaling of hourly extreme precipitation has been shown to drop off at high temperatures due to moisture limitation. This drop-off is expected to occur at higher temperatures under future conditions so that present scaling rates cannot be projected into the future (Prein et al. 2017a). It has been discussed whether temperature scaling can be a two-way causality because downdrafts of convective cells can influence the temperature if hourly temperature around the time of convection occurrence is used (Barbero et al. 2018). Because of these varying scaling rates, dew point temperature has been suggested and widely adopted as a more meaningful covariate (Lenderink et al. 2011).

To understand these varying scaling rates of sub-daily precipitation extremes, a number of studies have investigated the scaling of Lagrangian cell properties based on weather ra-

[3] *Yaneer Bar-Yam. "Concepts: Power Law". New England Complex Systems Institute. https://necsi.edu/power-law. Accessed: 28 November 2021.*

dars. They show that convective cells increase in area and intensity with temperature in central Europe (Lochbihler et al., 2017; Moseley et al., 2013; Purr et al., 2019), whereas no area increase and generally lower scaling rates were found in Mediterranean and semi-arid climate (Peleg et al., 2018).

3. Data

3.1. Radar Climatology

The radar-based precipitation climatology (Winterrath et al. 2017) developed by the national weather agency of Germany, Deutscher Wetterdienst, is used for tracking convective cells. This precipitation data set is based on radar data which has been quality checked, corrected, and adjusted to rain gauge measurements. The correction steps used for this product to derive precipitation from radar reflectivity include clutter filtering, distance-dependent signal correction, and removal of radar spokes. The 5-min dataset, the so-called YW-product (Winterrath et al. 2018a), is used for the tracking. For the comparison to stationary hourly precipitation intensities, the hourly dataset is, the so called RW-product (Winterrath et al. 2018b), is used. The analysis covers the period 2001-2016. The data set has a spatial resolution of 1 km x 1 km.

3.2. Reanalysis

ERA5, the 5th generation global reanalysis by ECMWF (Hersbach et al. 2020), is used to derive the environmental conditions of convective storms. The variables used to characterize convective storm conditions are dew point temperature at 2 m (T_d), convective available potential energy (CAPE), and bulk vertical wind shear (SH) calculated as vector difference between the wind in 500 hPa height and 10 m. ERA5 provides hourly values of atmospheric variables at a spatial resolution of 0.25° x 0.25°. Convective parameters calculated from ERA5 data have been compared with sounding data and the MERRA-2 reanalysis by Taszarek et al. (2020). ERA5 performs better than MERRA-2 for all variables but underestimates both mean and extreme values of CAPE and wind shear compared to rawinsoundings. An important consideration when relating cell properties to environmental conditions from reanalysis is the spatial and temporal representativity of the reanalysis. Precipitation scaling has been shown to depend on the time of temperature recording (Lenderink et al. 2011). Downdrafts and evaporative cooling of rain associated with convective storms lead to a decrease in surface temperature. Visser et al. (2021) found that using sub-daily atmospheric conditions before the start of the storm for determining scaling rates results in increased consistency of the scaling rates. However, since we use a reanalysis that parameterizes convection, it cannot be expected that the diurnal cycle of

convective precipitation is perfectly represented. The convection parameterization might trigger precipitation prematurely which leads to depleted CAPE and decreased dew point temperature, and thus the environmental conditions before storm onset do not necessarily represent the determining conditions for storm development. For these reasons, we relate convective environmental conditions at various times to cell properties. By default, we assign each cell to the 3-hourly values of CAPE, SH, and T_d before storm onset at its starting point. Additionally, we test the influence of sub-daily variability by using daily mean values.

4. Methods

4.1. COSMO-CLM Simulations

The Consortium for Small-Scale Modeling model in climate mode (COSMO-CLM, from now on abbreviated as CCLM) is used to downscale reanalysis data and output from general circulation models. For the evaluation part, the European Centre for Medium-Range Weather Forecast Interim Reanalysis (ERA-Interim) is downscaled to a horizontal grid spacing of 0.025° (≈2.8 km) via an intermediate nest with a grid spacing of 0.22° (≈25 km). At the lateral boundaries of the simulation domain, the model is nudged towards the driving data using Davies relaxation (Davies 1976). Within the simulation domain, no nudging is applied. The model domain of the inner nest covers central Europe (Figure 3) and is comprised of 368 * 306 grid points. The CCLM is a non-hydrostatic limited-area climate model based on the COSMO model (Steppeler et al. 2003), a model designed by the Deutsche Wetterdienst (DWD) for operational weather predictions. The climate limited-area modeling (CLM) community adapted this model to perform climate projections (Böhm et al. 2003, Rockel et al. 2008). We use the version COSMO5.0clm7 with the following setup. For time integration, the 5th order Runge–Kutta split-explicit time-stepping scheme is used with a time step of 25 s. The lower boundary fluxes are provided by the TERRA model. The radiative scheme is the Ritter and Geleyn scheme (Ritter & Geleyn 1992) and is called every 15 min. As recommended in Brisson et al. (2015), we use a one-moment microphysics scheme, including graupel in the finest nest, which provides a more realistic representation of deep convective clouds. While the parameterization of deep convection is switched off, shallow convection is still parameterized using the convection scheme after Tiedtke et al. 1989.

In addition, a COSMO-CLM hindcast simulation conducted at DWD was evaluated. This simulation was downscaled from the ERA5 reanalysis without an intermediate nest. Further specifications of this simulation can be found in Appendix D.

For the future projections, two continuous 30-yearlong simulations were performed: 1976–2005 (named *Historical* from now on) and 2071–2100 (named *RCP8.5*) at a resolution of 0.025. The model is forced by the global climate model EC-Earth (Hazeleger et al., 2012), in particular, realization r12i1p1 of the CMIP5 ensemble. The model setup, the nesting strategy, and the simulation domain is similar to the hindcast run driven by ERA-interim. The RCP8.5 emission scenario was used for the future simulation.

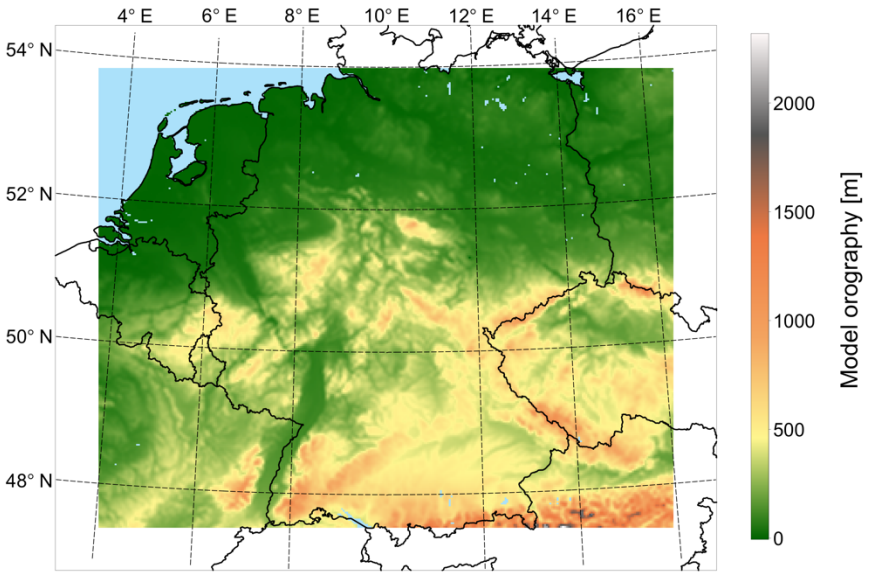

Figure 3: Model domain and model orography.

4.2. Tracking Algorithm

To obtain the properties of convective objects from model and radar data, we used a tracking algorithm. The tracking consists of three major steps:

1. Contiguous precipitation areas with precipitation intensity above a threshold of 8.5 mm/h (within 5 min), potential convective objects, are identified in the current and the subsequent time step. Contiguous areas are defined as pixels that share a common edge.
2. Wind information is used to predict the position of the object at the subsequent time step. To this end, a "cone of detection" is set up for each pixel of every object, and the cone is swept for precipitation objects from the subsequent time step. The axis of the cone is defined by the wind direction; the length of the cone is calculated as twice the wind speed. The opening angle of the cone is 45°. If a new cell is present in the cone, a probability value is assigned to the origin pixel of the cone, which links this pixel to the new cell. The probability value is highest in the center of the cone and drops off exponentially in all directions. As an example, Figure 4a shows the probability values for a single pixel in the case of purely westward wind. In this case, the probability is calculated according to the following formula:

$$Prob(0,0) = exp\left(-\sqrt{(Y_{cent} - y)^2 + \left(\frac{X_{max}}{2} - x\right)^2}\right) \quad (17)$$

where x and y are the indices in x and y direction starting at the original pixel (0,0). The parameter Y_{cent} denotes the centerline of the cone, and X_{max} is the length of the cone, as determined by the wind data. This procedure is repeated for wind information in three height levels (500, 700, and 850 hPa). Afterward, the height dependent probability values are averaged to obtain the final probability value.

3. In the next step, the probabilities of all pixels are summed up for each cell. If one single object is present in the cone, the corresponding objects from the current and the subsequent time step are connected. If multiple cells are present, the current cell is associated with the cell with the highest probability in the subsequent time step.

The properties that are extracted by the algorithm are cell lifetime, mean intensity, maximum intensity, area, cell speed, and track length. It should be noted that merges and splits of objects are not accounted for. If two cells merge, the cell track with the higher probability of association is continued, whereas the other track ends. The track that is not continued is regarded as an individual track in itself. Figure 4b shows an example of a tracked precipitation object.

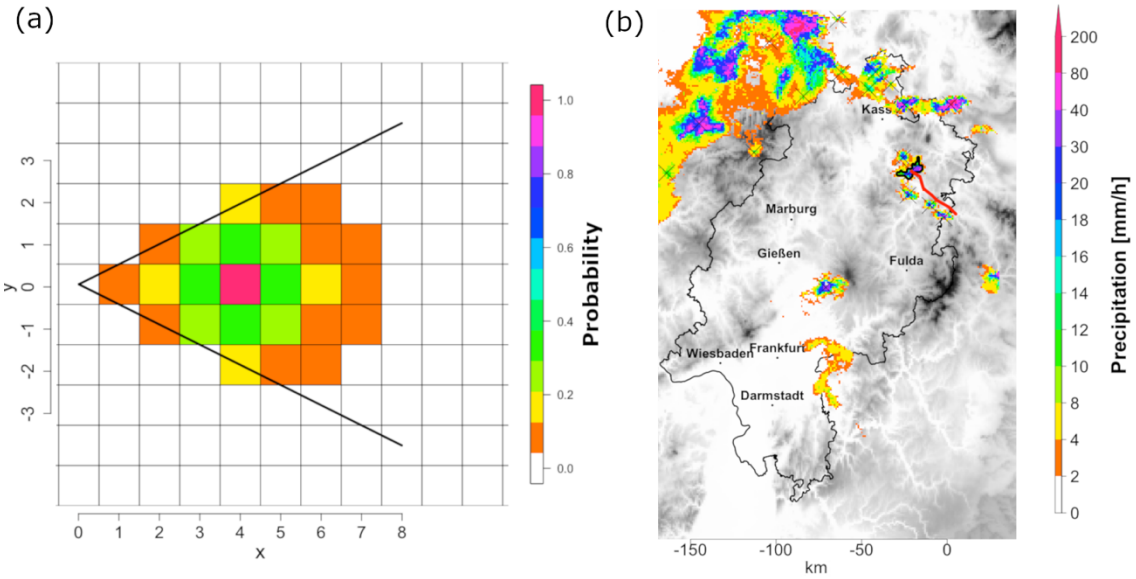

Figure 4: Visualization of the tracking algorithm: (a) detection probabilities for a cone with Xmax = 8 and Ycent = 0 (assuming a grid size of 1 km × 1 km and a time step of 5 min, this is equal to a westward wind of ca. 13.3 m/s), and (b) radar snapshot of a cell (shown is the 5-min precipitation intensity on 30 May 2008 at 21:40 (UTC) in colors and the detected cell track as red line).

Only cells with a lifetime of at least three time steps (=15 min) are considered for analysis. This condition reduces the chances of misinterpreting single clutter pixels in the radar data (which are still present but heavily reduced compared to operational radar products) as convective cells. Furthermore, the algorithm only selects precipitation areas larger than four grid boxes for the same reason. For consistency, this requirement is also kept when tracking the model data. This requirement is also justified because the effective resolution of any numerical model is always coarser than the grid spacing. For the purely radar-based investigation (section 5.1), the data is kept at the original grid in polar-stereographic projection with 1 km * 1 km grid size. For the comparison of model to radar data (section 5.2), both the model data and the radar data are conservatively remapped to a grid in polar stereographic projection with a grid size of 2.8 km * 2.8 km in order to have both data sets on a common, equidistant grid for ease of comparison. For the investigation of potential changes in the future (section 5.3), the model data is kept in its original grid.

The wind information used for estimating the position of each cell at the subsequent time step is taken from different sources for technical reasons. For the purely radar-based investigation (section 5.1), the ERA5 reanalysis was used. For the comparison of the model to the radar data (section 5.2), the ERA-Interim reanalysis was used in case of the radar

data (as ERA5 was not yet available at the time of investigation). In the case of the ERA-Interim driven simulation and the EC-Earth driven simulation, the wind information from the intermediate nest driving the finer simulation is used. In the case of the ERA5-driven simulation and the MIROC5-driven simulation, wind information from the inner nest could be used.

4.3. Calculation of Temperature and Moisture Scaling

To calculate scaling rates of cell properties we employ different techniques of *binning scaling*:

- For the investigation of convective cells based on radar observations (section 5.1), cells are grouped into 23 bins of dew point temperature, CAPE, or wind shear. The bin width varies in such a way that there is an approximately equal number of cells in each bin. As there are a total of ca. 1,350,000 cells in the area of investigation in the period 2001-2016, there are about 60,000 cells in each bin. The scaling rates s_p as a function of dew point temperature are computed for the highest percentiles p (90^{th}, 95^{th}, and 99^{th}) of all cell properties as the average fractional change of the respective quantity (e.g., precipitation sum, maximum intensity, etc.) Q from bin i to i+1 as:

$$\overline{s_p} = \frac{\sum_{i=1}^{23} s_{p,i}}{23} = ln\frac{Q_{p,i+1}}{Q_{p,i}} / (T_{i+1} - T_i) \quad (18)$$

  where T_i denotes dew point temperature of the respective bin i.
- For the comparison of convective cells in the COSO-CLM simulation driven by ERA-Interim with radar observations (section 5.2) we group the convective cells properties total precipitation, maximum area, and lifetime and mean intensity into temperature bins of 1 °C width and determine the 90^{th}, 95^{th}, and 99^{th} percentile for each bin. For the radar data, we use ERA-Interim 2-m temperature of the grid point closest to the origin of the convective cell. For the simulation data, we use the simulated 2-m temperature at the location of cell origin directly.
- For the investigation of potential changes in the future (section 5.3) The temperature and moisture scaling of cell properties are investigated by assigning 2m-temperature and 2m-dew point temperature to each cell. We use daily mean values

of temperature and dew point temperature from the driving, intermediate nest for the simulations driven by EC-Earth (because temperature and dew point temperature were not stored for the inner nest), whereas temperature and dew point temperature could be used from the inner nest directly for the MIROC5-driven simulations. For each cell, the respective conditions at the start location of the cell are used. Cells are sorted into bins of 1°C width for both temperature and dew point temperature. For each bin, the 95th and 99th percentiles of the investigated cell properties are computed.

5. Results and Discussion

The following chapter summarizes the answers to the research questions outlined in the introduction. A more detailed presentation of the results can be found in the 3 papers in the appendices A-C and the additional investigations in the appendices D and E.

5.1. Process Understanding

5.1.1. What is the effect of instability and wind shear on Lagrangian cell properties and the dew point temperature scaling of these properties?

Using the tracking algorithm described in section 4.2, we track convective cells in the radar data set (3.1) and connect them to large-scale environmental variables (dew point temperature, CAPE, and wind shear) from the ERA5 reanalysis (3.2). The highest percentiles of Lagrangian cell properties scale with dew point temperature at varying rates (Figure 5). While maximum intensity scales consistently at the CC-rate, the area and precipitation sum per cell scale at varying rates above the CC-rate.

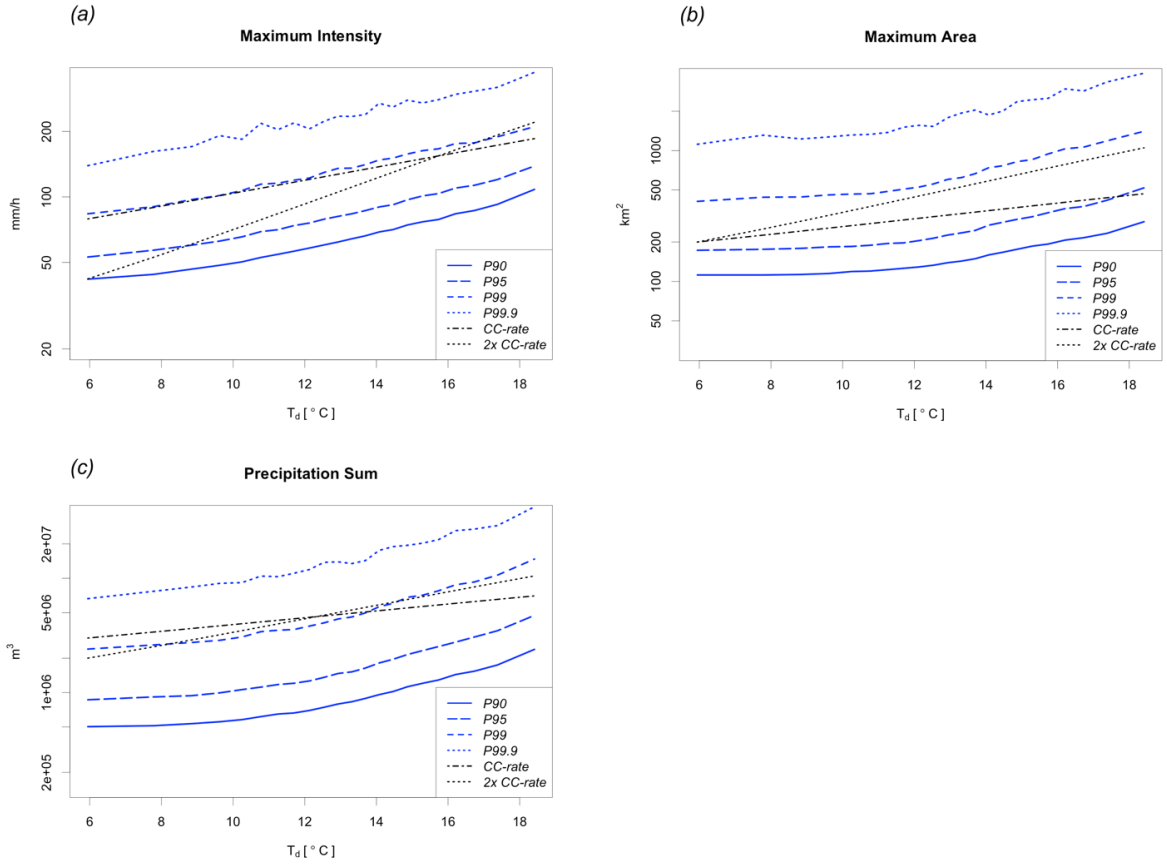

Figure 5: Dew point scaling of the cell properties (a) maximum intensity, (b) maximum area, and (c) precipitation sum (in blue). For orientation, the scaling CC- and 2x CC-rates are given (black). Note the logarithmic y-axis.

The super-CC scaling of the precipitation sum is caused by a covarying increase of static instability with dew point temperature and the effect of wind shear on cell area. In particular, the highest percentiles of daily maximum CAPE increase with T_d at varying rates well above the CC-rate. The increase is higher at high T_d values. The 95th percentile increases at rates around 4x CC-rate while the 99.9th percentile increases at around 3x CC-rate. The highest number of cells occurs at very high CAPE and T_d values. Because of the correlation between CAPE and T_d, cells are concentrated along a corridor of increasing CAPE and T_d values. The most extreme cells, in terms of maximum intensity, area, and precipitation sum, occur at high *CAPE*, T_d, and *SH* values (Figure 6). Wind shear increases the precipitation sum per cell mainly by increasing the cell's spatial extent (Figure 6a and 6c) and has little influence on the maximum intensity of cells (Figure 6d and 6e).

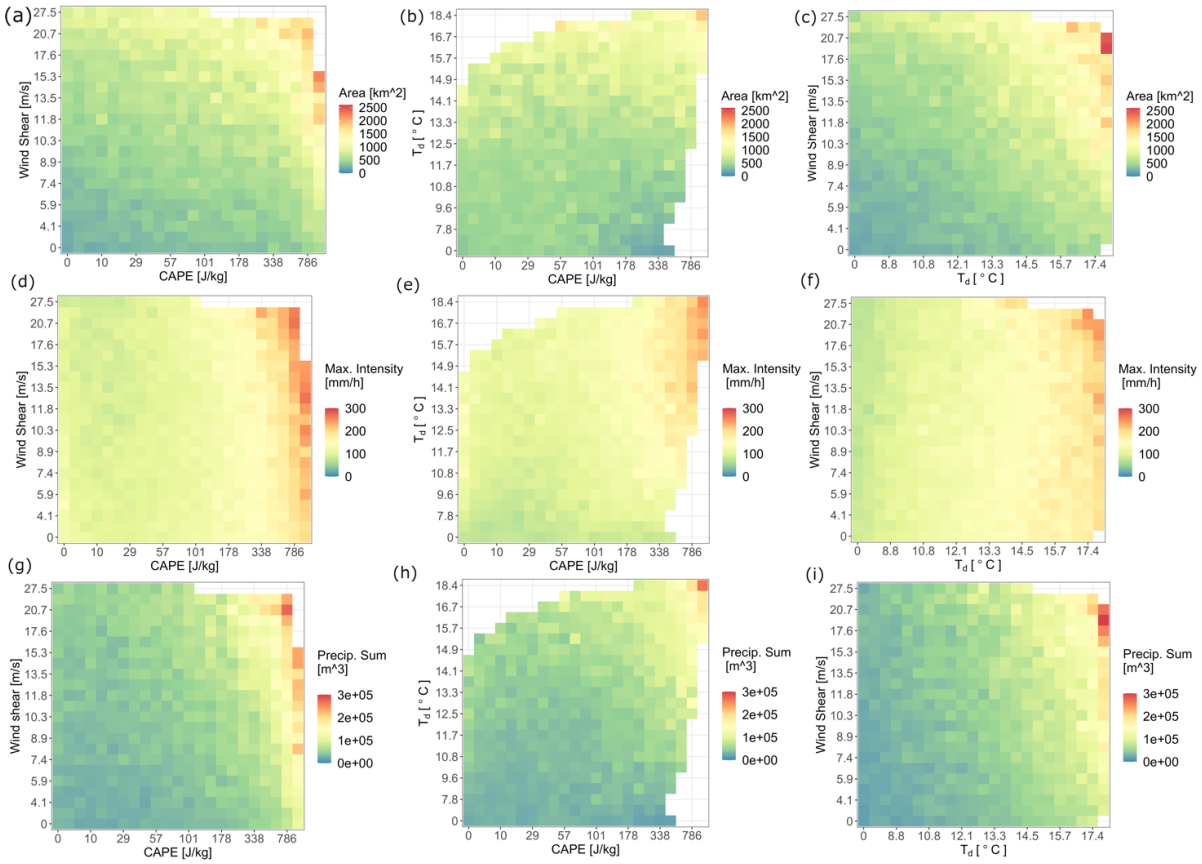

Figure 6: 99th percentile of cell properties depending on environmental variables CAPE, dew point temperature T_d, and wind shear SH.

The influence of CAPE and wind shear on dew point scaling is investigated by classifying convective cells according to their environmental CAPE and wind shear values. Cells are classified as “Low CAPE” cells if they occur in conditions below the median value of 87.5 J/kg or as “High CAPE” cells if they occur at a higher value. Similarly, cells are classified as “Low Wind Shear” cells if they occur in conditions below the median value of 11.2 m/s or as “High Wind Shear” cells if they occur at a higher value. Classifying the cells according to environmental CAPE shows the effects of the general increase of CAPE with dew point temperature: cells which occur at low dew point temperatures, occur predominantly at low CAPE values. Thus, the scaling curves of all cells shift gradually from the “Low CAPE” curve at low dew point temperatures to the “High CAPE” curve at high dew point temperatures (Figure 7a,c,e). The effect is smallest for the maximum area (Figure 7a), where it is only present for low dew point temperatures up to 12 °C, and larger for maximum intensity (Figure 7c) and precipitation (Figure 7e).

Concerning the influence of wind shear, the scaling curves of the 99th percentile are at higher values for the maximum area (Figure 7b) and the precipitation sum (Figure 7f) for

"High Wind Shear", whereas there is little influence on maximum intensity (Figure 7d) which is in line with the findings in the previous section. In contrast to CAPE, the scaling rates do not differ between cells occurring at high or low wind shear conditions and all the cells.

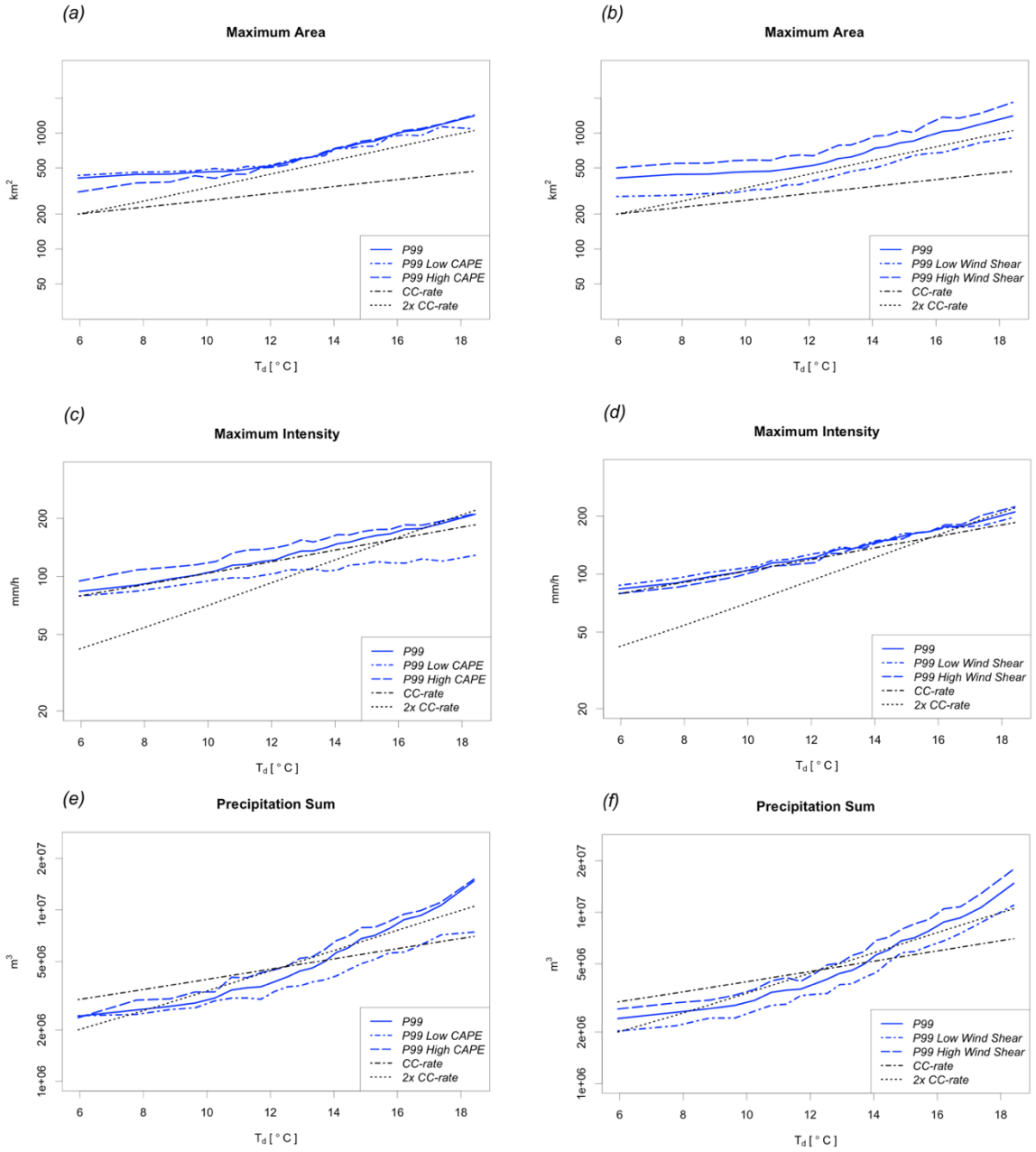

Figure 7: Dew point scaling of the cell properties maximum area, maximum intensity, and precipitation sum (in blue) depending on CAPE (left column), and wind shear (right column). For orientation, the scaling CC- and 2x CC-rates are given (black). Note the logarithmic y-axis.

5.1.2. To what extent does higher cell velocity offset the higher organization of convective cells in high-shear environments with respect to precipitation at fixed location?

From a Eulerian point of view, the increase of precipitation sum with wind shear is compensated by higher cell velocity, which leads to Eulerian precipitation scaling rates close to the CC-rate. To quantify the influence of wind shear on scaling for fixed location, we calculate the fixed location precipitation potential P_{fl} for each cell. The purpose of this quantity is to derive a measure of how much each cell can precipitate at fixed location based on its mean Lagrangian properties as derived from the tracking algorithm. It is calculated as

$$P_{fl} = I * t = \min\left(I * \frac{D}{v}, I * l\right) = \min\left(I * \frac{2\sqrt{A}}{v\sqrt{\pi}}, I * l\right),$$

where I denotes the mean precipitation intensity, t the duration of precipitation, D the diameter calculated based on the mean area of the cell, v the mean speed, A the cell area and l the lifetime of the cell.

P_{fl} shows varying scaling regimes over the dew point temperature range (Figure 8a). It increases at rates below the CC-rate for dew point temperatures below ~11 °C and slightly above the CC-rate, at a rate of 8.8 %/K, above 11 °C. The different percentiles increase at approximately similar rates. Concerning the influence of wind shear, the fixed location precipitation potential decreases with increasing wind shear (Figure 8b).

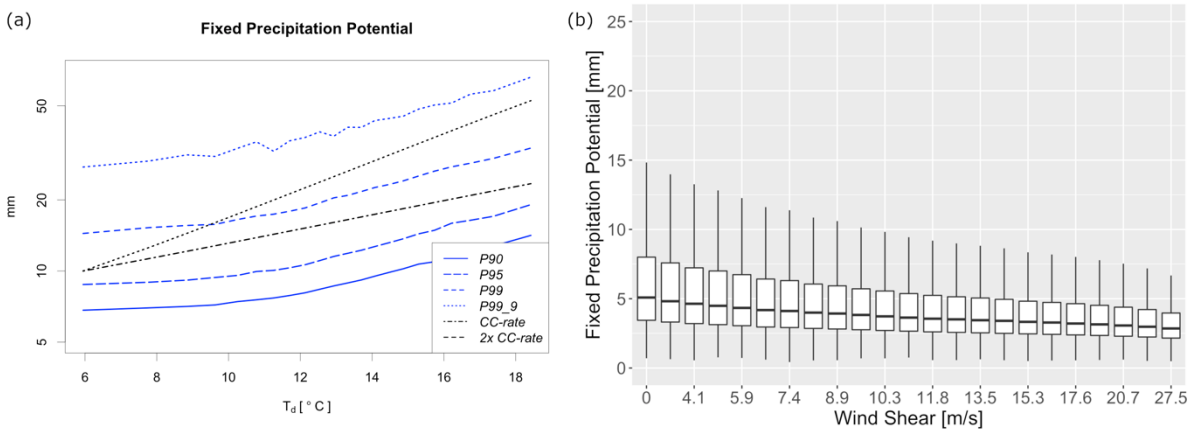

Figure 8: (a) Scaling of fixed location precipitation potential with dew point temperature; (b) wind shear dependence of fixed location precipitation potential.

Furthermore, it was investigated what kind of cells cause intense precipitation events at fixed locations. Intense precipitation events at fixed locations are defined as events with a precipitation amount of more than 25 mm in 1 h within an area of 1 km^2. This definition follows the warning criterion for severe precipitation (at level 3 out of 4) of Deutscher Wetterdienst. A convective cell is connected to a heavy precipitation event if it passes the grid box of heavy precipitation within the hour of its occurrence.
Cells that cause heavy precipitation at fixed locations (abbreviated as hp-cells) move comparably slow: the median cell speed of hp-cells is 8.3 m/s compared to 9.3 m/s for all cells. As cell speed is largely determined by wind shear, the frequency distribution of wind shear for hp-cells is also shifted to lower values compared to all cells.

5.2. Evaluation of the Convection-Permitting Climate Model COSMO-CLM

5.2.1. How well can a convection-permitting climate model represent the properties of convective cells?

Using the tracking algorithm described in section 4.2, we track convective cells in the radar data set (section 3.1) and in a COSMO-CLM simulation driven by the ERA-Interim reanalysis (CCLM-ERAi). A more detailed presentation of the results can be found in Appendix B. Additionally, we evaluated another COSMO-CLM simulation driven by the ERA5 reanalysis (CCLM-ERA5) to test if shortcomings in the previously mentioned simulation are inherent to the model or caused by simulation settings. A detailed description of the results of these simulations can be found in Appendix D.
The mean daily precipitation in observation and simulation data is 2.0 mm/d and 1.7 mm/d, respectively, resulting in a 14 % underestimation of total precipitation in the simulation. The model overestimates precipitation in mountainous regions, especially in the Black Forest in southwest Germany, and underestimates it in the lowlands of Northern Germany (Figure 9c). This points to an overestimation of the orographic intensification of precipitation in the simulations.
The analysis of convective cells is restricted to the summer half-year from April to September because convective precipitation mainly occurs in this period. The mean observed

and simulated summer precipitation (April to September) is 2.3 mm/d and 1.5 mm/d, respectively, resulting in an underestimation of 34 % in the simulation. Taking into account that convective precipitation occurs almost exclusively in the summer months in Germany, this indicates that the model underestimates convective precipitation more than stratiform precipitation. The underestimation is strongest in Northern Germany, while more realistic precipitation amounts are simulated in the South (Figure 9f).

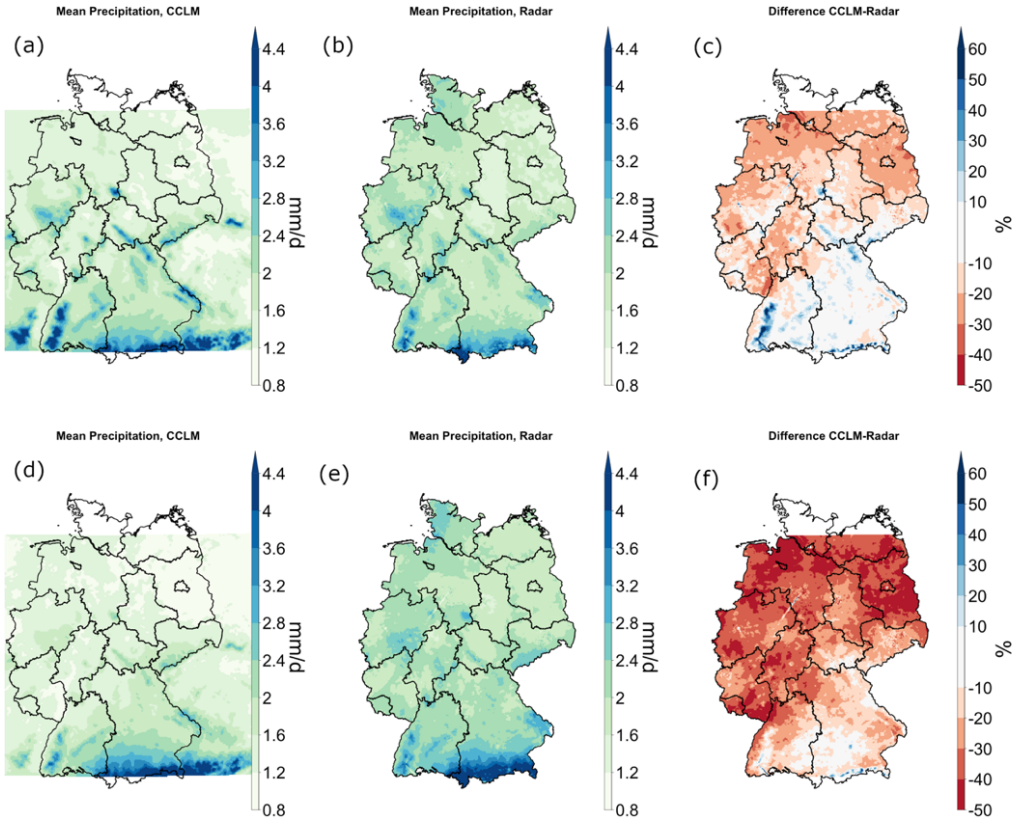

Figure 9: Mean precipitation intensities and differences in the period 2001–2015; (a–c) full year; (d–f) summer half-year (April–September).

The simulation underestimates convective activity, represented by the total number of convective cells, by 33 %. Convective precipitation, calculated as the precipitation sum of all convective cells, is very well matched with an overestimation of 2 %. The lifetime of convective cells ranges from 15 min (the lowest possible value as set by the tracking algorithm) to 7 h (Figure 10a). As expected, short-living cells are the most common form of convective cells. The simulation captures but underestimates the decrease in frequency with lifetime and produces too many long-living and too few short-living cells. Compar-

ing the lifetime distributions of the simulation and remapped radar data yields a Perkin's skill score (PSS) of 0.84. A possible reason for the overestimation of cell lifetime could be that tracks are more often lost in the radar data than in the simulation data by the tracking algorithm. The reason for this is that radar data provide snapshots of precipitation, whereas, in the model, precipitation is accumulated, which leads to a smoother precipitation field. This difference between accumulated and instantaneous precipitation also has a small influence on cell size and mean intensity. To estimate how many tracks are wrongfully split up by the tracking algorithm, we investigate the cell size at the first occurrence of the cell. If the cell only just started its life cycle, one would expect a small size close to the lower boundary of five grid points. If, on the other hand, the cell is the second part of a track that was wrongfully split up, it will have a larger extent. If we consider an initial area larger than 10 grid points (80 km^2) to be unrealistically large and discard those cells, then the underestimation of convective activity is only slightly reduced from 33 % to 28 %. The frequency distributions of total precipitation per cell (Figure 10b) and maximum cell area (Figure 10c) are very well matched with a PSS of 0.99 and 0.98, respectively. There are too few high-intensity cells (Figure 10d). The PSS for the mean intensity is 0.86.

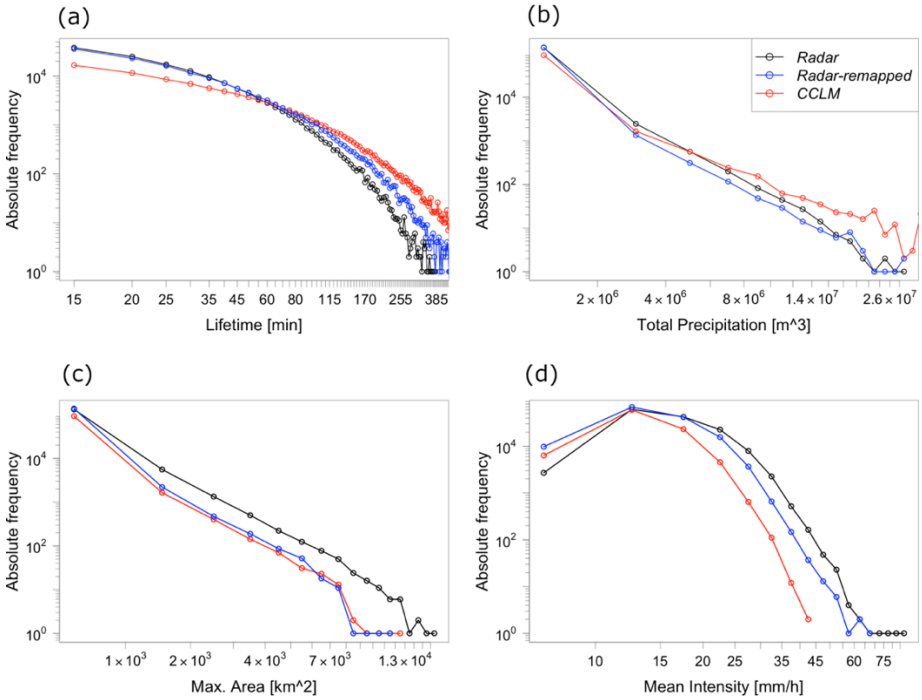

Figure 10: Frequency distributions of the cell properties (a) lifetime, (b) total precipitation, (c) maximum area, and (d) mean cell intensity as observed by the radar (black), by radar remapped to the model grid (blue,) and simulated (red).

To verify that it is really the long-living convective cells that have a high intensity and area, Figure 11 shows the distributions of mean intensity and of maximum area depending on the lifetime of the convective cells. To this end, cells are grouped into lifetime classes of 15-min width. A systematic increase in maximum area and mean intensity with lifetime can be seen in both the radar observations and the simulation. While the observed median maximum area is 226 km^2 for cells living 195 to 210 min, the median is only 25 km^2 for cells living 15 to 30 min. The observed median values of mean intensity of cells in the same lifetime classes are 21 mm/h for long-living and 12 mm/h for short-living cells. These relationships indicate that the detected short-living cells can either be single-cell storms or individual cells of a multicell storm. The long-living, large, and intense cells are organized forms of convective systems like squall lines, supercells, and mesoscale convective systems. The simulation systematically underestimates the increase in mean intensity with lifetime. The increase in maximum area is well matched.

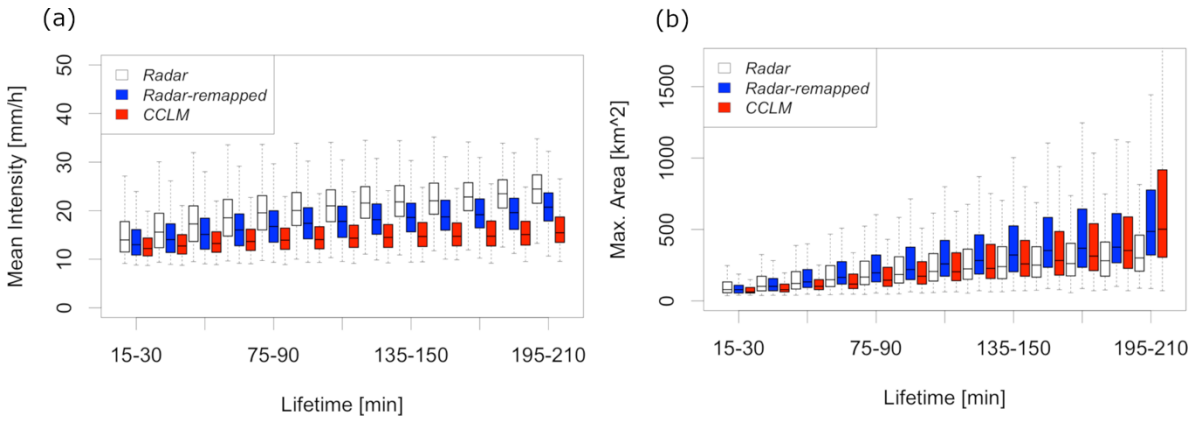

Figure 11: Dependence of (a) cell mean intensity and (b) cell maximum area on cell lifetime for radar observation and CCLM simulation. The boxes denote the 25th, 50th, and 75th percentiles. The whiskers denote the 5th and 95th percentile.

Figure 12 shows the spatial distribution of the occurrence of convective cells. Here, the occurrence of convective cells per grid-point for the period 2001–2015 is shown. The tracking algorithm stores the area and center of mass for each cell at every point in time. For this reason, no information about the actual shape of a cell is available. Instead, the cells are reconstructed as squares around the center of mass to match their original size. It has to be noted that every occurrence of a cell per 5-minute time step is counted. The value can, thus, be interpreted as the number of exceedances of a 5-minute precipitation intensity of 8.5 mm/h (the detection threshold of the tracking algorithm). Instead of count-

ing each cell only once (e.g., at its point of largest extent), this method represents the area affected by convective cells more realistically because cells can have widely varying areas and translation speeds.

Mountain ranges facilitate the triggering of deep convection through various processes (see Kirshbaum et al. (2018) for a review). Therefore, it is not surprising that the Alps and the pre-alpine region show the highest occurrence of convective cells. Low mountain ranges also show increased values compared to lowland regions. In general, there is a positive North–South gradient in convective activity. The mean intensity of convective cells is lower over the mountains (not shown). This can be explained by the fact that orographically induced convection is early in its life cycle in this area and, thus, has a relatively low intensity.

The simulation is capable of representing the increased convective activity in mountain areas. It overestimates the number of convective cells in the South and underestimates it in the North (Figure 12). However, there are areas of overestimation and underestimation in both parts of the investigated domain. Near the radar locations, overestimation prevails, while areas of underestimation tend to be located furthest away from the radar. More cells are initiated in the mountainous areas of Southern Germany than in the North. This supports the hypothesis that the more complex topography facilitates the onset of convection and, thus, eliminates the negative bias in the cell number present in Northern Germany.

Since the convective activity shows a different pattern in North and South Germany, which may be related to the different orography in these regions, we further investigate the height dependence of convective activity. Therefore, the convective cells are stratified by the terrain height at which they occur. While the cell number is underestimated by 15% in regions with a terrain height below 400 m a.s.l., the number of cells for terrain heights above 400 m a.s.l. is overestimated by 6%. The overestimation of convective precipitation in mountainous areas is in line with the results in Knist et al. (2018), who performed convection-permitting climate simulations over Germany using the WRF-model and compared the results to gauge data.

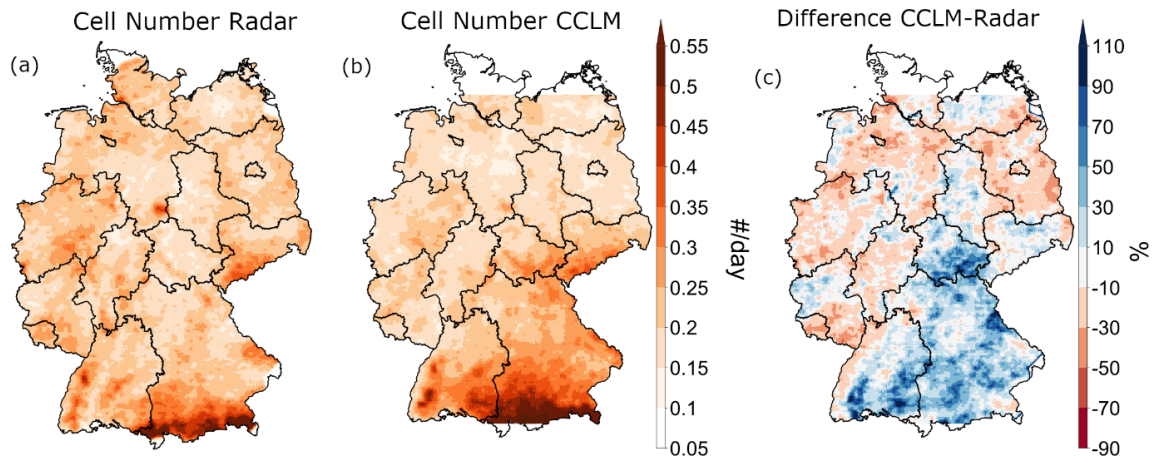

Figure 12: Spatial distribution of the number of convective cells; (a) observation, (b) simulation, (c) relative difference CCLM—radar.

The diurnal cycle of convective activity is slightly delayed in the simulation (Figure 13a). The afternoon maximum is observed at 15:50 (UTC), while the modeled maximum occurs around 16:30 (UTC). The number of cells initiated during the night and morning is well matched, whereas the daytime increase of convective activity is too small, resulting in 36% fewer cells being initiated in the afternoon and evening (between 13:00 UTC and 20:00 UTC). The maximum number of cell initiation is underestimated by 40%. Combined with the general overestimation of cell lifetime, this leads to an overestimation of cells present at each point in time during the night and an underestimation during the time of highest activity (Figure 13b). The mean intensity, defined as the mean over all cells of spatial mean intensity at every 5-min time step, increases during the daytime. The modeled increase of mean intensity is too weak.

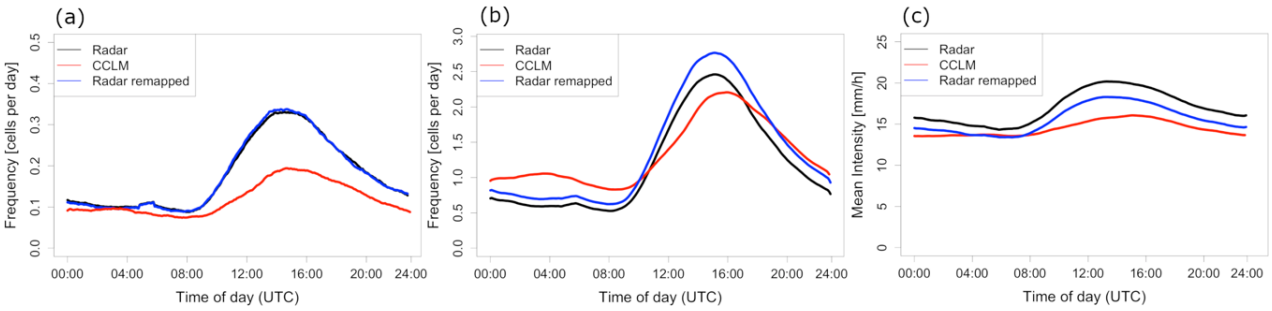

Figure 13: Diurnal cycle of convection; (a) cell number at cell initiation (every cell is counted once), (b) cell number at each individual time step (cells are counted multiple times, according to their lifetime), and (c) mean intensity of all cells at a certain point in time.

Results of the CCLM simulation driven by ERA5

The CCLM-ERA5 simulation produces more precipitation than CCLM-ERAi in the evaluation period 2001-2015. While total precipitation is overestimated by 6% in CCLM-ERA5 compared to the observations, it is underestimated by 14% in CCLM-ERAi. The underestimation of precipitation in Northern Germany is much less pronounced in CCLM-ERA5. During the summer months (Apr-Sep), mean precipitation is well simulated in CCLM-ERA5 with overestimation in the mountain ranges, which is compensated by underestimation in the lowlands.

Both simulations can represent the frequency distributions of cell properties showing the spectrum from short-living, unorganized convection to long-living, organized convection. However, there are more long-living cells in CCLM-ERA5, which could be caused by the better performance of the tracking algorithm resulting from more accurate wind information. Maximum cell intensity is better simulated in CCLM-ERA5, shown by a PSS value of 0.87 compared to 0.84 for CCLM-ERAi.

The diurnal cycle of convective cells is also better represented in CCLM-ERA5. While the diurnal cycle of cell initiation is virtually similar with a slightly later peak in CCLM-ERAi, the amplitude and the phase of the diurnal cycle are more realistic in CCLM-ERA5 when counting cells multiple times according to their lifetime. Furthermore, the phase and the amplitude of the diurnal cycles of mean and maximum intensity per cell are much better represented in CCLM as they do not underestimate the amplitude as strongly as CCLM-ERAi. For example, the diurnal maximum of mean intensity is 18.7 mm/h in the observations, 17.8 mm/h in CCLM-ERA5, and 16.1 mm/h in CCLM-ERAi.

Both simulations can represent the spatial distribution of increased initiation of convection in the alpine area and the lower mountain ranges but generally underestimate the initiation of convection. The underestimation of convective activity in Northern Germany (North of 52°N) is stronger in CCLM-ERAi (-47%) than in CCLM-ERA5 (-40%), whereas CCLM-ERAi initiates more convection in the pre-alpine area than CCLM-ERA5. This could be explained by the larger domain of CCLM-ERA5, which allows for convection to be triggered over the entire alps. Assuming a southerly flow, this would mean that convective cells have already depleted when reaching the northern end of the Alps.

Comparison of CCLM-ERAi simulation with GCM-driven simulation

So far, all of the evaluated simulations were driven by reanalysis data, which represent a best estimate of the large-scale atmospheric conditions. Using a GCM to provide the boundary data for the CCLM simulation introduces additional potential errors related to the representation of large-scale atmospheric conditions in the GCM. In order to assess the reliability of the simulations driven by the EC-Earth model, these simulations are briefly compared to the CCLM-ERAi simulation in terms of the frequency distributions of cell properties (Figure 14). It has to be noted that the simulation periods do not fully overlap: CCLM-ERAi covers the period 1976-2005, whereas *Historical* covers the period 1982-2011. Qualitatively, the frequency distributions of all cell properties are well represented. While the lifetime of cell is well captured (Figure 14a), the *Historical* simulation underestimates the area (Figure 14c) and intensity (Figure 14d) of cells compared to CCLM-EraI. In combination this leads to an underestimation of the total precipitation sum per cell (Figure 14b).

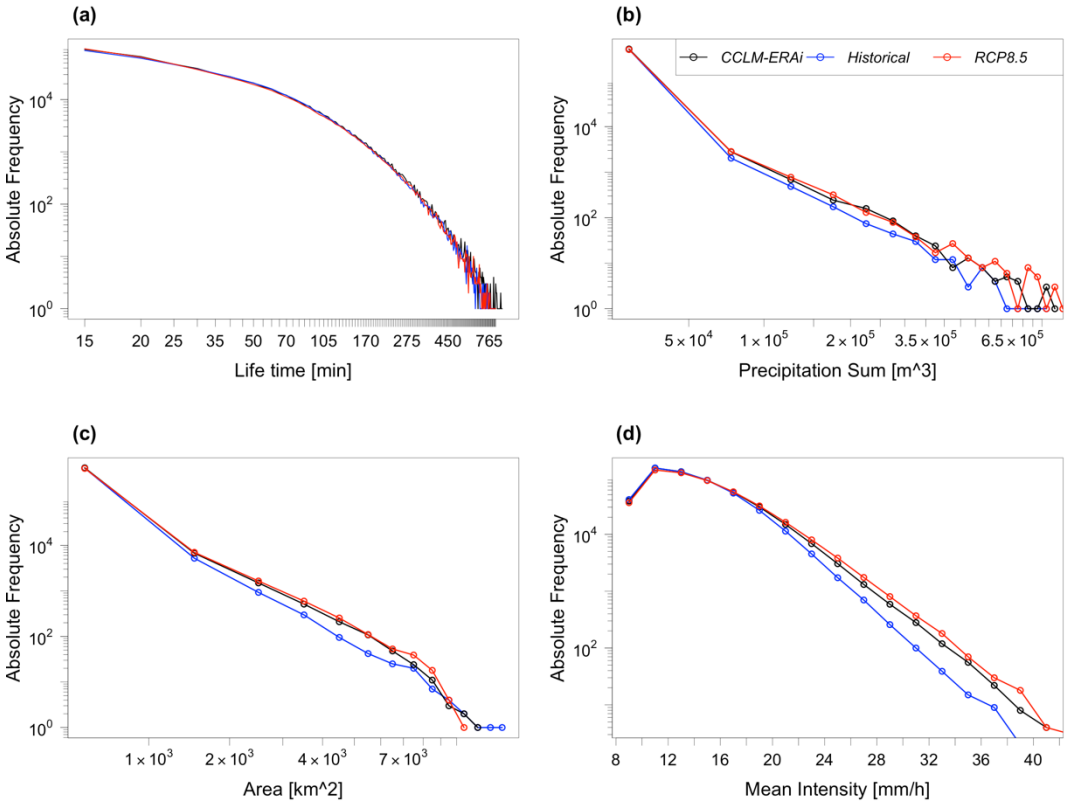

Figure 14: Frequency distributions of the cell properties (a) lifetime, (b) total precipitation, (c) maximum area, and (d) mean cell intensity in CCLM-ERAi (black), Historical (blue), and RCP8.5 (red).

5.2.2. Can the model reproduce the temperature scaling of cell properties?

The scaling of total precipitation, mean intensity, lifetime, and maximum area for both radar and simulation data is shown in Figure 15. Shown are the 90th, 95th, and 99th percentiles based on the simulation and the remapped radar data. For comparison, the 95th percentile of the original radar data is shown additionally. The general underestimation of the highest percentiles of the variables mean intensity and total precipitation, as well as the overestimation of lifetime, is also visible here. In contrast to these variables, the maximum area is well represented in the model, both in terms of absolute value and scaling rate. Generally, the rate at which mean intensity increases with temperature is well reproduced by the model. However, the underestimation of precipitation intensity for long-lasting, organized cells shown in the previous section is visible in the scaling rates of mean intensity. While the radar data shows an exponential increase up to the highest tem-

peratures, the simulated mean intensity flattens at 20 °C. The largest difference in scaling rate appears for the lifetime of convective cells.

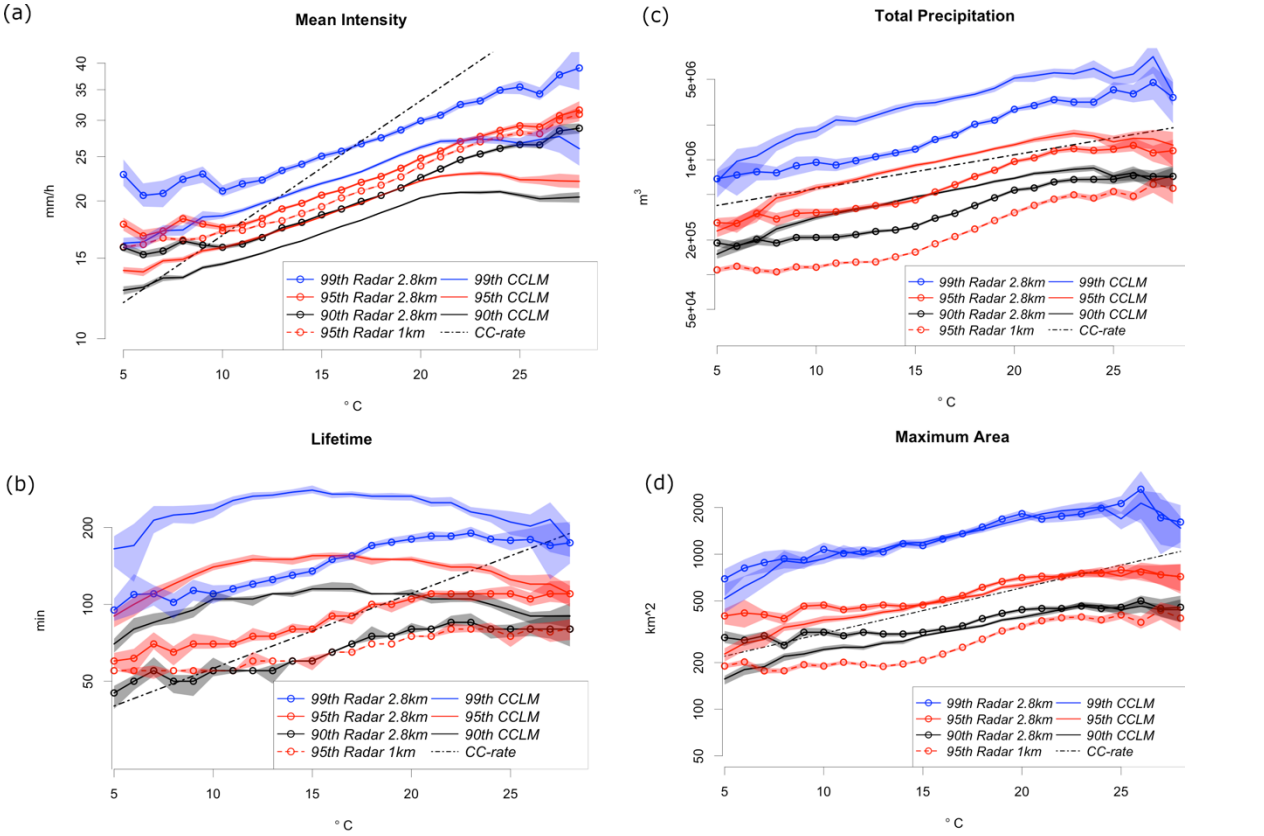

Figure 15: Temperature scaling of cell properties. (a) Spatial and temporal mean intensity of cells, (b) total precipitation, (c) lifetime, and (d) maximum area. Shaded areas denote the uncertainty range estimated by repeatedly calculating the respective quantile using bootstrapping. Note the logarithmic y-axis in all panels.

The radar data shows an increase in lifetime of ca. 5 % in the temperature range between 13 and 22 °C and flattens at higher temperatures. In contrast to this, the lifetime of convective cells in the simulation is mostly flat, with small increases only in the low-temperature range and a drop at high temperatures. An intensification of convective cells above the Clausius–Clapeyron rate, which supports the hypothesis of a positive feedback loop in the strength of convective cells with rising temperatures, is apparent from the scaling rate of the total precipitation. The scaling of the modeled total precipitation is larger than the Clausius–Clapeyron rate for the whole temperature range up to 23 °C, where it levels off. This leveling off is also frequently reported for scaling of extreme precipitation at fixed locations and attributed to limited moisture supply at high temperatures (Hard-

wick Jones et al. 2010, Chan et al. 2016). The observed total precipitation shows a slightly different behavior with a smaller increase at low temperatures and a larger increase starting at 15 °C.

5.3. Future Changes in Convective Cells

5.3.1. How will convective cells change in the future?

Cell properties are investigated by tracking precipitation from the two 30-yearlong CCLM simulations *Historical* and *RCP8.5* driven by EC-Earth (described in section 4.1). Additionally, the robustness of the results is assessed by repeating the analysis with two simulations driven by MIROC5 at the end of the section. A more detailed presentation of the results can be found in Appendix C. A detailed description of the results of the simulations driven by MIROC5 can be found in Appendix E.

While mean summer precipitation (Apr-Sep) is reduced by 15 % in the future period compared to historical conditions, mean convective precipitation (defined as the spatial and temporal mean of precipitation classified by the tracking algorithm) increases by 16 % (from 0.25 mm/d to 0.29 mm/d). This translates to an increase in the fraction of convective to total precipitation from 15.8 % to 21.8 %. The frequency of hourly precipitation at fixed location increases for intensities above 5 mm/h with the biggest relative changes for the highest percentiles. This increase in extreme hourly precipitation is caused by an increase in the number of large, long-living convective cells occurring at high temperature and moisture levels.

Changes in the frequency distribution of cell properties show a complex picture of the response of deep convection to climate warming. While the total number of cells and the lifetime does not change significantly in the future (Figure 16a), as simulated for the end of the 21st century under RCP8.5, there is a shift towards more intense (Figure 16b) and larger events (Figure 16c). In combination, this leads to higher precipitation sums per cell (Figure 16d).

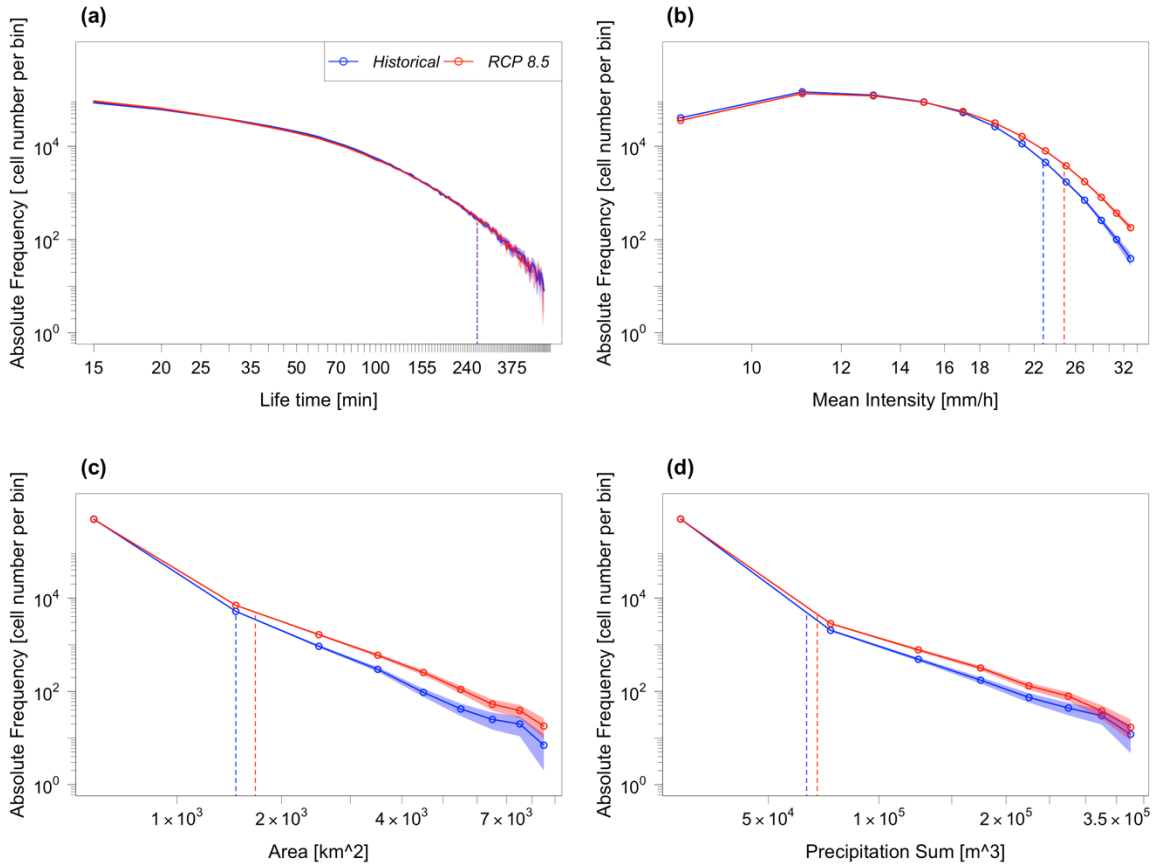

Figure 16: Frequency distribution of cell properties in the Historical (blue) and RCP8.5 (red) simulations: (a) lifetime, (b) mean intensity, (c) maximum area, (d) precipitation sum. Shaded areas denote the 95% confidence interval obtained from 1000 bootstrap samples of all cells. Dashed, vertical lines denote the 99th percentiles. Circles show the midpoints of bins.

The relative increase is strongest for the highest percentiles for all of these properties (mean and maximum intensity, area, and precipitation sum). However, caution should be taken when interpreting results related to the most severe cells as the precipitation intensity is underestimated by the model, especially for long-lasting, organized convection (see previous section). Table 1 summarizes the relative changes. The trend scaling (relative changes divided by the mean temperature change signal, Zhang et al., 2017) is slightly above the CC-rate for the highest percentiles of precipitation sum and maximum area and below the CC-rate for mean and maximum intensity.

Table 1: Relative changes in cell characteristics (from Historical to RCP8.5).

Change in %	Lifetime	Maximum Area	Precipitation Sum	Mean Intensity	Maximum Intensity	Mean Speed
Mean	-2.1	+13.4	+18.3	+3.3	+8.3	+9.0
Median	0.0	+9.1	+3.2	+2.4	+5.8	+7.9
P95	0.0	+16.9	+16.9	+6.4	+12.6	+10.0
P99	0.0	+27.9	+27.0	+9.3	+15.8	+11.0
P99.9	+1.1	+32.0	+30.6	+11.3	+19.1	+13.4
Trend Scaling of P99 [%/K]	0.0	+8.2	+7.9	+2.7	+4.6	+3.2

The diurnal cycle of convective activity changes towards fewer convective cells during the afternoon maximum and more cells during the nighttime (Figure 17a). In combination with the increase in mean precipitation intensity per cell (Figure 17b), this leads to up to 50% more convective precipitation during nighttime and a small decrease during the afternoon maximum (Figure 17c). The afternoon decrease in cell number is primarily caused by fewer slow-moving cells despite the fact that there is no change in the large-scale wind speed.

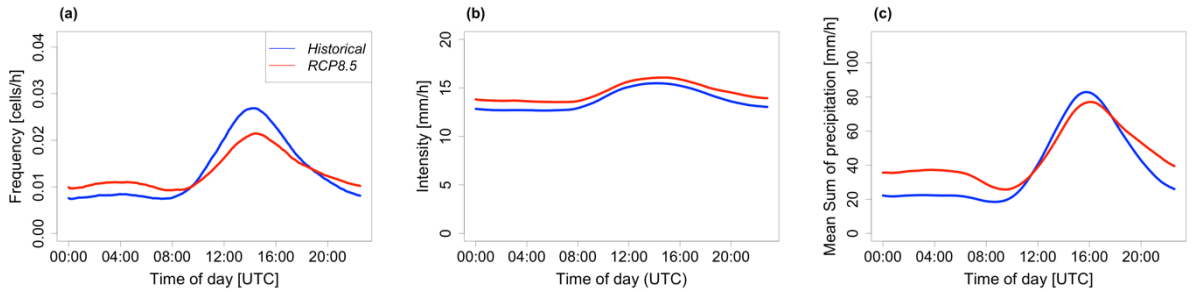

Figure 17: Diurnal cycle of (a) number of cells, (b) mean intensity per cell, and (c) mean sum of convective precipitation.

Although the total number of cells stays approximately constant in the future, the change in cell number varies considerably in space (Figure 18a). In South-West Germany, the number of convective cells decreases while in the North-East increases prevail. However, these changes are not uniform, and changes between increases and decreases occur at small spatial scales of about 10-100 km. This pattern is not related to orography and is

likely caused by internal variability of the convective cells. Mean intensity increases throughout the domain (Figure 18b). The sum of convective precipitation, which can be derived as cell number times mean intensity, therefore, shows a pattern similar to the number of convective cells (Figure 18c).

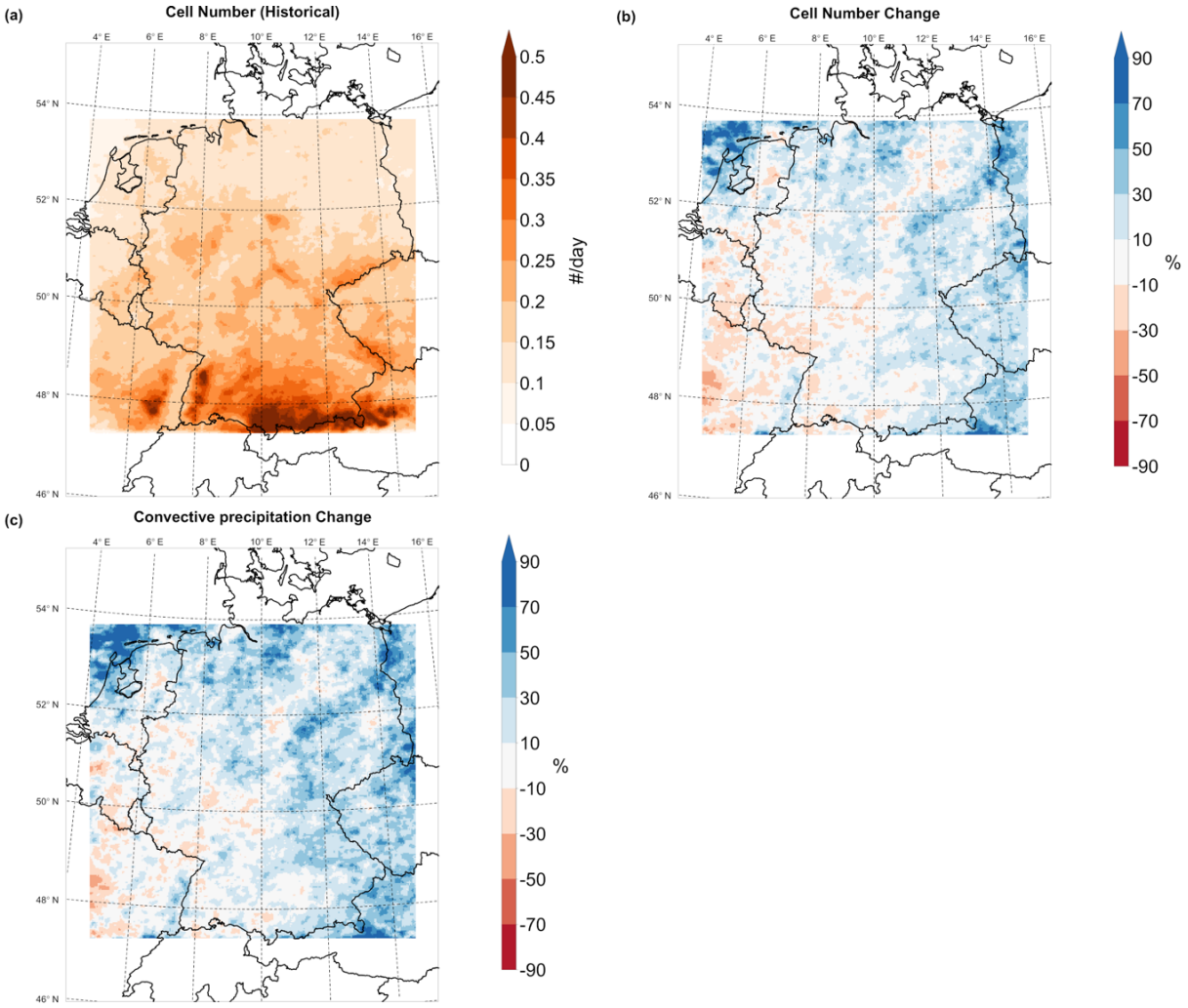

Figure 18: Spatial distribution of (a) cell number in the Historical simulation, (b) relative change in cell number in RCP8.5 compared to Historical, and (c) relative change in convective precipitation sum.

Results of the CCLM simulations driven by MIROC5

In the MIROC5-driven simulations (MIROC5-CCLM), precipitation decreases by 9% from 2.0 mm/h in Hist to 1.8 mm/h in RCP8.5 in the summer months (Apr-Sep). Thus, this projection shows a smaller decrease than the EC-Earth driven simulation (ECE-CCLM) of -15%. The mean temperature change is 4.4 K in the full simulation domain and 4.5 K in the ECE domain (compared to 3.4 K in the EC-Earth simulation). The frequency distributions of the cell properties lifetime, area, precipitation sum, and intensity are qualitatively similar to the EC-Earth simulation but differ quantitatively in a number of ways. While cell area is quite similar in both simulations, cells are longer living and more intense in MIROC5-CCLM. For estimating the changes in cell properties, again, we calculate the relative changes of different percentiles for future conditions compared to present conditions. As in ECE-CCLM, the relative changes are highest for the highest percentiles (Table 2). The relative changes of all cell properties are higher in MIROC5-CCLM than in ECE-CCLM for the high percentiles and about the same for the median (except for precipitation sum, which is 3,2% and thus lower in ECE-CCLM). This higher increase in extreme cells seems to be caused by the higher temperature change signal, as can be seen from the trend scaling. Trend scaling of P99 is very similar in ECE-CCLM and MIROC5-CCLM. The scaling rates do not differ more than 1.5% between the two simulations. The largest difference in scaling rates occurs for maximum intensity which is higher in the MIROC5 simulation. As in ECE-CCLM, the scaling rates for maximum area and precipitation sum are very close to the CC-rate. The simulation of the diurnal cycle is very similar in MIROC5-CCLM compared to ECE-CCLM showing a damped afternoon maximum of convective activity.

Table 2: Relative changes in cell characteristics (from Historical to RCP8.5) for the ECE domain.

Change in %	Lifetime	Maximum Area	Precipitation Sum	Mean Intensity	Maximum Intensity	Mean Speed
Mean	0,20	22,5	30,25	4,95	13,1	9,38
Median	-10,00	16,70	11,60	2,00	5,10	8,10
P75	0,00	18,20	18,70	5,30	12,20	10,80
P90	0,00	23,80	26,00	9,00	18,20	12,00
P99	4,50	40,60	44,70	15,70	31,60	11,90
Trend scaling of P99 (%/K)	1,0	7,60	8,20	3,2	6,1	2,50

5.3.2. Is the scaling behavior of Lagrangian cell properties similar in present and future conditions?

At first, the results of the ECE-CCLM simulation are described, followed by the description of the MIROC5-CCLM simulations. The temperature scaling curves of cell properties peak at higher values in the future (Figure 19). This is caused by more abundant humidity at these high temperatures, resembling the scaling curves of extreme hourly precipitation at fixed locations. In contrast to the temperature scaling, dew point scaling curves in historical and future conditions are consistent across the whole dew point temperature range.

The Clausius-Clapeyron scaling of cell area and maximum cell intensity in combination leads to super Clausius-Clapeyron scaling (ca. 14%/K) of the precipitation sum per cell.

The scaling curves under historical and future conditions are most similar for the highest percentiles. The differences for the lower percentiles reflect the complex changes in the properties of convective cells related to, e.g., the change in the diurnal cycle. The similar dew point scaling curves for the highest percentiles of cell properties facilitate inference of the upper limit of convective cell properties from large-scale humidity values.

The fact that the number of convective cells per dew point temperature bin changes both in absolute and relative terms (number of cells per occurrence of dew point temperature bin) prevents inference of extreme precipitation at fixed locations. This is also illustrated

by the differences in the dew point temperature scaling curves of extreme precipitation at fixed locations.

In contrast to the ECE-CCLM simulations, the scaling rates differ for present and future conditions in MIROC5-CCLM. Concerning the temperature scaling, the scaling rates are higher in future conditions for all cell properties over the whole temperature range Again, this is in contrast to the ECE-CCLM simulation where temperature-scaling is similar in the intermediate temperature range and the difference between present and future are higher peak values in the future. Concerning dew point scaling, the differences are not as large as for temperature scaling but still larger than in the ECE-CCLM simulation.

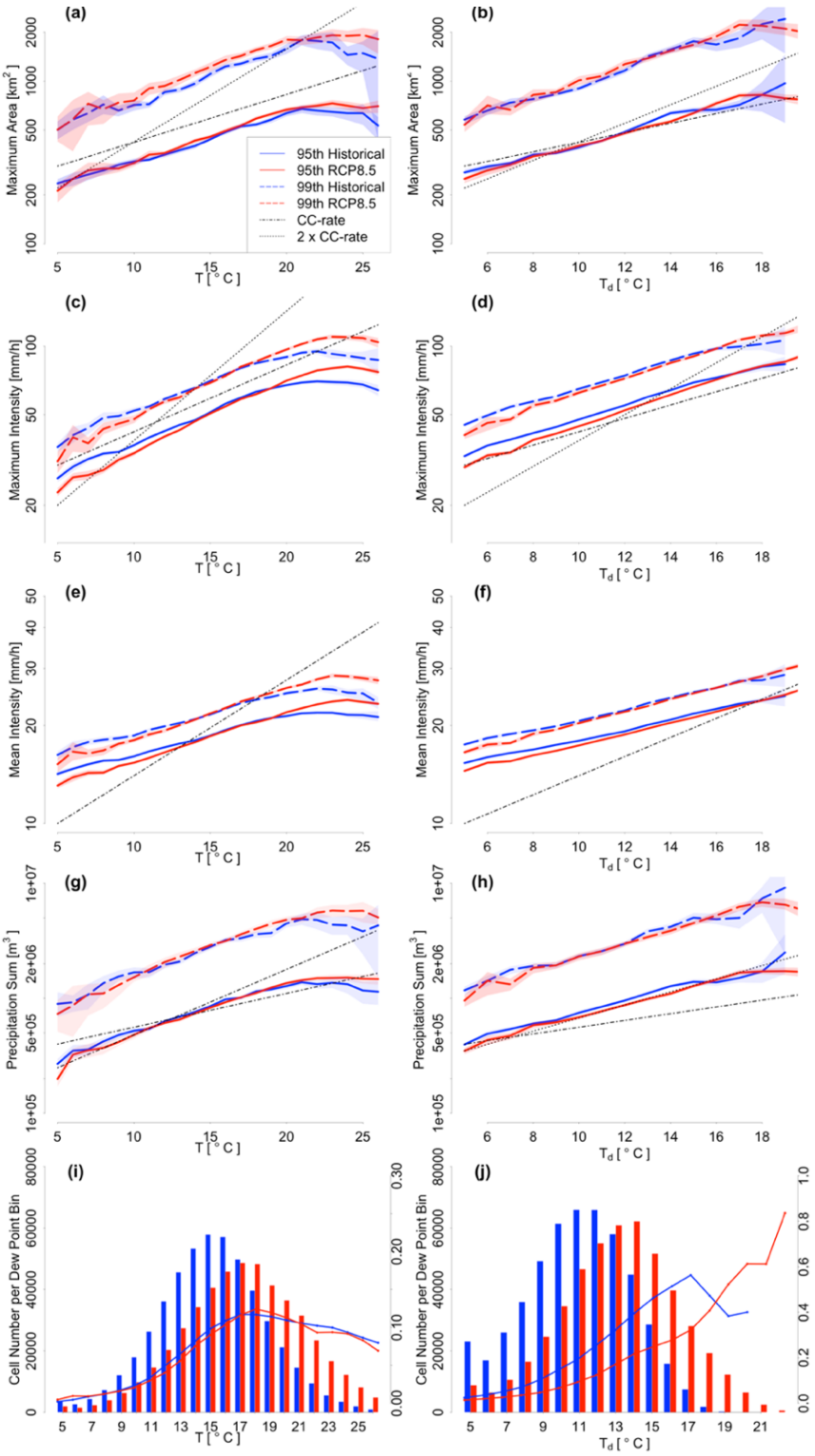

Figure 19: Temperature scaling (left column) and dew point temperature scaling (right column) of cell properties. (a) and (b): maximum area; (c) and (d): maximum intensity; (e) and (f): mean intensity; (g) and (h): precipitation sum. Shaded areas denote the uncertainty range caused by varying bin occupancy, obtained from bootstrapping cells in each bin. (i) and (j) show the frequency distribution of cells, where bars denote the absolute number of cells per temperature or dew point temperature class (left y-axis) and lines denote the relative number of cells per occurrence of temperature or dew point temperature class (right y-axis).

6. Conclusions

In this thesis, the properties of convective rain cells and their potential changes under global warming were investigated for Germany. Firstly, the influence of the environmental conditions CAPE, vertical wind shear, and dew point temperature on cell properties was investigated in the current climate using radar and reanalysis data.

It was shown that the cell area is strongly influenced by vertical wind shear, with higher wind shear leading to larger cells. In contrast, wind shear has very little influence on the maximum intensity of cells. Consequently, different Lagrangian cell properties scale with dew point temperature at varying rates. While the maximum intensity of cells scales with dew point temperature consistently at the CC-rate, the area of cells increases at varying rates, namely at the CC-rate below 12 °C and at 2x CC-rate above. The precipitation sum scales at above CC-rate at varying rates which increase with dew point temperature. Different processes are discussed in the literature as a cause for super Clausius-Clapeyron scaling of extreme precipitation, for example a positive feedback of updraft strength with moisture supply (Lenderink et al. 2017) or increased convective organization at higher temperatures (Lochbihler et al. 2019). As CAPE is correlated with dew point temperature, we conclude that besides these processes, the super-CC scaling is at least partially caused by more unstable stratification of the pre-storm environment at high dew point temperatures. Precipitation scaling at fixed locations is lower than the Lagrangian scaling rate of the total precipitation sum per cell due to the compensating effect of higher cell speed at high wind shear. This means that the increase in cell speed with increasing wind shear overcompensates the increase in cell area caused by increased convective organization. Another finding that illustrates this point is that intense precipitation events at fixed locations are caused by cells that, in the mean, move slower than all cells. The fact that *binning scaling* rates are modulated by vertical wind shear and CAPE makes it unlikely that present scaling rates for fixed locations can be transferred into the future as both variables are projected to change under global warming.

Potential changes of convective rain cell properties in the future were investigated using the convection-permitting climate model COSMO-CLM. To assess if the model is capable of representing climate statistics of convective cell properties, it was first evaluated by comparing Lagrangian cell properties to the observed cell properties discussed above.

The model is capable of reproducing the total amount of convective precipitation, as well as the frequency and properties of convective cells ranging from short-living, small cells

to long-living, intense cells. However, the number of convective cells is underestimated. This underestimation is compensated by an overestimation of cell lifetime. A possible explanation for the underestimation of convective activity and the overestimation of cell lifetime could be that the grid size of 2.8 km is too coarse to capture boundary layer inhomogeneities, which facilitate the initiation of convection; thus, the number of cells is reduced. The underestimation of mean intensity and maximum intensity of large, long-living cells suggests model deficiencies in representing large, organized forms of convection. This underestimation is reduced when using the ERA5 reanalysis instead of ERA-Interim as driving data. To evaluate the model's capability of representing the properties of extreme convective cells at different temperatures, we investigate the temperature scaling of cell properties. While the model can reproduce the increases in mean intensity and area of extreme convective cells with temperature, it fails to reproduce the increasing cell lifetime seen in observations. The simulated scaling of total precipitation shows a continuous increase above the Clausius–Clapeyron rate, which indicates dynamical changes in extreme convective cells with increasing temperature. The observations show different scaling rates with a value close to the Clausius–Clapeyron rate at temperatures below 15 °C and higher values above. More detailed investigations are needed to understand these differences. These results suggest that the evaluation of coarse-grained (e.g., hourly) precipitation fields is insufficient for revealing challenges in convection-permitting simulations.

Potential changes in the properties of convective cells were investigated for the end of the 21st century under the high emission scenario RCP8.5. Changes in the frequency distribution of cell properties show a complex picture of the response of deep convection to climate warming. While the total number of cells and the lifetime do not change in the future according to the projections, there is a shift towards larger and more intense events. In combination, this leads to higher precipitation sums per cell. The relative increase of mean and maximum cell intensity, cell area, and precipitation sum is largest for the highest percentiles meaning that the most extreme events intensify the most. The *trend scaling* rates for the 99th percentile are within 1.5 % in the two investigated simulations. This indicates that it may be possible to infer the upper limit of cell properties from the mean temperature change signal to a certain degree. However, two simulations are too few to estimate a robust range for the scaling rates.

The diurnal cycle of convective activity changes towards fewer convective cells during the afternoon maximum and more cells during the nighttime. Combined with the increase

in mean precipitation intensity per cell, this leads to up to 50% more convective precipitation during nighttime and a small decrease during the afternoon maximum. The afternoon decrease in cell number is primarily caused by fewer slow-moving cells despite the fact that there is no change in the large-scale wind speed. In combination with an increase in CIN this points to less air-mass convection in the future projections meaning that it becomes more difficult to initiate convective storms without a dynamical trigger mechanism. However, once convection is initiated, the increase in CAPE and near-surface humidity leads to more intense cells, which, in turn, can produce stronger cold pools and thus trigger new cells, which could explain the shift towards later times of day. These findings are in line with results from the USA, where a shift towards more extreme and less moderate events because of increased CAPE and CIN values is reported (Rasmussen et al. 2020). This process could mitigate the increase of intense precipitation at fixed locations because intense hourly precipitation is often caused by slow-moving cells, as previously described.

The temperature *binning scaling* curves of cell properties peak at higher values in the future, resembling the scaling curves of extreme hourly precipitation at fixed locations. In contrast to the temperature scaling, dew point scaling curves in historical and future conditions are consistent across the whole dew point temperature range. The Clausius-Clapeyron scaling of cell area and maximum cell intensity leads to super Clausius-Clapeyron scaling (ca. 14 %/K) of the precipitation sum per cell. Similar to the reanalysis data investigated in the first part of the thesis, there is a correlation of dew point temperature with CAPE, which can partially explain scaling above the Clausius-Clapeyron rate.

The scaling curves under historical and future conditions are similar for the highest percentiles in the simulation driven by EC-Earth. The differences for the lower percentiles reflect the complex changes in the properties of convective cells related to, e.g., the change in diurnal cycle. The similar dew point scaling curves for the highest percentiles of cell properties facilitate inference of the upper limit of convective cell properties from large-scale humidity values. However, the fact that the number of convective cells per dew point temperature bin changes both in absolute and relative terms (number of cells per occurrence of dew point temperature bin) prevents inference of extreme precipitation at fixed locations. In contrast to these findings, the scaling curves for the highest percentiles are different between present and future in the MIROC5 simulation. Further studies are necessary to understand the reasons for these discrepancies. Future research could build on the evaluation of Lagrangian cell properties to develop a BIAS correction meth-

od based on cell properties with the aim of assessing the hydrological consequences of the projected increase in heavy precipitation events. Concerning future changes of convective precipitation, more projections are necessary to determine the uncertainty related to large-scale changes in the general circulation as general circulation models vary in their representation of climate change in mid-latitudes.

Appendices

A. Paper 1: Convective Rain Cell Properties and the Resulting Precipitation Scaling in a Warm Temperate Climate

Submitted as:
Purr, Christopher; Erwan Brisson; K. Heinke Schlünzen; and Bodo Ahrens. 2021. " Convective rain cell properties and the resulting precipitation scaling in a warm temperate climate" to *Quarterly Journal of the Royal Meteorological Society.*

Abstract

Convective precipitation events have been shown to intensify at rates exceeding the Clausius-Clapeyron rate (CC-rate) of ca. 7 %/K under current climate conditions. In this study, we relate atmospheric variables (low-level dew point temperature, convective available potential energy, and vertical wind shear), which are regarded as ingredients for severe deep convection, to properties of convective rain cells (cell area, maximum precipitation intensity, lifetime, precipitation sum, and cell speed). The rain cell properties are obtained from a rain gauge-adjusted radar data set in a mid-latitude region, which is characterized by a temperate climate with warm summers (Germany). Different Lagrangian cell properties scale with dew point temperature at varying rates. While the maximum precipitation intensity of cells scales consistently at the CC-rate, the area and precipitation sum per cell scale at varying rates above the CC-rate. We show that this super-CC scaling is caused by a covarying increase of convective available potential energy with dew point temperature. Wind shear increases the precipitation sum per cell mainly by increasing the spatial cell extent. From a Eulerian point-of-view, this increase is partly compensated by a higher cell velocity, which leads to Eulerian precipitation scaling rates close to and slightly above the CC-rate. Thus, Eulerian scaling rates of convective precipitation are modulated by convective available potential energy and vertical wind shear making it unlikely that present scaling rates can be applied to future climate conditions. Furthermore, we show that cells

that cause heavy precipitation at fixed locations occur at low vertical wind shear and, thus, move relatively slow compared to typical cells.

A.1 Introduction

Convective precipitation is expected to intensify with global warming (Trenberth et al. 2003). This intensification is also projected for warm temperate climates in mid-latitudes (Purr et al. 2021). However, the rate of increase and the role of thermodynamic and dynamic processes remain uncertain. The water holding capacity of the atmosphere, governed by the Clausius-Clapeyron (CC) equation, is frequently used as a baseline estimate on how much extreme precipitation will change with global warming (Westra et al. 2014). Two different approaches have been used to estimate the increase in extreme precipitation with temperature: *trend scaling* and *binning scaling*, sometimes also referred to as *apparent scaling* (Zhang et al. 2017). While *trend scaling* describes the ratio of precipitation extremes in different climate states scaled by the mean temperature change, *binning scaling* calculates the dependence of extreme precipitation on day-to-day temperature variability in the current climate period. *Binning scaling* has been frequently used in recent years due to a lack of long-term observations of sub-daily precipitation. *Binning scaling* rates above the CC rate of 7%/K have been reported for convective precipitation extremes on sub-daily timescales in warm temperate climate in a number of studies (e.g. Lenderink & van Meijgaard 2008, Berg et al. 2013). Different explanations have been given for this super-CC scaling. Firstly, it has been attributed to a positive feedback mechanism between moisture supply at cloud base and updraft speed in convective clouds (Lenderink et al. 2017). Secondly, the increasing degree of convective organization at higher temperatures has been suggested to cause more intense precipitation (Moseley et al. 2016). This hypothesis has been established from idealized LES simulations which show that the precipitation field is organized into fewer but more intense precipitation cells at higher temperatures (Lochbihler et al. 2019). Additionally, the statistical effect that at high temperatures extreme precipitation is increasingly caused by convection was shown by Berg et al. (2013). The temperature scaling of both hourly extreme precipitation at fixed location (Prein et al. 2017) and of Lagrangian cell properties (Purr et al. 2019) has been shown to drop-off at high temperature due to moisture limitation. Because of these varying scaling rates, dew point temperature has been suggested and widely adopted as a more meaningful covariate (Lenderink et al. 2011). It has been questioned whether binning scaling rates

can be extrapolated to the future as other environmental conditions which influence convective storms besides low-level moisture might change, too (Bao et al. 2017, Sun et al 2020). These environmental conditions, which determine the strength of a convective cell to a large degree, are vertical instability, and vertical wind shear (see e.g. Weisman and Klemp (1982) or Rasmussen and Blanchard (1998)).Vertical instability is often measured by convective available potential energy (CAPE). Although CAPE is useful for predicting the strength of convection it is mainly related to maximum vertical velocity in the updraft (Markowski and Richardson 2010, p. 43) and only indirectly to precipitation intensity. Precipitation intensity can be influenced by various additional processes, like entrainment rates and evaporation below cloud base. Precipitation efficiency, the ratio of total precipitation of a convective cloud to the moisture inflow at cloud base, has been shown to be strongly influenced by vertical wind shear (Weisman & Klemp 1982, Market & Allen 2003, Chen et al. 2015). In general, vertical wind shear influences the degree of organization of convective storms via various processes. Firstly, it increases the organization of convective storms by separating the updraft from the downdraft (and precipitation) region. Furthermore, it can facilitate the development of super cells by tilting horizontal vortices into the vertical and thus creating a rotating updraft. The spectrum of convective storms ranges from unorganized single convective cells at low wind shear via multi-cells, which are characterized by the repeated development of new cells in the vicinity of old ones, at intermediate wind shear to supercells and mesoscale convective systems at high wind shear (Houze 2014).

Besides increasing the severity of convective storms (Kaltenboeck & Steinheimer, 2014), high wind shear also increases the horizontal velocity of convective storms. Storm velocity increases because convective storms move approximately with the mean tropospheric wind and the commonly used bulk wind shear is largely determined by the wind in the 500 hPa level. In general, long-living cells are larger, more intense (Purr et al. 2019) and move faster. Because the high speed balances the higher precipitation intensity to some extent, it is not a priori clear to what extent intense fast-moving cells or less intense slow-moving cells cause heavy precipitation at fixed locations.

Due to their small spatial and temporal scale, convective storms are notoriously difficult to observe. When investigating extreme precipitation many observational studies rely on gauge data, although it has been shown that gauge data sets are only representative for spatial scales of up to 11 km for hourly accumulation periods (Bohnenstengel et al. 2011) and miss about 80% of hourly extreme precipitation events in Germany (Lengfeld et al.

2020) due to sparse sampling in space. Nonetheless, some interesting relations were found: for example, Lepore et al. (2016) investigated conditions leading to hourly precipitation extremes in the contiguous United States and found CAPE and dew point temperature to be the best predictors for precipitation intensity.

The shortcomings of in-situ measurements can be remedied by remote sensing techniques to an ever increasing degree. Remote sensing data used for investigating convective storms include lightning data (Wapler 2013, Brisson et al. 2021) and weather radars (e.g. Moseley et al. 2013, Lochbihler et al. 2017). Kunz et al. (2020) combined radar data with storm reports and reanalysis data to investigate hailstorms in Central Europe. They found that vertical wind shear provides a good predictor for the size of hail stones as frontal storms associated with high wind shear tend to form larger hail stones. The progress of weather radars has made it possible to track convective storms in data sets that currently cover time periods of up to two decades (e.g. Peleg et al. 2018). While many studies track convective cells based on radar reflectivity, few radar data sets offer reliable estimates of ground-level precipitation. For this reason, Lagrangian properties of convective rain events have seldomly been quantitatively connected to precipitation at fixed locations. As an example for this kind of study, Schumacher & Johnson (2005) showed that about 2/3 of daily extreme precipitation is caused by Mesoscale Convective Systems and investigated the MCS's properties.

The influence of the environmental conditions described above on storm properties has not yet been studied in observational data on decadal time scales to the authors' knowledge. Therefore, we attempt to establish a link between the influence of environmental conditions on storm properties focusing on the effect of wind shear on storm velocity and the resulting precipitation at fixed locations in this study. Besides process understanding, investigating the effect of large-scale environmental conditions on cell properties is beneficial in the context of model evaluation and climate change. Firstly, the results obtained here can be used for evaluating convective clouds in convection-permitting weather and climate models. While Purr et al. (2019) already evaluated the frequency distribution and temperature scaling of convective cells in a regional climate model, a more thorough evaluation linking cell properties to environmental conditions would be advantageous. Additionally, convection parameterizations could be tested, especially with respect to the influence of wind shear on mesoscale organization (Rio et al. 2019, Yano & Moncrieff 2016). In the context of climate change, linking convective cell properties to environmental conditions could be used to develop a statistical model, which allows de-

riving convective cell properties for future conditions from environmental variables provided by hydrostatic RCMs. Currently, these RCMs are used to investigate frequency changes in severe convection environments, which are usually defined as environments with certain amounts of instability and wind shear without knowing how convective cells will react to the changes (Púčik et al. 2017). Therefore, we aim at answering the following questions:

1. What is the effect of instability and wind shear on Lagrangian cell properties and the dew point temperature scaling of these properties?
2. To what extent does higher cell velocity offset the higher organization of convective cells in high-shear environments with respect to precipitation at fixed location?

We use a novel, gauge-adjusted radar climatology, which provides continuous precipitation data in time and space. Properties of convective storms causing extreme sub-daily precipitation are investigated by tracking convective cells in 5-min radar data (Section A.2.1 and A.3.1). To estimate the influence of wind shear, instability, and low-level moisture we connect the cell properties to the corresponding large-scale atmospheric conditions using ERA5 reanalysis data (Section A.2.2). Reanalysis data is used instead of sounding data because of their high temporal and spatial frequency. While soundings are often taken only 2 or 4 times a day and hundreds of kilometers away from a convective storm, the ERA5 reanalysis provides hourly values at 0.25° resolution. For the United States, Lepore et al. (2015) found that rainfall intensity is better correlated with CAPE from reanalysis than with CAPE computed from atmospheric soundings. The results are presented in Chapter A.4 for univariate and multivariate dependence of Lagrangian cell properties on environmental variables (Section A.4.1, A.4.2), and thus question 1 is addressed. The relation of cell properties to precipitation at fixed locations, which adresses question 2, is provided in Section A.4.3.

A.2 Data

A.2.1 Radar climatology

We use the radar-based precipitation climatology (Winterrath et al. 2017) developed by the national meteorological service of Germany, Deutscher Wetterdienst, for tracking convective cells. This precipitation data set is based on radar data, which has been quality

checked, corrected, and adjusted to rain gauge measurements. The correction steps used for this product to derive precipitation from radar reflectivity include clutter filtering, distance dependent signal correction and removal of radar spokes. For the tracking we use the 5-min dataset, the so called YW-product (Winterrath et al. 2018a). For the comparison to stationary hourly precipitation intensities, we use the hourly dataset, the so called RW-product (Winterrath et al. 2018b). Our analysis covers the summer half years (Apr-Sep) of the period 2001-2016. Focusing in the summer half year is sufficient as convective rain events occur almost exclusively in this time (Lengfeld et al. 2021). The data sets have a spatial resolution of 1 km x 1 km.

A.2.2 Environmental variables

We use ERA5, the 5th generation global reanalysis by ECMWF (Hersbach et al. 2020), to derive environmental conditions of convective storms. The variables used to characterize convective storm conditions are dew point temperature at 2 m (T_d), convective available potential energy (*CAPE*), and bulk vertical wind shear (*SH*) calculated as vector difference between the wind in 500 hPa height and 10 m. ERA5 provides hourly values of atmospheric variables at a spatial resolution of 0.25° x 0.25°. Convective parameters calculated from ERA5 data have been compared with sounding data and the MERRA-2 (Modern-Era Retrospective Analysis for Research and Applications version 2, Gelaro et al. 2017) reanalysis by Taszarek et al. (2020). ERA5 performs better than MERRA-2 for all variables but underestimates both mean and extreme values of CAPE and wind shear compared to rawinsoundings.

An important consideration when relating cell properties to environmental conditions from reanalysis is the spatial and temporal representativity of the reanalysis data. Precipitation scaling has been shown to depend on the timing of the temperature recording relative to the storm occurrence (Lenderink et al. 2011). Downdrafts and evaporative cooling of rain associated with convective storms lead to a decrease in surface temperature. Visser et al. (2021) found that using sub-daily atmospheric conditions before the start of the storm for determining scaling rates results in increased consistency of the scaling rates. However, since we use a reanalysis that parameterizes convection it cannot be expected that the diurnal cycle of convective precipitation is perfectly represented. The convection parameterization might trigger precipitation prematurely which leads to depleted CAPE and decreased dew point temperature, and thus the environmental conditions before storm

onset do not necessarily represent the determining conditions for storm development. For these reasons, we relate convective environmental conditions at two different times to cell properties. By default, we assign each cell to the 3-hourly values of CAPE, *SH,* and T_d before storm onset at its onset location. Additionally, we test the influence of sub-daily variability by using daily mean values.

A.3 Methods

A.3.1 Convective cell tracking

Because of its high temporal and spatial resolution, the radar data allows for a quasi-continuous monitoring of convective cells. We use a tracking algorithm to derive convective cell properties from the radar data. The algorithm is described in detail in Purr et al. (2019). In summary, convective cells are tracked in three major steps:

1. Contiguous precipitation areas with precipitation intensity above a threshold of 8.5 mm/h (within 5 minutes), are identified in the current and the subsequent time step as potential convective objects. The minimum cell area is set to four grid points.
2. Wind information from the ERA5 reanalysis is used to predict the position of the cell at the subsequent time step. To this end, a "cone of detection" is set up for each pixel of every cell in the current time step. If a new cell is present in the cone, a probability value is assigned to the origin pixel of the cone, which links this pixel to the new cell.
3. The probability values of all pixels are summed up for each cell. If a single cell is present in the cone, the corresponding objects from the current and the subsequent time step are connected. If multiple cells are present, the current cell is associated with the cell with the highest probability in the subsequent time step.

Cells must have a lifetime of at least three time steps, equal to 15 min, to be considered for analysis. This condition ensures that potential radar artifacts are not considered in the analysis. Cell mergers and splits are dealt with as follows: If two cells merge, the cell track with the higher probability of cell association is continued. The other track is regarded as an individual track in itself. The same applies to cells that split. The properties that are obtained by the algorithm for each cell are: (1) lifetime ; (2) mean intensity, i.e., the temporal and spatial mean over the entire lifetime; (3) maximum intensity, i.e., the

highest grid-point intensity during the entire lifetime; (4) maximum area, defined as the maximum instantaneous area over the entire lifetime; (5) precipitation sum, i.e., the total spatial and temporal precipitation sum over the entire lifetime; and (6) mean speed, defined as the temporal mean speed of the cells' center of mass. The center of mass is defined as average position of all cell pixels, weighted according to their precipitation intensity. Figure A1 provides an example of detected cells and a selected cell track (red line).

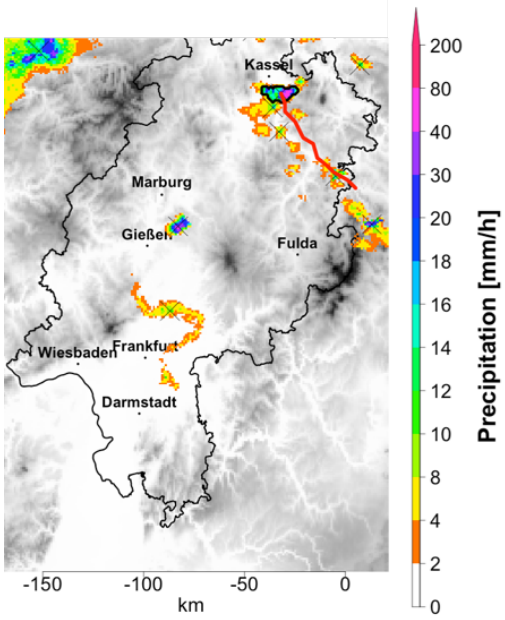

Figure A1: Radar snapshot of a convective cell. Shown is the 5-min precipitation intensity on 30 May 2008 at 21:50 (UTC) in colors and an exemplary detected cell track as a red line. The track starts with cell detection at 21:00 (UTC) and is shown up to the time of the snapshot.

A.3.2 Calculation of scaling rates

To investigate the influence of environmental conditions on cell properties, cells are grouped into 23 bins of dew point temperature, CAPE, or wind shear. The bin width varies in such a way that there is an approximately equal number of cells in each bin. As there are a total of ca. 1,350,000 cells in the area and period of investigation, there are about 60,000 cells in each bin.

The scaling rates s_p as function of dew point temperature T_d are computed for the highest percentiles p (90^{th}, 95^{th}, 99^{th}, and 99.9^{th}) of all cell properties as the average fractional change of the respective quantity (e.g., precipitation sum, maximum intensity, etc.) Q from bin i to i+1 as:

$$\bar{s_p} = \frac{\sum_{i=1}^{23} s_{p,i}}{23} = ln\frac{Q_{p,i+1}}{Q_{p,i}} / (T_{d\,i+1} - T_{d\,i})$$

$T_{d\,i}$ denotes dew point temperature of the respective bin i.

A.4 Results

A.4.1 Univariate dependence of cell properties on environmental variables

The environmental variables influence the investigated cell properties, maximum intensity, maximum area, and precipitation sum by varying degrees. In general, an increase in CAPE or dew point temperature increases the severity of convective cells as expected. Foremost, maximum intensity (Figure A2a and Figure A2b) and area (Figure A2d and Figure A2e) increase with these variables. To a lesser extent, lifetime of convective cells increases, too (Figure A2g and Figure A2h). The 75th (99th) percentile of lifetime increases from 30 min (95 min) for CAPE values between 0 and 0.75 J/kg to 40 min (140 min) for CAPE values above 1284 J/kg. The maximum area of cells is relatively constant for low CAPE values up to ~200 J/kg and increases for higher values. In contrast, it increases more uniformly with dew point temperature.

The maximum intensity increases approximately linearly with CAPE and exponentially with dew point temperature (note the varying bin widths in Figure A2a and A2b). Wind shear exerts a strong control on cell area (Figure A2f). While the 99th percentile of cell area is 85 km^2 for the wind shear class 0-2 m/s, it is 160 km^2 for wind shear above 25 m/s. Interestingly, the maximum cell intensity decreases with wind shear (Figure A2c). As a result, the total precipitation sum per cell increases strongly with increasing CAPE and dew point temperature but only slightly with increasing wind shear (Figure A2j-l). The overall increase in maximum intensity and precipitation sum with CAPE is non-monotonic for very low CAPE values with decreasing values from 0 J/kg to 10 J/kg. This decrease is smaller when using daily mean CAPE values. For example, the 99th percentile of maximum intensity decreases from 113 mm/h for CAPE values between 0 J/kg and 0.8 J/kg to 95 mm/h for values between 10 J/kg and 15.5 J/kg when using CAPE values before storm onset whereas it increases from 85 mm/h to 87 mm/h when using daily mean CAPE values. The mean cell speed is constant across the dew point range, decreases slightly with increasing CAPE values, and increases with wind shear (not shown). However, an increase in wind shear leads to a smaller increase in cell speed. While the median

cell speed is 7.0 m/s in the 0 m/s wind shear bin it increases to 14 m/s for 27.5 m/s wind shear.

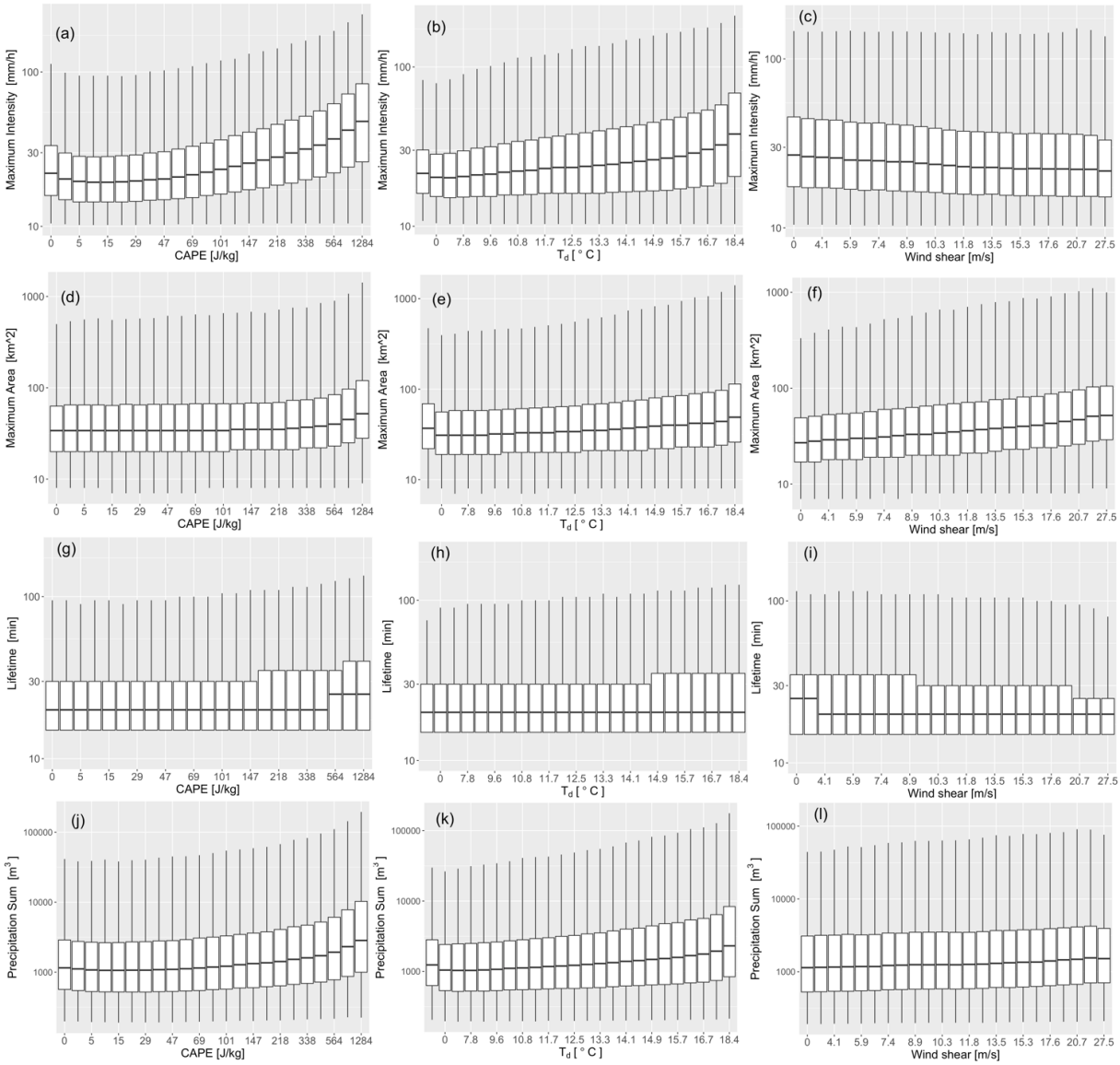

Figure A2: Dependence of cell properties on environmental variables. Cells are grouped into bins as explained in section A3.2. The lower and upper hinges denote the 25th, and 75th percentiles, respectively. The lower and upper whiskers denote the 5th and 99th percentiles, respectively. Note the logarithmic y-axis.

Maximum intensity scales consistently over the dew point range at the CC-rate, except for very high T_d suggesting that maximum intensity is mainly constrained by moisture availability (Figure A3a). The scaling rates range from 7.7 %/K for s_{99} to 8.0 %/K for s_{95}. In contrast, cell area scales at different rates below and above a threshold of ~12 °C. The scaling rates are below the CC-rate below this threshold and at about the 2*CC-rate above this threshold (Figure A3b). Furthermore, the scaling rates of the different percentiles are

more variable than for maximum intensity with values from 8.4%/K for s_{90} to 11.4%/K for $s_{99.9}$. These varying rates suggest that area is not controlled by dew point temperature alone and that the scaling rates are influenced by other variables like vertical wind shear. Like cell area, the total precipitation sum also shows an increase in scaling rates with dew point temperature (Figure A3c). However, there is no distinct shift but a gradual increase of scaling rates from about the CC-rate at low dew point temperatures to more than 2*CC-rate at high dew point temperatures. Using daily mean T_d instead of the value before storm onset does not change the shape of the scaling curves and influences the scaling rates only slightly. The scaling rates for maximum intensity increase to a range of 8.1%/K (s_{99}) to 8.5%/K ($s_{99.9}$). The scaling rates for cell area and precipitation sum per cell using daily mean T_d are similar to the scaling rates using environmental conditions before storm onset.

Concerning the possible uncertainty estimation of scaling rates, the data set does not provide error ranges. However, the data set was evaluated against gauge data by Kreklow et al. (2020) who found an underestimation of high intensity precipitation. As the highest precipitation intensities occur predominantly at high dew point temperatures, this underestimation implies that the radar-based scaling rates can be seen as the lower bound of the real scaling rates.

It has been shown that the occurrence of moderate hourly precipitation (>15mm/h) is clearly coupled to orography, whereas extreme precipitation (>40 mm/h) is independent from orography (Lengfeld et al. 2019). For this reason we separately investigated low-land and mountainous regions, defined as areas below or above 400 m elevation, to determine any differences in the scaling depending on region. However, no difference in scaling between low-lands and mountainous regions was found.

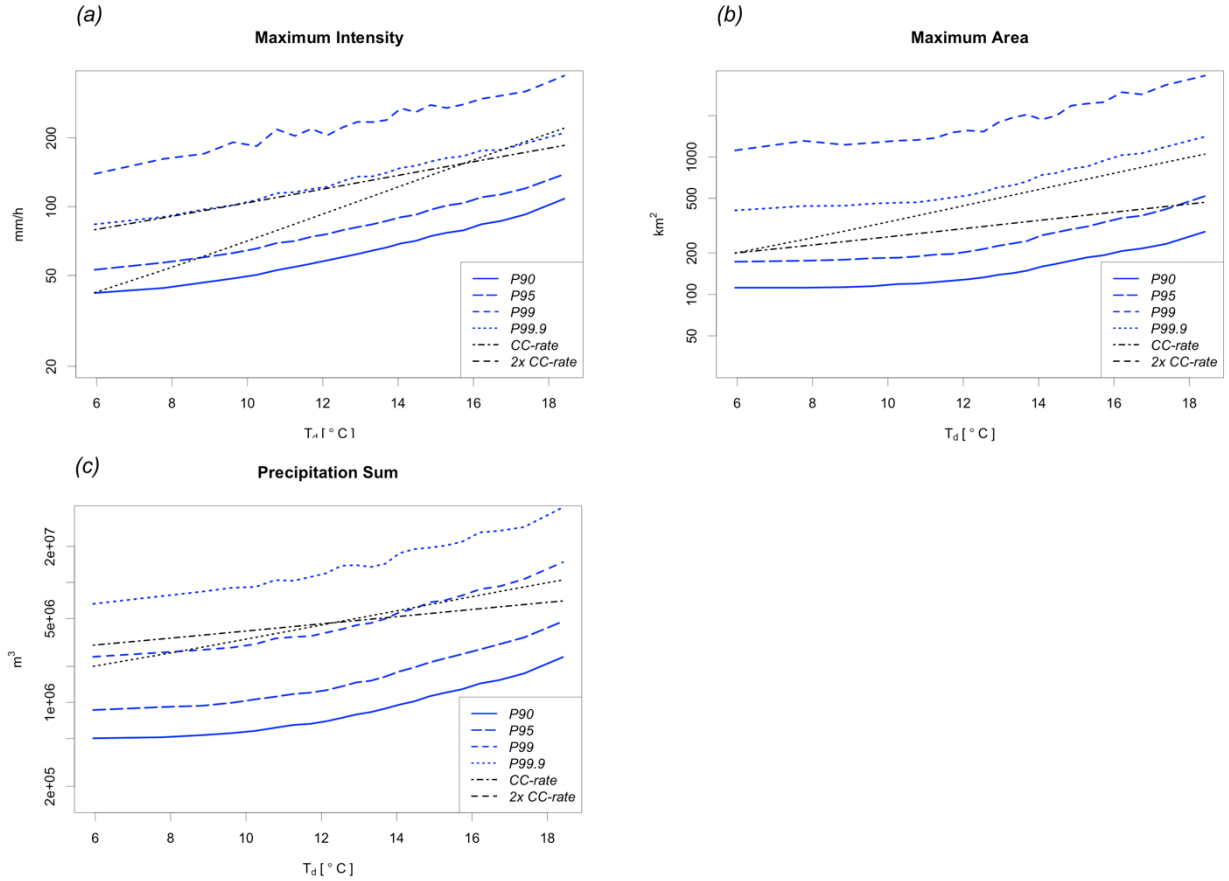

Figure A3: Dew point scaling of the cell properties (a) maximum intensity, (b) maximum area, and (c) precipitation sum (in blue). For orientation, the scaling CC- and 2xCC-rates are given (black). Note the logarithmic y-axis.

A.4.2 Multivariate dependence of cell properties on environmental variables

We investigate cell properties and frequency of cells depending on combinations of environmental variables. In *CAPE-SH* space, the convective cells occur mainly at low CAPE, high shear values (*SH*) or high CAPE, low shear values (Figure A4a). While for low CAPE convection seems implausible at first sight, low CAPE, high shear convection is frequently observed in the US (see e.g. Sherburn et al. 2016). Besides, it cannot be completely ruled out that strong stratiform precipitation cells are detected by the tracking algorithm.

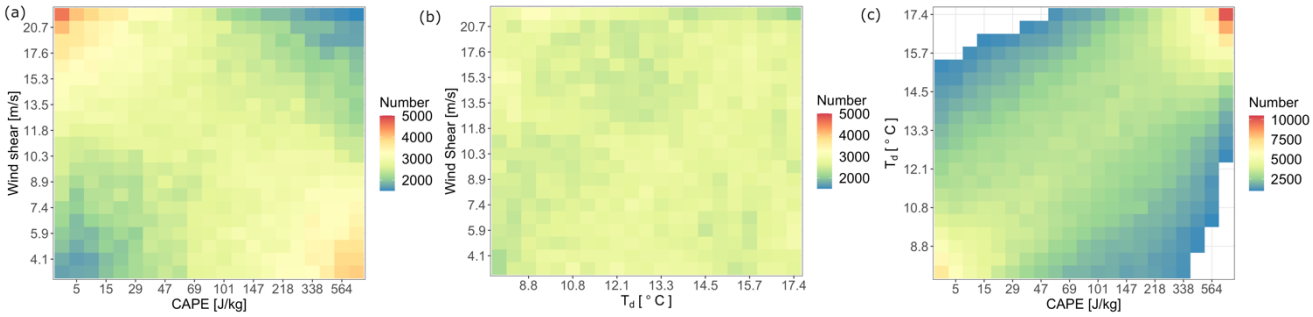

Figure A4: (a-c) Occurrence of cells depending on values of the environmental variables CAPE, dew point temperature Td, and wind shear SH. Note the different colour bar in subfigure (c).

In T_d-*SH*-space (Figure A4b), the cell numbers are approximately homogeneously distributed. However, there seems to be a slightly increased number of cells occurring at low T_d and high shear values, which are separated from cells occurring at higher T_d values. These cells could be related to fronts, which are characterized by high wind shear and may occur at low T_d values. In CAPE- T_d -space, the highest number of cells occurs at very high CAPE and T_d values. Furthermore, cells are concentrated along a corridor of increasing CAPE and T_d values (Figure A4c). The reason for this is that CAPE increases with T_d. We find an increase of the highest percentiles of daily maximum CAPE with daily T_d for all days of the investigation period 2001-2016 at varying rates well above the CC-rate in the ERA5 reanalysis (Figure A5). The 95th percentile increases at rates around 4x CC-rate while the 99.9th percentile increases at around 3x CC-rate for dew point temperatures above 7 °C. These values are well above the CC-increase found in a simplified model which simulates peak CAPE under varying boundary-layer moisture in a continental environment (Agard and Emanuel 2017).

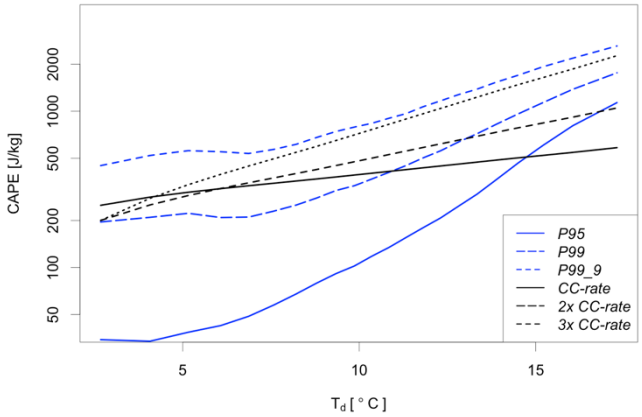

Figure A5: Increase of daily maximum CAPE with dew point temperature.

The most extreme cells, in terms of maximum intensity, area and precipitation sum, occur at high *CAPE*, T_d, and *SH* values (Figure A6). Low-CAPE, high-shear cells are not among the most extreme cells but have the lowest maximum intensity (Figure A6d). Again, wind shear is correlated predominantly with the area of cells (Figure A6a and Figure A6c) and has little influence on the maximum intensity of cells (Figure A6d and Figure A6e).

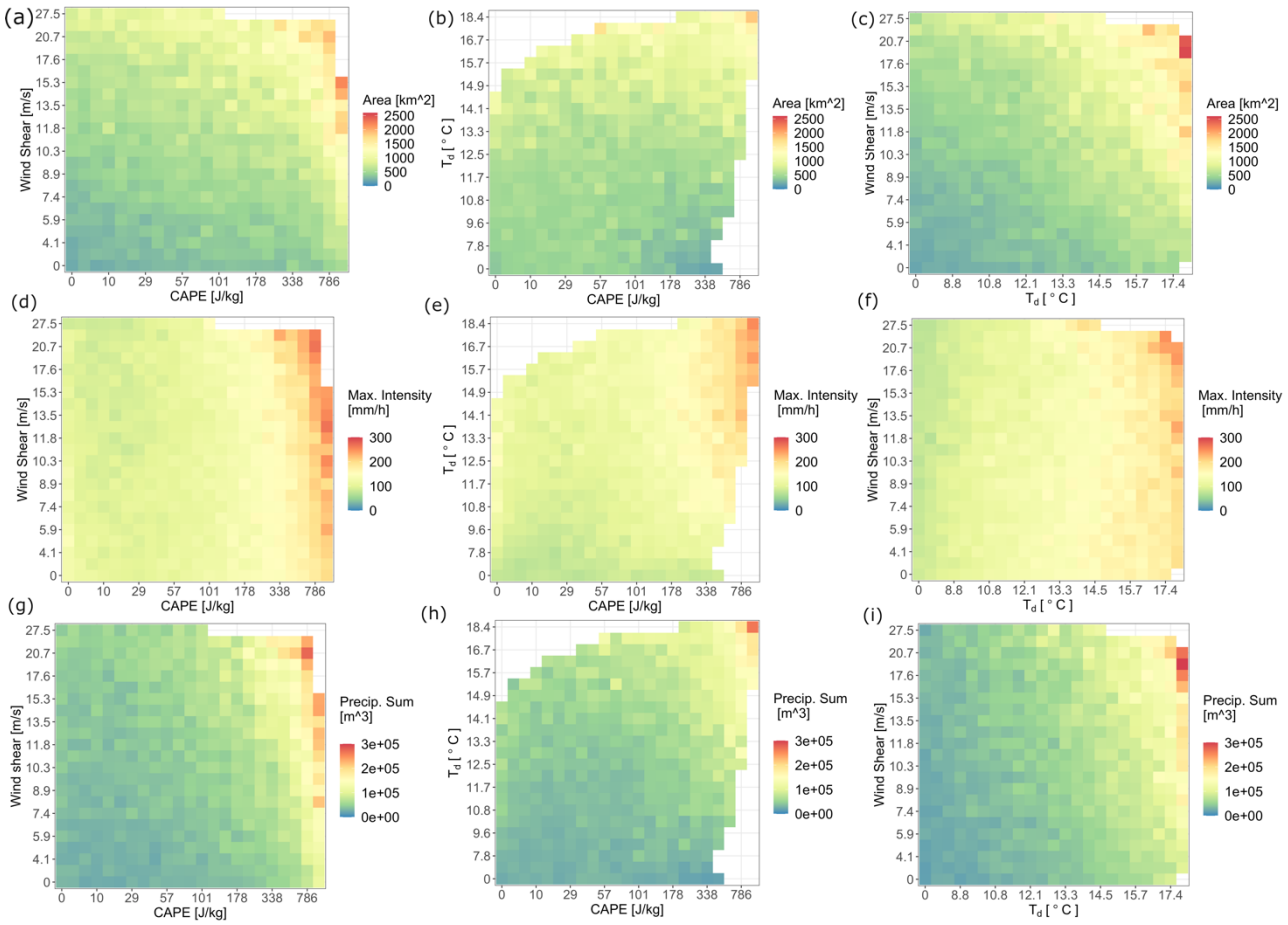

Figure A6: 99th percentile of cell properties depending on environmental variables CAPE, dew point temperature Td, and wind shear SH.

The influence of CAPE and wind shear on dew point scaling is investigated by classifying convective cells according to their environmental CAPE and wind shear values. Cells are classified as “Low CAPE” cells if they occur in conditions below the median value of 87.5 J/kg or as “High CAPE” cells if they occur at a higher value. Similarly, cells are classified as “Low Wind Shear” cells if they occur in conditions below the median value of 11.2 m/s or as “High Wind Shear” cells if they occur at a higher value. Classifying the cells according to environmental CAPE shows the effects of the general increase of CAPE with dew point: cells which occur at low dew point temperatures, occur predomi-

nantly at low CAPE values. Thus, the scaling curves of all cells shift gradually from the "Low CAPE" curve at low dew point temperatures to the "High CAPE" curve at high dew point temperatures (Figure A7a,c,e). The effect is smallest for the maximum area (Figure A7a), where it is only present for low dew point temperatures up to 12 °C, and larger for maximum intensity (Figure A7c) and precipitation (Figure A7e).

Concerning the influence of wind shear, the scaling curves of the 99th percentile are at higher values for the maximum area (Figure A7b) and the precipitation sum (Figure A7f) for "High Wind Shear", whereas there is little influence on maximum intensity (Figure A7d) which is in line with the findings in the previous section. In contrast to CAPE, the scaling rates do not differ between cells occurring at high or low wind shear conditions and all the cells.

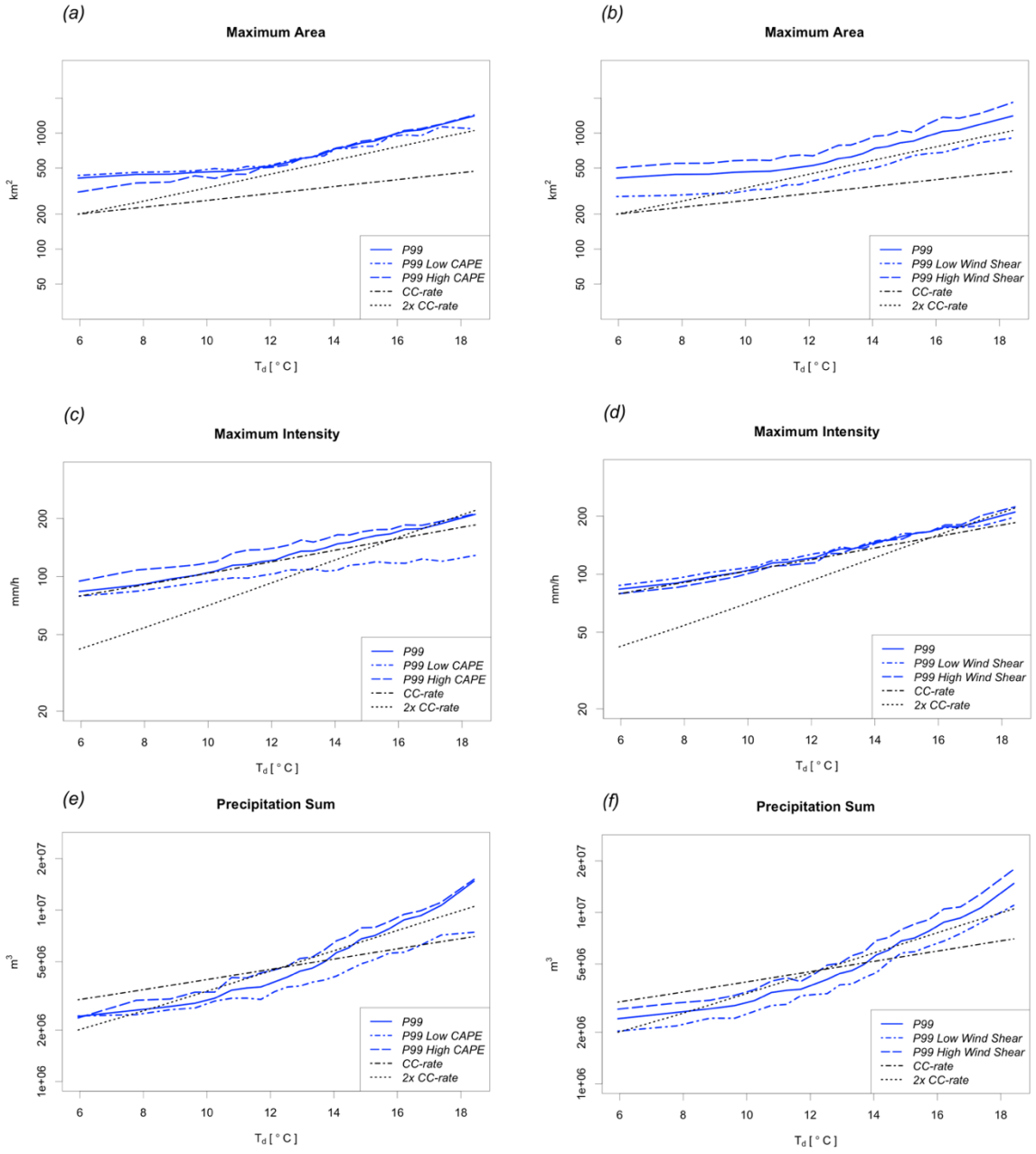

Figure A7: Dew point scaling of the cell properties maximum area, maximum intensity, and precipitation sum (in blue) depending on CAPE (left column), and wind shear (right column). For orientation, the scaling CC- and 2x CC-rates are given (black). Note the logarithmic y-axis.

A.4.3 Relation of cell properties to precipitation at fixed location

We now investigate the relationship between Lagrangian cell properties and their potential to cause extreme precipitation for fixed locations. We use two methods to describe this relationship: (1) calculation of fixed location precipitation potential using Lagrangian

cell properties, (2) selection of all heavy precipitation events at fixed locations and investigation of the convective cells which caused these extreme events.

(1) Precipitation potential for fixed locations

To investigate the influence of wind shear on scaling for fixed location, we define the fixed location precipitation potential P_{fl} for each cell. The purpose of this quantity is to derive a measure of how much each convective cell can precipitate at a fixed location based on its mean Lagrangian properties as derived from the tracking algorithm. P_{fl} is calculated as

$$P_{fl} = I * t = \min\left(I * \frac{D}{v}, I * l\right) = \min\left(I * \frac{2\sqrt{A}}{v\sqrt{\pi}}, I * l\right),$$

where I denotes the mean precipitation intensity, t the duration of precipitation, D the diameter calculated based on the mean area of the cell, v the mean speed, A the cell area and l the lifetime of the cell. The duration of the rain event at fixed location is either calculated as the minimum of the diameter divided by the mean cell speed or taken as the cell lifetime. This condition accounts for the fact that a precipitation event at fixed location can only last as long as the moving cell causing it.

P_{fl} shows varying scaling regimes over the dew point range (Figure A8a). It increases at rates below the CC-rate for dew point temperatures below ~11°C and slightly above the CC-rate, at a rate of 8.8%/K, above 11°C. The different percentiles increase at approximately similar rates. Concerning the influence of wind shear, the fixed location precipitation potential decreases with increasing wind shear (Figure A8b).

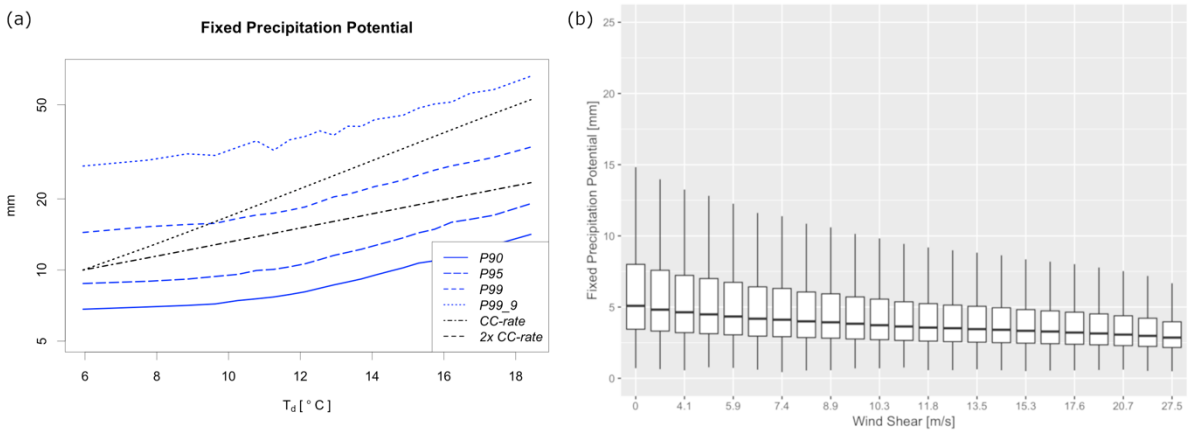

Figure A8: (a) Scaling of fixed location precipitation potential with dew point; (b) Wind shear dependence of fixed location precipitation potential.

Convective cells causing heavy precipitation events

We define heavy precipitation events at fixed locations as events with a precipitation amount of more than 25 mm in 1 h within an area of 1 km^2 (equal to one grid box of the radar data set). This definition follows the warning criterion for severe precipitation (at level 3 out of 4) of Deutscher Wetterdienst. A convective cell is connected to a heavy precipitation event if it passes the grid box of heavy precipitation within the hour of its occurrence.

Cells that cause heavy precipitation at fixed locations (abbreviated as hp-cells from now on) move comparably slow (Figure A9a). The median cell speed of hp-cells is 8.3 m/s compared to 9.3 m/s for all cells. As cell speed is largely determined by wind shear, the frequency distribution of wind shear for hp-cells is also shifted to lower values compared to all cells (Figure A9b).

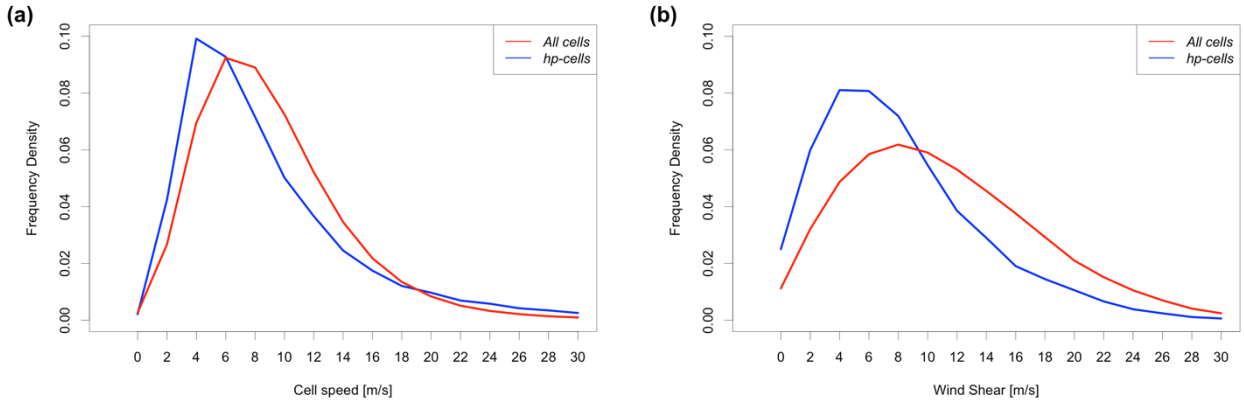

Figure A9: Frequency densities of (a) cell speed of all cells and hp-cells, and (b) environmental wind shear for all cells and hp-cells.

A.5 Discussion and conclusion

We showed that Lagrangian cell properties scale with dew point temperature at varying rates under current climate conditions. The maximum intensity of cells scales consistently at the CC-rate, implicating that the maximum intensity of cells is governed by thermodynamics. The area of cells increases at varying rates, namely at the CC-rate below 12 °C and at 2x CC-rate above, which implicates a dynamic control. Indeed, cell area is strongly influenced by vertical wind shear, with higher wind shear leading to larger cells. This behavior reflects the well-known increase of convective organization by vertical wind shear. In contrast, wind shear has very little influence on the maximum intensity of cells. The precipitation sum scales at above CC-rate with higher scaling rates at higher dew point temperature. In summary, the strongest convective cells as measured by the precipitation sum per cell occur at high wind shear, high CAPE and high dew point conditions.

Scaling for fixed location is lower than the Lagrangian scaling rate of total precipitation sum per cell due to the compensating effect of higher cell speed at high wind shear. The scaling rate of fixed precipitation potential (8.8%/K) is in line with other studies which report super-CC scaling for Germany (Berg et al. 2013, Ali et al. 2021). Thus, local differences in scaling rates of sub-daily precipitation at fixed location, which vary between the CC-rate and 2x CC-rate, are modulated by differences in properties of convective storms. While we cannot distinguish between different processes discussed in the literature, like a positive feedback loop of cloud dynamics or the effect of self-organization in the current analyses, we point out that the increase of environmental CAPE with dew point temperature can serve as an explanation for super-CC scaling of sub-daily precipitation without assuming changes in the storm dynamics. Although it is well known that moist air is less dense, little attention has been paid to the fact that buoyancy (as measured by CAPE) increases with dew point on climatological time scales when discussing super CC-scaling of sub-daily extreme precipitation. We conclude that super-CC scaling is at least partially caused by more unstable stratification of the pre-storm environment at high dew point temperatures.

The role of convective self-organization for the intensification of convective precipitation is currently an active area of research (e.g. Moseley, 2016, Lochbihler et al. 2019). Convective self-organization describes the process of convective cells to form clusters that tend to produce higher precipitation intensities and react differently to environmental conditions than unorganized convection. Often, convective self-organization is investigat-

ed by tracking precipitation and differentiating between cells that merge or split and solitary tracks. Preliminary analyses show that the average number of splits and mergers per cell increases consistently with increasing dew point temperature from ca. 0.2 splits and merges per cell at 6 °C to 0.95 at 19 °C. Further investigations are needed to understand the role of mesoscale organization and the role of cold pools in detail.

The fact that scaling rates are modulated by vertical wind shear and CAPE makes it unlikely that present scaling rates for fixed locations can be transferred into the future. However, the results obtained in this paper can be used to infer how convective events might change by using a more quantitative description, like multivariate regression, of the relationship of cell properties to environmental conditions. As an alternative to purely statistical inference, convection-permitting climate simulations can be used to investigate changes in convective cells. As shown in Purr et al. (2021), the dew point scaling of convective cell properties is similar in present and future conditions for the highest percentiles. Thus, the dew point scaling of cell properties shown in section 4.1 might also be valid in the future climate. However, the frequency distribution of cells depending on dew point temperature changes. To understand the changes in the frequency distribution, other variables might have to be taken into consideration. For example, changes in convective inhibition have been shown to change the population of convective cells in the future (Rasmussen et al. 2020). These changes potentially include a decreasing number of slow-moving convective cells in the afternoon (Purr et al. 2021). Combined with the fact that slow-moving cells have a higher potential for heavy precipitation at fixed location as shown in section 4.3 this indicates a compensating effect on heavy precipitation. Again, this illustrates the fact that present scaling rates at fixed locations cannot simply be extrapolated into the future (Fowler et al. 2021). Future research should investigate the role of different formulations of convective parameters like storm relative helicity or lifted index to better understand the organization of convective storms. Furthermore, the role of fronts and convergence lines as trigger mechanisms and the effect of orography or urban areas for triggering and enhancing convective cells should be further investigated.

B. Paper 2: Convective Shower Characteristics Simulated with the Convection-Permitting Climate Model COSMO-CLM

Published as:
Purr, Christopher; Erwan Brisson; and Bodo Ahrens. 2019. "Convective Shower Characteristics Simulated with the Convection-Permitting Climate Model COSMO-CLM" *Atmosphere* 10, no. 12: 810. https://doi.org/10.3390/atmos10120810

Abstract

This paper evaluates convective precipitation as simulated by the convection-permitting climate model (CPM) Consortium for Small-Scale Modeling in climate mode (COSMO-CLM) (with 2.8 km grid-spacing) over Germany in the period 2001–2015. Characteristics of simulated convective precipitation objects like lifetime, area, mean intensity, and total precipitation are compared to characteristics observed by weather radar. For this purpose, a tracking algorithm was applied to simulated and observed precipitation with 5-min temporal resolution. The total amount of convective precipitation is well simulated, with a small overestimation of 2%. However, the simulation underestimates convective activity, represented by the number of convective objects, by 33%. This underestimation is especially pronounced in the lowlands of Northern Germany, whereas the simulation matches observations well in the mountainous areas of Southern Germany. The underestimation of activity is compensated by an overestimation of the simulated lifetime of convective objects. The observed mean intensity, maximum intensity, and area of precipitation objects increase with their lifetime showing the spectrum of convective storms ranging from short-living single-cell storms to long-living organized convection like supercells or squall lines. The CPM is capable of reproducing the lifetime dependence of these characteristics but shows a weaker increase in mean intensity with lifetime resulting in an especially pronounced underestimation (up to 25%) of mean precipitation intensity of long-living, extreme events. This limitation of the CPM is not identifiable by classical evaluation techniques using rain gauges. The simulation can reproduce the general increase of the highest percentiles of cell area, total precipitation, and mean intensity with temperature but fails to reproduce the increase of lifetime. The scaling rates of mean intensity and

total precipitation resemble observed rates only in parts of the temperature range. The results suggest that the evaluation of coarse-grained (e.g., hourly) precipitation fields is insufficient for revealing challenges in convection-permitting simulations.

Keywords: precipitation; tracking; convective storms; convection-permitting simulation; COSMO-CLM

B.1 Introduction

The correct representation of deep convection in climate models is essential for assessing the risks associated with this phenomenon like wind gusts, hail, lightning, and flash floods. Convection-permitting climate models (CPMs) that simulate deep convection explicitly improve the representation of the diurnal cycle of precipitation and the simulation of extreme precipitation intensities on short time scales compared to models that parameterize convection (Ban et al. 2014, Kendon et al. 2014, Prein et al. 2015, Brisson et al. 2016). The vast majority of studies evaluating precipitation in CPMs use rain gauge data or gridded precipitation data sets based on gauge data as observations. However, this traditional evaluation of precipitation has limitations for evaluating convective precipitation since the typical dimension of convective storms is smaller than the distance between stations. This can lead to an underestimation of storm frequency and storm peak intensity (Schroeer et al. 2018a). An evaluation of the space-time dynamics of convective cells requires the finer spatial and temporal resolution of remote sensing techniques. Since the temporal and spatial resolution of radar data is finer than the characteristic scales of convective clouds, it allows for continuous tracking of convective cells over their life cycle. Although mainly used for now-casting purposes, tracking of radar data to derive characteristics of convective cells on climatological time scales has been done in a few studies, for example by Lochbihler et al. (2017) or Moseley et al. (2013). Precipitation output of convection-permitting climate models has rarely been used for tracking so far. Brisson et al. (2017) simulated selected days of high convective activity and compared the life cycle of precipitation intensity of convective cells to radar data. Prein et al. (2020) conducted a comparison of hourly precipitation from a CPM and radar data in order to evaluate the model's capability to simulate mesoscale convective systems in North America. To the authors' knowledge, sub-hourly precipitation output from continuous CPM simulation has

not been evaluated yet. This is why we apply a tracking algorithm to 5-min precipitation output of a CPM and to a newly developed 5-min precipitation climatology based on gauge adjusted radar data. The first aim of this study is to evaluate the characteristics of convective precipitation objects (the term convective cells is used synonymously from now on) in a CPM in terms of lifetime, mean precipitation intensity, area, and total precipitation.

Because of climate change, the hydrological cycle is expected to intensify with increasing temperatures, leading to changes in intensity, frequency, and duration of precipitation events Trenberth et al. (2003). The question of how the characteristics of deep convection and the accompanying extreme short-term precipitation events will change is still being discussed. Observational studies (Lenderink and van Meijgaard 2008; Berg et al. 2003) have reported intensification of hourly precipitation above the Clausius–Clapeyron rate (the increase of the saturation water vapor pressure with temperature) of ca. 7%/K. Different hypotheses have been suggested to explain this behavior, for example, the invigoration of convective cells through a positive feedback loop caused by increased moisture availability at higher temperatures leading to increased latent heat release in the updraft of convective cells, which, in turn, leads to higher updraft speeds and increased moisture convergence at the cloud base (Lenderink et al. 2017). Moseley et al. 2013 investigated the life cycle of convective precipitation cells by tracking radar data. They showed a stronger increase in mean intensity of convective precipitation cells with temperature than for stratiform cells. The application of a tracking algorithm allows us to investigate the temperature dependence of cell characteristics. Therefore, the second aim of this study is to gain insights into how well the model can reproduce the temperature scaling of cell characteristics observed in the radar data.

The paper is structured as follows: In the following section, the model setup and the radar data will be introduced, followed by a description of the cell tracking algorithm. The subsequent result section starts with an evaluation of stationary precipitation statistics. Afterward, the characteristics and spatial distribution of convective cells in the convection-permitting simulation are compared to the radar data. The section is concluded by the investigation of the temperature dependence of the cell characteristics. In the final section, the results are summarized, and conclusions are drawn.

B.2 Data and Methods

B.2.1 Model Setup

The Consortium for Small-Scale Modeling model in climate mode (COSMO-CLM, from now on abbreviated as CCLM) is used to downscale the European Centre for Medium-Range Weather Forecast Interim Reanalysis (ERA-Interim) to a horizontal grid spacing of 0.025° (≈2.8 km) via an intermediate nest with a grid spacing of 0.22° (≈25 km). At the lateral boundaries of the simulation domain, the model is nudged towards the driving data using Davies relaxation (Davies 1976). Within the simulation domain, no nudging is applied. The model domain of the inner nest covers central Europe (Figure B1). The CCLM is a non-hydrostatic limited-area climate model based on the COSMO model (Steppeler et al. 2003), a model designed by the Deutsche Wetterdienst (DWD) for operational weather predictions. The climate limited-area modeling (CLM) community adapted this model to perform climate projections (Böhm et al. 2003, Rockel et al. 2008). We use the version COSMO5.0clm7 with the following setup. For time integration, the 5th order Runge–Kutta split-explicit time-stepping scheme is used with a time step of 25 s. The lower boundary fluxes are provided by the TERRA model. The radiative scheme is the Ritter and Geleyn scheme (Ritter and Geleyn 1992) and is called every 15 min. As recommended in Brisson et al. 2015, we use a one-moment microphysics scheme, including graupel in the finest nest, which provides a more realistic representation of deep convective clouds. While the parameterization of deep convection is switched off, shallow convection is still parameterized using the convection scheme after Tiedtke et al. (1989). The simulation covers the period from 1983 to 2015. Surface temperature and precipitation output are stored every 5 min. Since the evaluation data set is available from 2001, the evaluation period is 2001–2015.

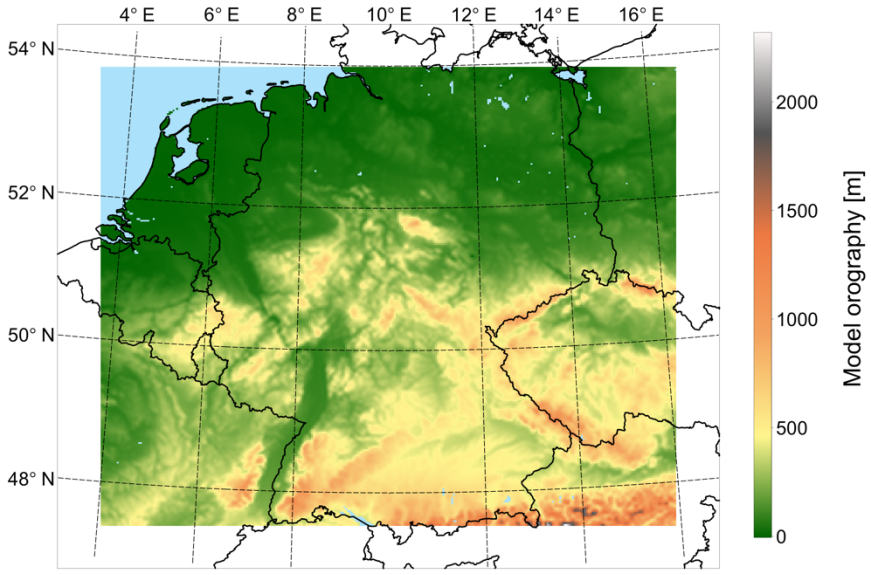

Figure B1: Model domain and model orography.

B.2.2 Radar Data

As a reference for the model evaluation, we use the radar-based precipitation climatology developed by DWD (Winterath et al. 2017). This precipitation data set is based on radar data that has been quality checked and adjusted to rain gauge measurements. The correction steps used for this product to derive precipitation from radar reflectivity include clutter filtering, distance-dependent signal correction, and removal of radar spokes. For the tracking, we use the 5-min dataset (YW-product) (Winterath et al. 2018a). For the comparison of mean precipitation and for the comparison of stationary hourly precipitation intensities, we use the hourly dataset (RW-product) (Winterath et al. 2018b). The full data set covers the time period 2001–2018. The data set has a spatial grid resolution of 1 km × 1 km. For the evaluation, the radar data is conservatively remapped to 2.8 km × 2.8 km. In order to assess the impacts of this remapping on the tracking results, the results of tracking the data in the original resolution are often shown in addition.

B.2.3 Tracking Algorithm

To obtain the characteristics of convective objects from model and radar data, we use a tracking algorithm. The tracking consists of three major steps:

Contiguous precipitation areas with precipitation intensity above a threshold of 8.5 mm/h (within 5 min), potential convective objects, are identified in the current and the subsequent time step. Contiguous areas are defined as pixels that share a common edge.

Wind information is used to predict the position of the object at the subsequent time step. To this end, a "cone of detection" is set up for each pixel of every object, and the cone is swept for precipitation objects from the subsequent time step. The axis of the cone is defined by the wind direction; the length of the cone is calculated as twice the wind speed. The opening angle of the cone is 45°. If a new cell is present in the cone, a probability value is assigned to the origin pixel of the cone, which links this pixel to the new cell. The probability value is highest in the center of the cone and drops off exponentially in all directions. As an example, Figure B2a shows the probability values for a single pixel in the case of purely westward wind. In this case, the probability is calculated according to the following formula:

$$\mathrm{Prob}(0,0) = \exp\left(-\sqrt{(\mathrm{Y_{cent}} - \mathrm{y})^2 + \left(\frac{\mathrm{X_{max}}}{2} - \mathrm{x}\right)^2}\right)$$

where x and y are the indices in x and y direction starting at the original pixel (0,0). The parameter Y_{cent} denotes the centerline of the cone, and X_{max} is the length of the cone, as determined by the wind data. This procedure is repeated for wind information in three height levels (500, 700, and 850 hPa). Afterward, the height dependent probability values are averaged to obtain the final probability value.

In the next step, the probabilities of all pixels are summed up for each cell. If one single object is present in the cone, the corresponding objects from the current and the subsequent time step are connected. If multiple cells are present, the current cell is associated with the cell with the highest probability in the subsequent time step.

The characteristics that are extracted by the algorithm are cell lifetime, mean intensity, maximum intensity, area, cell speed, and track length. It should be noted that merges and splits of objects are not accounted for. If two cells merge, the cell track with the higher probability of association is continued, whereas the other track ends. The track that is not continued is regarded as an individual track in itself. Figure B2b shows an example of a tracked precipitation object.

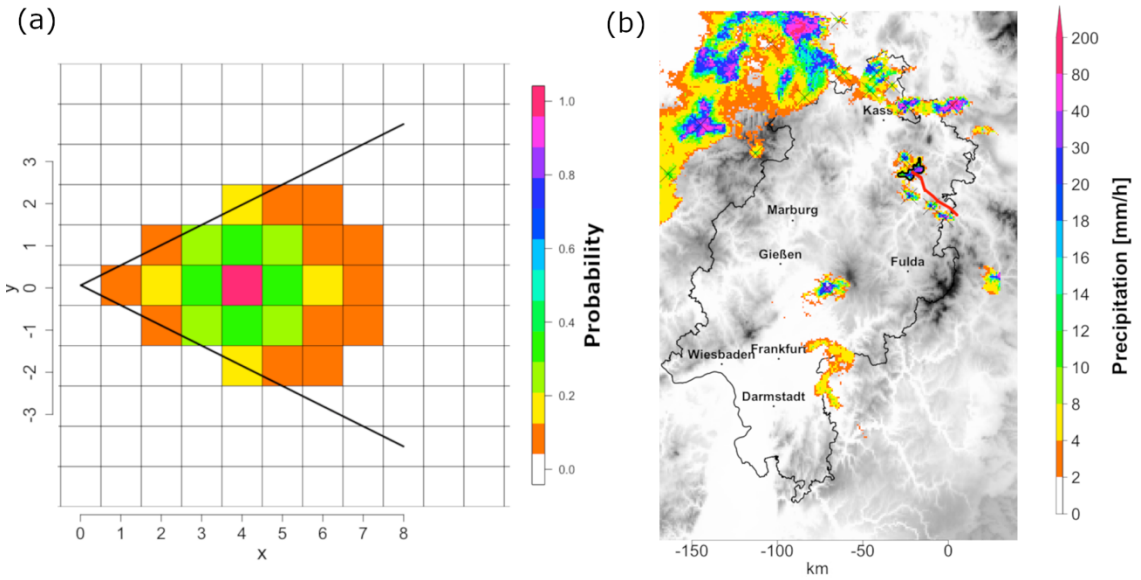

Figure B2: Visualization of the tracking algorithm: (a) detection probabilities for a cone with Xmax = 8 and Ycent = 0 (assuming a grid size of 1 km × 1 km and a time step of 5 min, this is equal to a westward wind of ca. 13.3 m/s), and (b) radar snapshot of a cell (shown is the 5-min precipitation intensity on 30 May 2008 at 21:40 (UTC) in colors and the detected cell track as red line).

Only cells with a lifetime of at least three time steps (=15 min) are considered for analysis. This condition reduces the chances of misinterpreting single clutter pixels in the radar data (which are still present but heavily reduced compared to operational radar products) as convective cells. Furthermore, the algorithm only selects precipitation areas larger than four grid boxes for the same reason. For consistency, this requirement is also kept when tracking the model data. This requirement is also justified because the effective resolution of any numerical model is always coarser than the grid spacing. When applying the tracking algorithm to the model data, the model data is conservatively remapped to the polar stereographic projection of the radar data in order to have both data sets on a common, equidistant grid for ease of comparison. The wind information used for estimating the position of each cell at the subsequent time step is taken from the ERA-Interim reanalysis in case of the radar data. In the case of the simulation data, the wind information from the intermediate nest driving the finer simulation is used.

B.3 Results and Discussion

B. 3.1 Precipitation Statistics

We first evaluate the mean precipitation sum in the simulation with respect to the radar climatology on the common 2.8-km grid. The highest precipitation amount is found in the Alps (Figure B3). Least precipitation occurs in the North-East of Germany. The mean daily precipitation in observation and simulation data is 2.0 mm/d and 1.7 mm/d, respectively, resulting in a 14% underestimation of total precipitation in the simulation. Considering that no bias correction (Dobler and Ahrens 2008) has been applied, this is in line with other CPM evaluations. The model overestimates precipitation in mountainous regions, especially in the Black Forest in southwest Germany, and underestimates it in the lowlands of Northern Germany. This points to an overestimation of the orographic intensification of precipitation in the simulations. Unfortunately, no measurement uncertainty is provided for the radar data. Since other gridded precipitation data sets also show considerable deviations from each other (Prein and Gobiet 2017), a detailed comparison of the radar data set to other precipitation data would be beneficial. In a first comparison to a daily gridded observational dataset for precipitation, temperature, and sea level pressure in Europe (E-OBS, version 20.e, Cornes et al. 2018), we find that areal mean precipitation in the radar data is 5.9% smaller than in E-OBS. This is in line with Winterrath et al. (2017), who compared the radar data to a station-based data set and found the precipitation amount in the radar data to be smaller, especially in mountain areas. The spatial pattern of underestimation in the North and overestimation in the mountains is also present when comparing the simulation to the E-OBS data set (not shown).

We restrict our analysis of convective cells to the summer half-year from April to September because convective precipitation mainly occurs in this period. The mean observed and simulated summer precipitation (April to September) is 2.3 mm/d and 1.5 mm/h, respectively, resulting in an underestimation of 34% in the simulation. Taking into account that convective precipitation occurs almost exclusively in the summer months in Germany, this indicates that the model underestimates convective precipitation more than stratiform precipitation. The underestimation is strongest in Northern Germany, while more realistic precipitation amounts are simulated in the South.

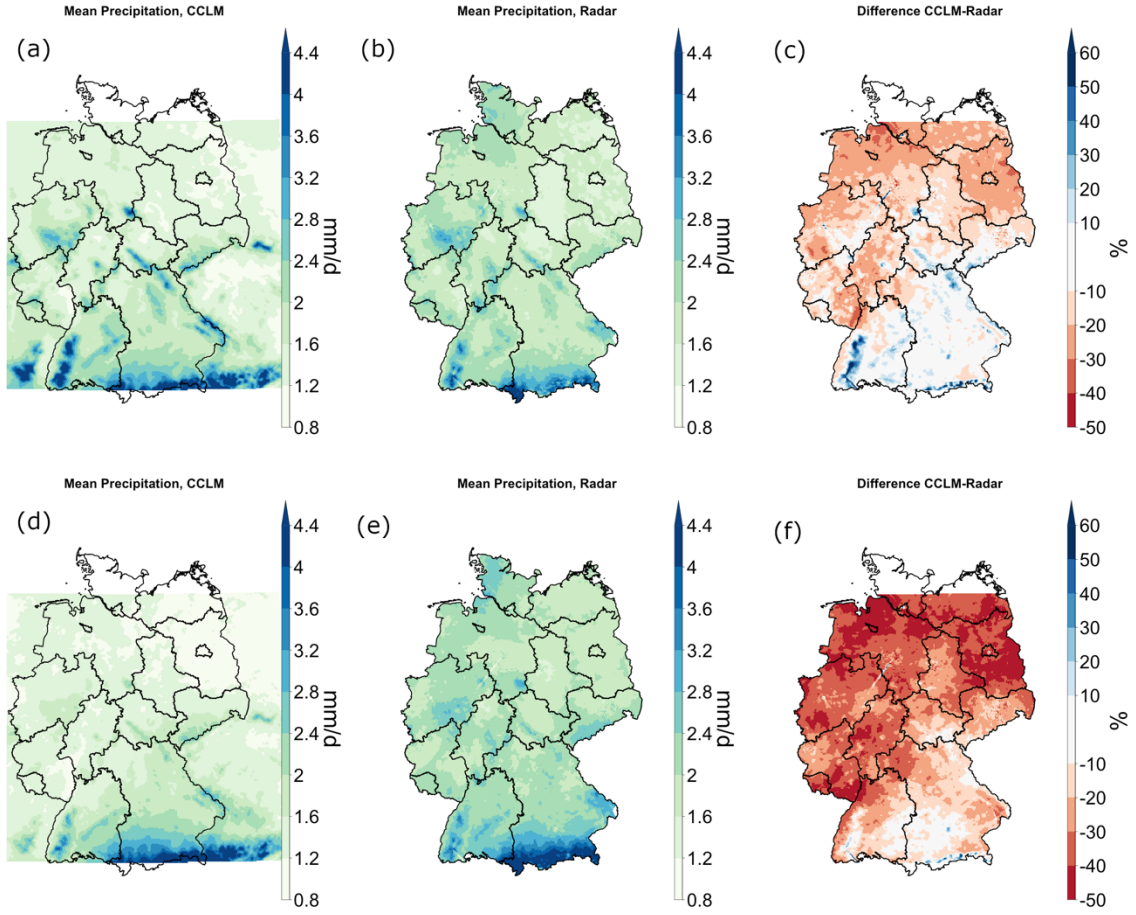

Figure B3: Mean precipitation intensities and differences in the period 2001–2015; (a–c) full year; (d–f) summer half-year (April–September).

The simulated probability distribution of hourly precipitation compares well with the observed one (Figure B4). The observed wet hour frequency defined as hours with precipitation above 0.1 mm/h is 8.5 %; the simulated wet hour frequency is 9.6%. The Perkin's Skill Score (PSS), which calculates the overlapping area between observed and modeled probability distribution function (Perkins et al. 2007), is 0.89 for the wet hour frequency. The simulation considerably underestimates precipitation occurrence in the range below 12 mm/h. This range contributes 95% to the total observed precipitation sum and is underestimated by ca. 28%. The precipitation sum resulting from intensities between 12 mm/h and 50 mm/h is overestimated by 12%. The occurrence of hourly precipitation sums above 50 mm/h is underestimated by 32%. Considering the 5-min intensity distribution, the model always underestimates precipitation intensity. The drop-off at the highest 5-min intensities corresponds well with the drop-off at the hourly time scale. However,

the fact that there is no overestimation of high intensities corresponding to the one at the hourly time scale points to differences in the dynamics of convective cells.

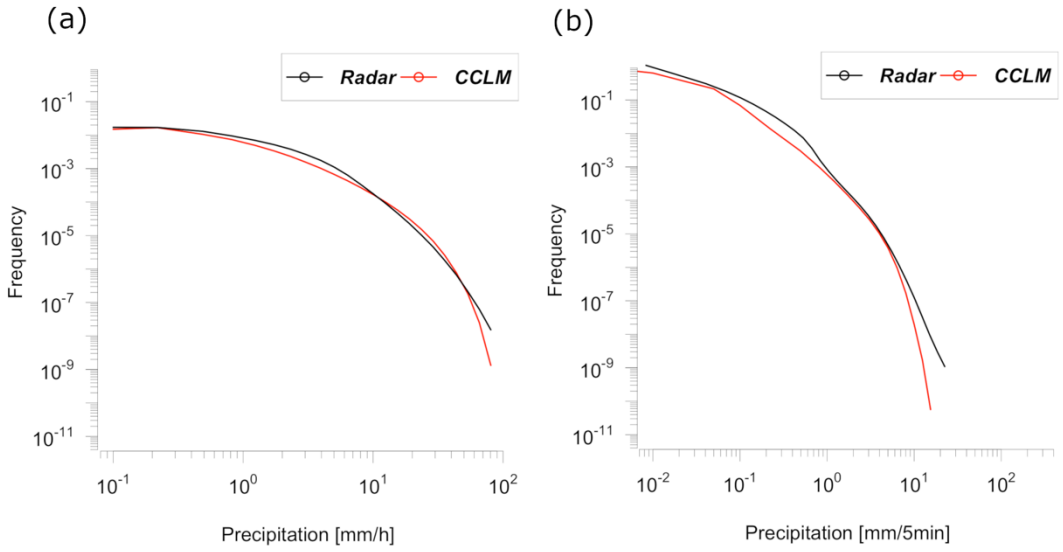

Figure B4: Frequency distribution of (a) hourly and of (b) 5-min precipitation intensities from radar observations (black) and CCLM simulation (red).

B.3.2. Frequency and Characteristics of Convective Cells

In this subsection, we compare the simulated frequency distributions of cell characteristics with the radar characteristics. The simulation underestimates convective activity, represented by the total number of convective cells, by 33%. Convective precipitation, calculated as the precipitation sum of all convective cells, is very well matched with an overestimation of 2%. The lifetime of convective cells ranges from 15 min (the lowest possible value as set by the tracking algorithm) to 7 h (Figure B5). As expected, short-living cells are the most common form of convective cells. The simulation captures but underestimates the decrease in frequency with lifetime and produces too many long-living and too few short-living cells. Comparing the lifetime distributions of the simulation and remapped radar data yields a PSS of 0.84. A possible reason for the overestimation of cell lifetime could be that tracks are more often lost in the radar data than in the simulation data by the tracking algorithm. The reason for this is that radar data provide snapshots of precipitation, whereas, in the model, precipitation is accumulated, which leads to a smoother precipitation field. This difference of accumulated versus instantaneous precipitation also has a small influence on cell size and mean intensity. To estimate how many

tracks are wrongfully split up by the tracking algorithm, we investigate the cell size at the first occurrence of the cell. If the cell only just started its life cycle, one would expect a small size close to the lower boundary of five grid points. If, on the other hand, the cell is the second part of a track that was wrongfully split up, it will have a larger extent. If we consider an initial area larger than 10 grid points (80 km^2) to be unrealistically large and discard those cells, then the underestimation of convective activity is only slightly reduced to 28%.

The frequency distributions of cell area and total precipitation per cell are very well matched with a PSS of 0.99 and 0.98, respectively. There are too few high-intensity cells. The PSS for the mean intensity is 0.86.

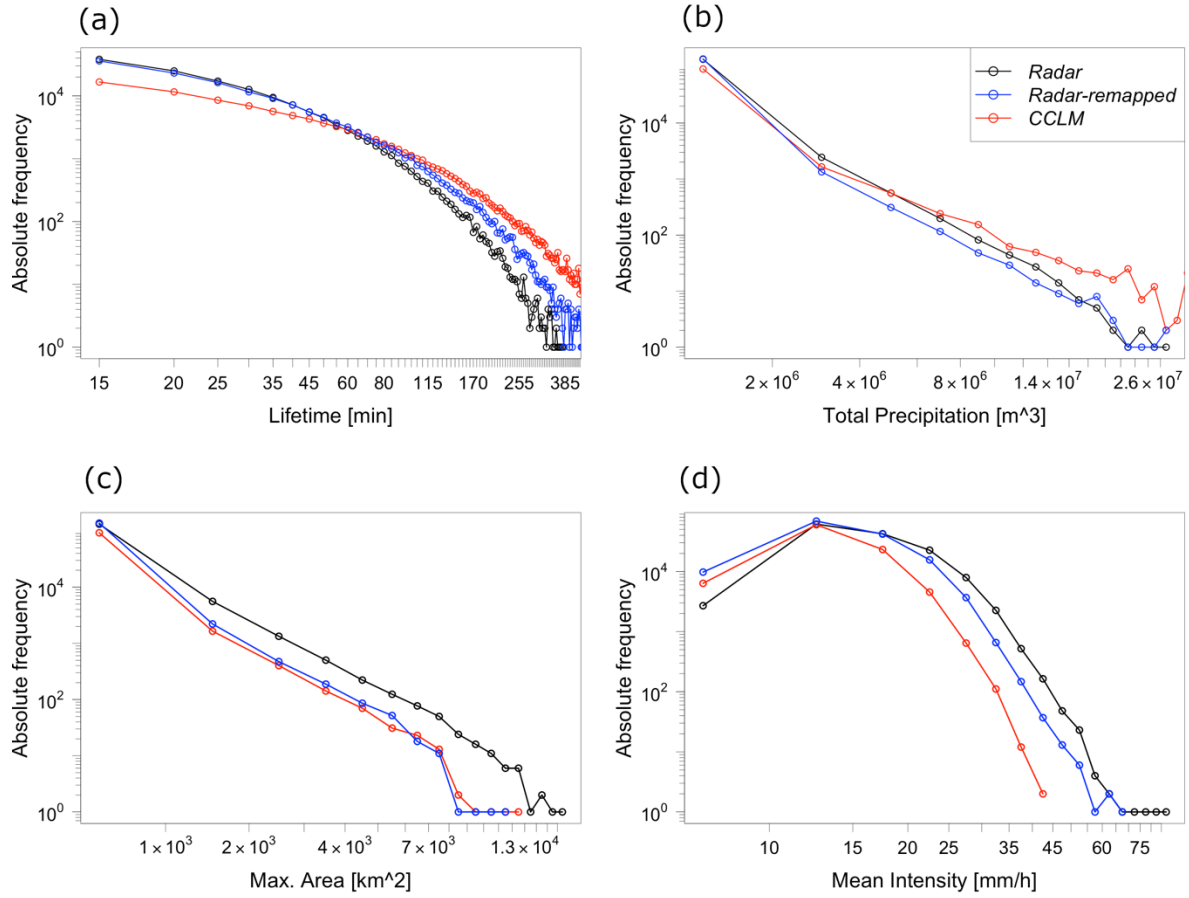

Figure B5: Frequency distributions of the cell characteristics (a) lifetime, (b) total precipitation, (c) maximum area, and (d) mean cell intensity as observed by the radar (black), by radar remapped to the model grid (blue) and simulated (red).

To verify that it is really the long-living convective cells that have a high intensity and area, Figure B6 shows the distributions of mean intensity and of maximum area depending on the lifetime of the convective cells. To this end, cells are grouped into lifetime

classes of 15-min width. A systematic increase in maximum area and mean intensity with lifetime can be seen in both the radar observations and the simulation. While the observed median maximum area is 226 km^2 for cells living 195 to 210 min, the median is only 25 km^2 for cells living 15 to 30 min. The observed median values of mean intensity of cells in the same lifetime classes are 21 mm/h for long-living and 12 mm/h for short-living cells. These relationships indicate that the detected short-living cells can either be single-cell storms or individual cells of a multicell storm. The long-living, large, and intense cells are organized forms of convective systems like squall lines, supercells, and mesoscale convective systems. The simulation systematically underestimates the increase in mean intensity with lifetime. The increase in maximum area is well matched.

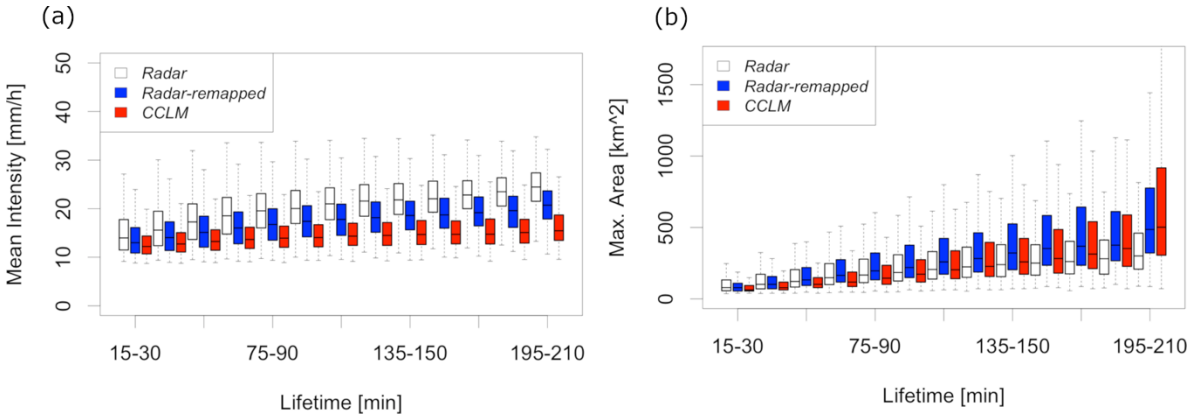

Figure B6: Dependence of (a) cell mean intensity and (b) cell maximum area on cell lifetime for radar observation and CCLM simulation. The boxes denote the 25th, 50th, and 75th percentiles. The whiskers denote the 5th and 95th percentile.

B.3.3 Spatial Distribution of Cell Characteristics

Figure B7 shows the spatial distribution of the occurrence of convective cells. Here, the occurrence of convective cells per grid-point for the period 2001–2015 is shown. The tracking algorithm stores the area and center of mass for each cell at every point in time. For this reason, no information about the actual shape of a cell is available. Instead, the cells are reconstructed as squares around the center of mass to match their original size. It has to be noted that every occurrence of a cell per 5-minute time step is counted. The value can, thus, be interpreted as the number of exceedances of a 5-minute precipitation intensity of 8.5 mm/h (the detection threshold of the tracking algorithm). Instead of counting each cell only once (e.g., at its point of largest extent), this method represents the area affected by convective cells more realistically because cells can have widely varying areas and translation speeds.

Mountain ranges facilitate the triggering of deep convection through various processes (see Kirshbaum et al. 2018 for a review). Therefore, it is not surprising that the Alps and the pre-alpine region show the highest occurrence of convective cells. Low mountain ranges also show increased values compared to lowland regions. The overall pattern matches the climatology of convective activity derived from lightning data presented in Wapler and James 2013. In general, there is a positive North–South gradient in convective activity. The mean intensity of convective cells is lower over the mountains (not shown). This can be explained by the fact that orographically induced convection is early in its life cycle in this area and, thus, has a relatively low intensity.

In general, the simulation is capable of representing the increased convective activity in mountain areas. It overestimates the number of convective cells in the South and underestimates it in the North (Figure B7). However, there are areas of overestimation and underestimation in both parts of the investigated domain. Near the radar locations, overestimation prevails, while areas of underestimation tend to be located furthest away from the radar. More cells are initiated in the mountainous areas of Southern Germany than in the North. This supports the hypothesis that the more complex topography facilitates the onset of convection and, thus, eliminates the negative bias in the cell number present in Northern Germany.

Since the convective activity shows a different pattern in North and South Germany, which may be related to the different orography in these regions, we further investigate the height dependence of convective activity. Therefore, the convective cells are stratified by the terrain height at which they occur. While the cell number is underestimated by 15% in regions with a terrain height below 400 m a.s.l., the number of cells for terrain heights above 400 m a.s.l. is overestimated by 6%. The overestimation of convective precipitation in mountainous areas is in line with results in Knist et al. (2018), who performed convection-permitting climate simulations over Germany using the WRF-model and compared the results to gauge data.

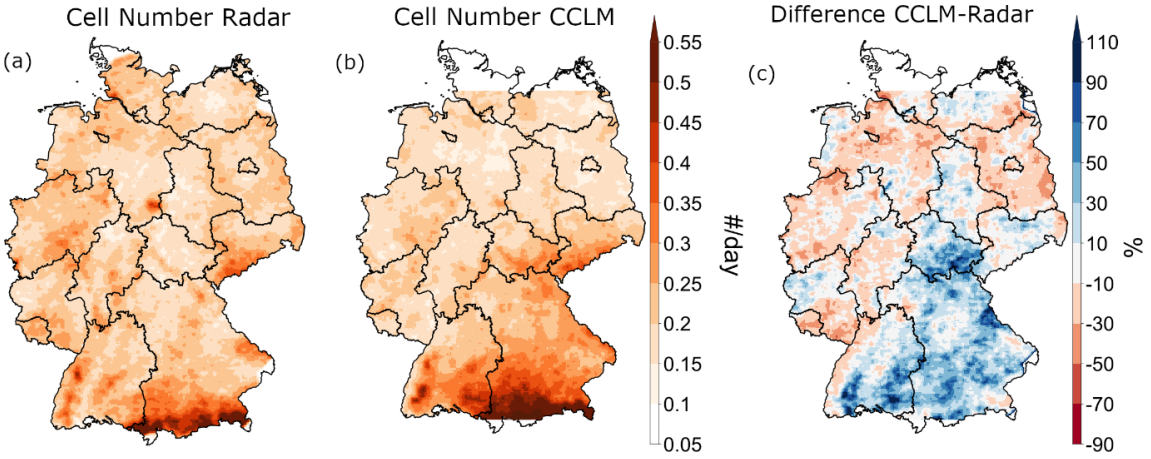

Figure B7: Spatial distribution of the number of convective cells; (a) observation, (b) simulation, (c) relative difference CCLM—radar.

B.3.4 Diurnal Cycle

The diurnal cycle of convective activity in Central Europe has a pronounced maximum in the afternoon, which is caused by daytime land surface heating (Pfeifroth et al. 2013). The diurnal cycle of convective activity is slightly delayed in the simulation (Figure B8a). The afternoon maximum is observed at 15:50 (UTC), while the modeled maximum occurs around 16:30 (UTC). The number of cells initiated during the night and morning is well matched, whereas the daytime increase of convective activity is too small, resulting in 36% fewer cells being initiated in the afternoon and evening (between 13:00 UTC and 20:00 UTC). The maximum number of cell initiation is underestimated by 40%. Combined with the general overestimation of cell lifetime, this leads to an overestimation of cells present at each point in time during the night and an underestimation during the time of highest activity (Figure B8b). The mean intensity, defined as the mean over all cells of spatial mean intensity at every 5-min time step, increases during the daytime. The modeled increase of mean intensity is too weak.

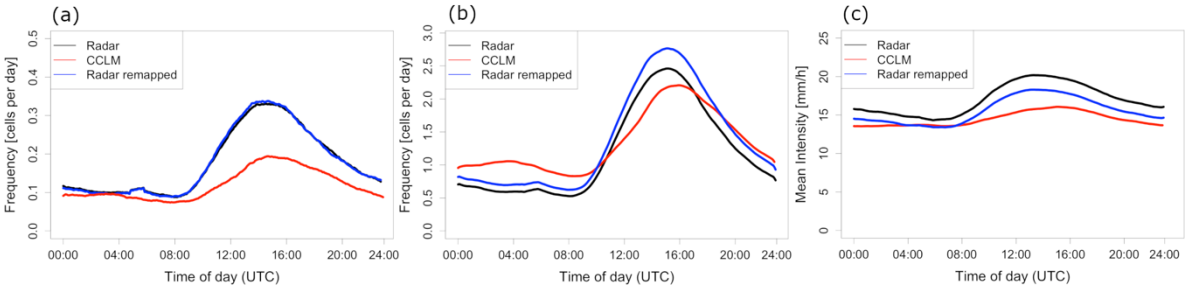

Figure B8: Diurnal cycle of convection; (a) cell number at cell initiation (every cell is counted once), (b) cell number at each individual time step (cells are counted multiple times, according to their lifetime), and (c) mean intensity of all cells at a certain point in time.

While the peak of convective activity in areas with an elevation below 400 m is underestimated, the convective activity above 400 m is well simulated (Figure B9). The sum of convective precipitation is overestimated in mountainous areas, which is caused by an overestimation of cell size during the daytime, which is especially pronounced in the afternoon.

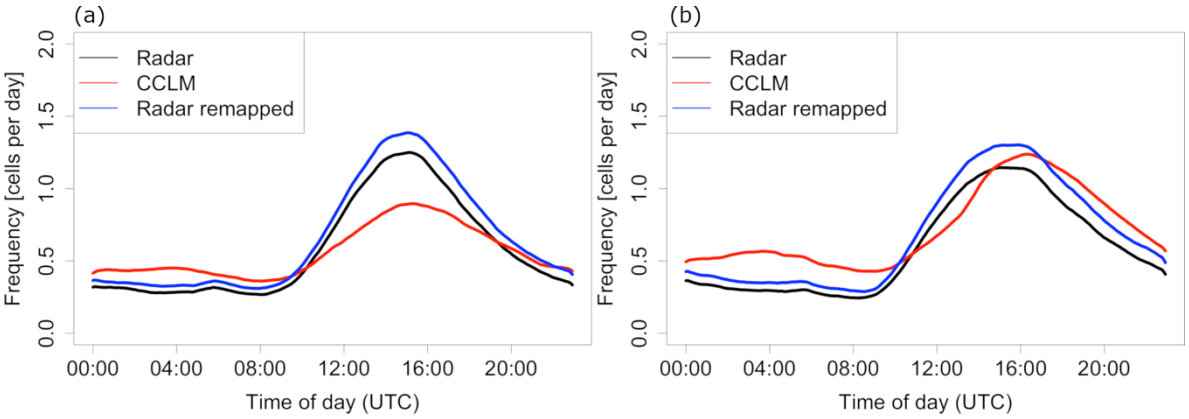

Figure B9: Dependence of the diurnal cycle of cell initiation. (a) Cells originating over terrain with an elevation <400 m. (b) Cells originating over terrain with an elevation >400 m.

B.3.5 Temperature Scaling of Cell Characteristics

In this subsection, we investigate the temperature scaling of cell properties like total precipitation, area, and mean intensity. We assign the mean daily temperature to each cell. Mean daily temperature is chosen instead of, for example, hourly temperature, to minimize the effect of local processes like cold pool formation on the scaling rate (Lenderink and van Maijgaard 2008; Barbero et al. 2018). For the radar data, we use ERA-Interim 2-m temperature of the grid point closest to the origin of the convective cell. For the simula-

tion data, we use the simulated 2-m temperature at the location of cell origin directly. Afterward, we group the convective cells properties total precipitation, maximum area, and lifetime and mean intensity into temperature bins of 1 °C width and determine the 90th, 95th, and 99th percentile for each bin.

The scaling of total precipitation, mean intensity, and lifetime and maximum area for both radar and simulation data is shown in Figure B10. Shown are the aforementioned percentiles based on the simulation and the remapped radar data. For comparison, the 95th percentile of the original radar data is shown additionally. The general underestimation of the highest percentiles of the variables mean intensity and total precipitation, as well as the overestimation of lifetime, is also visible here. In contrast to these variables, the maximum area is well represented in the model both in absolute value as well as the scaling rate. Generally, the rate at which mean intensity increases with temperature is well reproduced by the model. However, the underestimation of precipitation intensity for long-lasting, organized cells shown in Section B.3.2 is visible in the scaling rates of mean intensity. While the radar data shows an exponential increase up to the highest temperatures, the simulated mean intensity flattens at 20 °C. The largest difference in scaling rate appears for the lifetime of convective cells. The radar data shows an increase in lifetime of ca. 5% in the temperature range between 13 and 22 °C and flattens at higher temperatures. In contrast to this, the lifetime of convective cells in the simulation is mostly flat with small increases only in the low-temperature range and a drop at high temperatures. An intensification of convective cells above the Clausius–Clapeyron rate, which supports the hypothesis of a positive feedback loop in the strength of convective cells with rising temperatures, is apparent from the scaling rate of the total precipitation. The scaling of the modeled total precipitation is larger than the Clausius–Clapeyron rate for the whole temperature range up to 23 °C, where it levels off. This leveling off is also frequently reported for scaling of extreme precipitation at fixed locations and attributed to limited moisture supply at high temperatures (Hardwick et al. 2010, Chan et al. 2016). The observed total precipitation shows a slightly different behavior with a smaller increase at low temperatures and a larger increase starting at 15 °C.

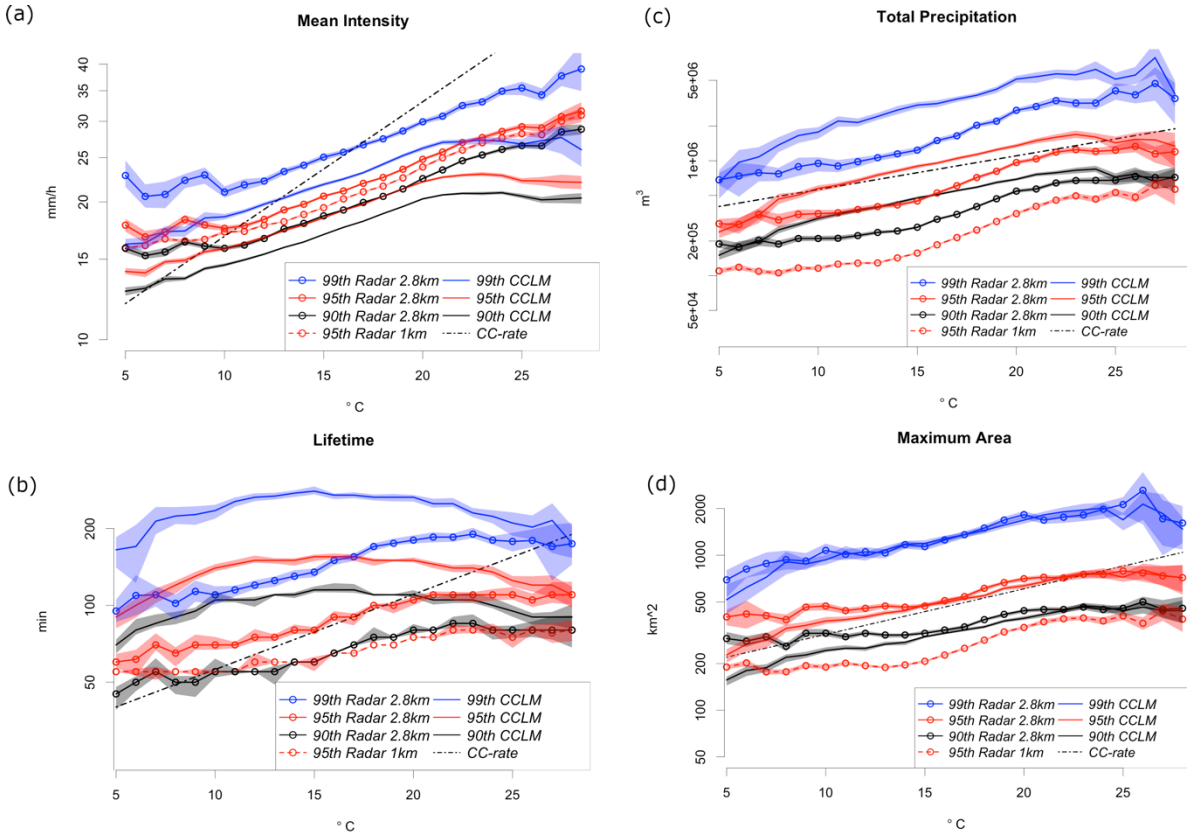

Figure B10: Temperature scaling of cell characteristics. (a) Spatial and temporal mean intensity of cells, (b) total precipitation, (c) lifetime, and (d) maximum area. Shaded areas denote the uncertainty range estimated by repeatedly calculating the respective quantile using bootstrapping. Note the logarithmic y-axis in all panels.

B.4 Conclusions

In this study, we evaluate the representation of convective precipitation objects in a CPM by applying a tracking algorithm to 5-min precipitation output and a newly developed 5-min radar climatology over Germany. The model is capable of reproducing the total amount of convective precipitation, as well as the frequency and characteristics of convective cells ranging from short-living, small cells to long-living, intense cells. However, the number of convective cells is underestimated. This underestimation is compensated by an overestimation of cell lifetime. A possible explanation for the underestimation of convective activity and the overestimation of cell lifetime could be that the grid size of 2.8 km is too coarse to capture boundary layer inhomogeneities, which facilitate the initiation of convection; thus, the number of cells is reduced. At the same time, convective available potential energy (CAPE) can accumulate longer without being consumed by convection, and the cells that manage to evolve can live longer. The observed enhanced convec-

tive activity in the mountain ranges is reproduced by the model. However, convective activity is underestimated in the lowlands of Northern Germany and overestimated in the mountainous regions of Southern Germany. This supports the hypothesis that the grid size is too coarse to fully represent the initiation of deep convection without the help of orographic forcing. However, it cannot be ruled out that other model deficiencies contribute to this bias. The difference in representing convective precipitation in mountainous areas and lowland regions agrees with an evaluation of the WRF-CPM (Knist et al. 2018). The fact that both models overestimate convective precipitation in the mountains whilst giving correct amounts in the lowlands might indicate a general, model-independent problem, such as resolution, which is 2.8 km in both studies. The underestimation of mean intensity and maximum intensity of large, long-living cells suggests model deficiencies in representing large, organized forms of convection. To evaluate the model's capability of representing the characteristics of extreme convective cells at different temperatures, we investigate the temperature scaling of cell characteristics. While the model can reproduce the increases in mean intensity and area of extreme convective cells with temperature, it fails to reproduce the increasing cell lifetime seen in observations. The simulated scaling of total precipitation shows a continuous increase above the Clausius–Clapeyron rate, which indicates dynamical changes in extreme convective cells with increasing temperature. The observations show different scaling rates with a value close to the Clausius–Clapeyron rate at temperatures below 15 °C and higher values above. More detailed investigations are needed to understand these differences. Further studies could investigate the scaling behavior of forced vs. unforced convection. Additionally, the combination of the tracking algorithm with spectral methods characterizing the organization of the precipitation field, for example, Brune et al. (2018), could yield insight into the organization of deep convection.

The approach presented here can be used for more detailed process studies of deep convection in regional climate models, for example, focusing on different synoptical situations with potentially different types of convection, as investigated in Wapler et al. (2015). It might also be beneficial to evaluate the consequences of changing the model setup by increasing resolution or switching to a more sophisticated (i.e., two-moment) microphysics scheme. Furthermore, this study can be the basis for gaining confidence in the representation of different types of convection in order to use the output from RCMs for hydrological applications. One idea could be to construct a synthetic time series of convective precipitation objects that are derived from RCM output and bias-corrected

with radar data to estimate the hydrological consequences of the projected increase in heavy precipitation events.

Author Contributions: Conceptualization, B.A., E.B., and C.P.; Methodology, E.B., and C.P.; Software, C.P. and E.B.; Formal Analysis, C.P.; Investigation, C.P. and E.B.; Resources, B.A.; Data Curation, E.B., and C.P.; Writing-Original Draft, C.P.; Writing-Review and Editing, C.P., E.B., and B.A.; Visualization, C.P.; Supervision, B.A.; Project Administration, B.A., Funding Acquisition, B.A.

Acknowledgments: We thank the „Hessisches Landesamt für Naturschutz, Umwelt und Geologie“ and the „Rheinland-Pfalz Kompetenzzentrum für Klimawandelfolgen“ for funding the project “Konvektive Gefährdung über Hessen und Rheinland-Pfalz” in the course of which the results of this paper were obtained. Furthermore, we thank DWD for providing the radar data. The radar data is publicly available at Winterrath (2018a, 2018b). The simulations were performed on the LOEWE-CSC high-performance computer of the Frankfurt University.

Funding: This research was funded by „Hessisches Landesamt für Naturschutz, Umwelt und Geologie“ and „Rheinland-Pfalz Kompetenzzentrum für Klimawandelfolgen“, project name: “Konvektive Gefährdung über Hessen und Rheinland-Pfalz”.
Conflicts of Interest: The authors declare no conflict of interest.

C. Paper 3: Convective Rain Cell Characteristics and Scaling in Climate Projections for Germany

Published as:
Purr, Christopher; Erwan Brisson, Bodo Ahrens. 2021. Convective rain cell characteristics and scaling in climate projections for Germany. *International Journal of Climatology*. 41: 3174– 3185. https://doi.org/10.1002/joc.7012

Abstract

Extreme convective precipitation is expected to increase with global warming. However, the rate of increase and the understanding of contributing processes remain highly uncertain. We investigated characteristics of convective rain cells like area, intensity, and lifetime as simulated by a convection-permitting climate model in the area of Germany under historical (1976-2005) and future (end-of-century, RCP8.5 scenario) conditions. To this end, a tracking algorithm was applied to 5-min precipitation output. While the number of convective cells is virtually similar under historical and future conditions, there are more intense and larger cells in the future. This yields an increase in hourly precipitation extremes, although mean precipitation decreases. The relative change in the frequency distributions of area, intensity, and precipitation sum per cell is highest for the most extreme percentiles, suggesting that extreme events intensify the most.

Furthermore, we investigated the temperature and moisture scaling of cell characteristics. The temperature scaling drops off at high temperatures, with a shift in drop-off towards higher temperatures in the future, allowing for higher peak values. In contrast, dew point temperature scaling shows consistent rates across the whole dew point range. Cell characteristics scale at varying rates, either below (mean intensity), at about (maximum intensity and area), or above (precipitation sum) the Clausius-Clapeyron rate. Thus, the widely investigated extreme precipitation scaling at fixed locations is a complex product of the scaling of different cell characteristics. The dew point scaling rates and absolute values of the scaling curves in historical and future conditions are closest for the highest percentiles. Therefore, near-surface humidity provides a good predictor for the upper limit of e.g. maximum intensity and total precipitation of individual convective cells. However,

the frequency distribution of the number of cells depending on dew point temperature changes in the future, preventing statistical inference of extreme precipitation from near-surface humidity.

Keywords: precipitation, tracking, convection-permitting simulation, COSMO-CLM, Clausius-Clapeyron scaling, convective storms

C.1 Introduction

The question of how extreme precipitation will change in the future due to climate change is of high relevance due to the potentially severe hazards accompanying it. While daily precipitation extremes are projected to increase close to the Clausius-Clapeyron (CC) rate of ca. 7%/K on average in mid-latitudes, the change of precipitation extremes at regional level and on shorter time scales (e.g. hourly) is still uncertain (Zhang et al., 2017).

Observational studies show that the temperature scaling of extreme precipitation can divert from the CC-rate on sub-daily timescales (Lenderink et al., 2008), especially in the case of convective precipitation (Berg et al. 2013). Furthermore, Schroeer and Kirchengast (2018b) showed that the scaling can vary considerably at small spatial scales and depending on the season.

Since hourly precipitation extremes are primarily caused by convective precipitation in mid-latitudes, it is necessary to use models that can simulate deep convection explicitly, so- called convection-permitting climate models (CPMs). CPMs substantially improve the representation of convective precipitation, especially in terms of extreme precipitation, in contrast to coarser models, parameterizing deep convection (Prein et al., 2015; Brisson et al., 2016). Convection-permitting simulations agree on an increase in extreme hourly precipitation with global warming showing the highest increases for the highest percentiles (Knist et al., 2018).

A common way of investigating extreme precipitation in CPMs is calculating the temperature scaling of precipitation extremes. The temperature scaling on the hourly scale found in CPM studies varies between values slightly below (Fosser et al., 2017) or above the CC-rate (Kendon et al., 2014; Knist et al., 2018). What is common among these studies is that the scaling curves keep their characteristic shape but are shifted towards higher peak values at high temperatures in future conditions (Prein et al., 2017a). This suggests that

atmospheric conditions with sufficient humidity are present at higher temperatures in the future.

Varying scaling rates in observations and shifting scaling curves in CPMs indicate that the dynamics of deep convection and changes in the large-scale environment have a strong influence on the scaling rate and that the temperature scaling of extreme hourly precipitation under current climate conditions cannot be used to infer how convective events might react to climate change.

The rationale behind the procedure of relating extreme precipitation to near-surface temperature is that near-surface temperature provides a proxy for absolute humidity if relative humidity remains unchanged. However, the severity and structure of deep convective storms are determined by at least two additional ingredients besides near-surface moisture: static instability, as measured, for example, by convective available potential energy (CAPE), and wind shear (Weismann and Klemp, 1982). When coarse regional or global climate models (grid spacing larger than 4 km) are used to investigate how severe convection might change in a warmer climate, a combination of these three parameters is usually used to calculate changes in the frequency of thermodynamic environments favorable for convection (e.g., Seeley and Romps, 2015). Púčik et al. (2017) found an increase in storm favoring environments in Europe based on an ensemble of 14 regional climate models.

Solid understanding of the changes in deep convection and the processes involved can strengthen the reliability and plausibility of results. Therefore, we apply a tracking algorithm to 5-min precipitation output from the regional climate model COSMO-CLM to investigate convective rain cells' characteristics under historical and future conditions. Applying such a Lagrangian approach has the advantage of being able to monitor precipitating convective cells along their entire lifecycle. Observational studies based on weather radars show that convective cells increase in area and intensity with temperature in central Europe (Lochbihler et al., 2017; Moseley et al., 2013; Purr et al., 2019), whereas no area increase and generally lower scaling rates were found in Mediterranean and semi-arid climate (Peleg et al., 2018). Prein et al. (2017b) investigated the characteristics of Mesoscale Convective Systems in the USA by applying a tracking algorithm to hourly precipitation data from a CPM. They found an increase in the storm size and storm intensity for future conditions using a pseudo-global warming approach. Rasmussen et al. (2018) found an increase in intense convective precipitation events and a decrease in moderate events for North America at the end of the century. They used the WRF-model

in a pseudo global warming setup. They attributed these changes to increases in both CAPE and convective inhibition (CIN).
This study compares cell characteristics and their dependence on near-surface temperature and humidity in two 30-year periods, covering historical (1976-2005) and future (2071-2100) conditions. We relate the scaling of cell characteristics to the scaling of precipitation at fixed locations and discuss the influence of static stability and wind shear on the scaling rates.
In section 2 we describe the simulations that were performed and the tracking algorithm. The setup we use here has been shown to represent convective cell characteristics adequately in Purr et al. (2019). In this former study we evaluated the same model setup as used here but driven by reanalysis instead of a general circulation model. We will refer to these evaluation results specifically by stating the model's limitations in representing the individual cell characteristics in the respective result sections. The following section describes the setup of the CPM simulations, the tracking algorithm, and the way the temperature and moisture scaling was calculated. In the result section we first show "traditional" precipitation statistics such as change in mean precipitation and frequency distribution of hourly precipitation. Afterward, we investigate the overall frequency distributions of cell characteristics as well as their diurnal cycle and spatial distribution. Subsequently, the dependence of cell characteristics on near-surface temperature and dew point temperature is investigated. At the end, we discuss the influence of the large-scale environment described by CAPE and wind shear and potential limitations of the current study.

C.2 Methods

C.2.1 COSMO Simulations

The simulations analyzed in this study were performed with the Consortium for Small-Scale Modeling in climate mode (COSMO-CLM) model. The COSMO-CLM model is a non-hydrostatic limited-area climate model, based on the COSMO model (Steppeler et al. 2003), a model designed by the Deutsche Wetterdienst (DWD) for operational weather predictions. The climate limited-area modeling (CLM) community adapted this model to perform climate projections (Böhm et al. 2006; Rockel et al. 2008). For time integration, the 5th order Runge-Kutta split-explicit time stepping scheme is used. The lower boundary

fluxes are provided by the TERRA model (Doms et al. 2018). The radiative scheme is the Ritter and Geleyn (1992) scheme. As recommended in Brisson et al. (2015), we used a one-moment microphysics scheme, including graupel in the finest nest, which provides a more realistic representation of deep convective clouds. Shallow convection is parameterized using the convection scheme after Tiedtke (1989).

Two continuous 30-year long simulations were performed: 1976-2005 (named *Historical* from now on) and 2071-2100 (named *RCP8.5*) at a resolution of 0.025°. The model is forced by the global climate model EC-Earth (Hazeleger et al. 2012), in particular realization r12i1p1 of the CMIP5 ensemble, in a one-way nesting setup with an intermediate COSMO-CLM nest which has a resolution of 0.22°. The RCP8.5 emission scenario was used for the future simulation. The model domain covers an area in central Europe (Figure C1) and comprises 368 x 306 grid points.

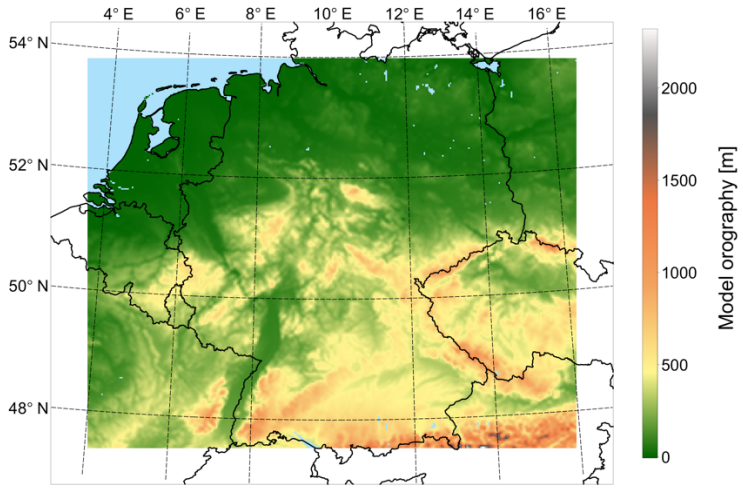

Figure C1: Model domain of the 0.025° simulation. Colors indicate the model orography in the evaluation region. The non-colored margin is the relaxation zone, which is not used for evaluation.

C.2.2 Tracking algorithm

We use a tracking algorithm to obtain convective cell characteristics from model simulations. A detailed description of the tracking algorithm can be found in Purr et al. (2019). In summary, the tracking algorithm consists of three major steps:

Contiguous precipitation areas with precipitation intensity above a threshold of 8.5 mm/h (within 5 minutes), potential convective objects, are identified in the current and the subsequent time step. The minimum cell area is set to 4 grid points.

Wind information is used to predict the position of the cell at the subsequent time step. To this end, a "cone of detection" is set up for each pixel of every cell in the current time step. If a new cell is present in the cone, a probability value is assigned to the origin pixel of the cone, which links this pixel to the new cell.

The probability values of all pixels are summed up for each cell. If a single cell is present in the cone, the corresponding objects from the current and the subsequent time step are connected. If multiple cells are present, the current cell is associated with the cell with the highest probability in the subsequent time step.

Cells are considered for analysis only if they are traceable for at least three time steps. It should be noted that cell mergers and splits are not accounted for. If two cells merge, the cell track with the higher probability of cell association is continued. The other track is regarded as an individual track in itself. The same applies to cells that split. The characteristics that are extracted by the algorithm for each cell are: (1) lifetime; (2) mean intensity, i.e., the temporal and spatial mean over the entire lifetime; (3) maximum intensity, i.e., the highest grid-point intensity during the entire lifetime; (4) maximum area, defined as the maximum instantaneous area over the entire lifetime; (5) precipitation sum, i.e., the total spatial and temporal precipitation sum over the entire lifetime; and (6) mean speed, defined as the temporal mean speed of the cells' center of mass.

C.2.3 Temperature- and moisture-scaling methods

The temperature and moisture scaling of cell characteristics are investigated by assigning 2m-temperature and 2m-dew point temperature to each cell. We use daily mean values of temperature and dew point temperature from the driving, intermediate nest. For each cell, the respective conditions at the start location of the cell are used.

Cells are sorted into bins of 1°C width for both temperature and dew point. For each bin, the 95th and 99th percentiles of the investigated cell characteristics are computed. The scaling rates s_i are computed as the fractional change of the respective quantity (e.g., precipitation sum, maximum intensity, etc.) P from bin i to i+1 as: $s_i = ln\frac{P_{i+1}}{P_i}/(T_{i+1} - T_i)$

where T denotes temperature or dew point temperature for temperature and dew point temperature scaling, respectively.

C.3 Results and discussion

The following section starts by describing the simulations' general precipitation statistics, and putting them into context with other regional climate simulations. Afterward, the frequency distributions, spatial distribution, and diurnal cycle of convective cell characteristics are analyzed in subsection C.3.2. The scaling of these characteristics with temperature and dew point temperature is investigated in subsection C.3.3, followed by a description of the influence of CAPE and wind shear on these scalings.

C.3.1 Mean and extreme precipitation

Mean summer precipitation (Apr-Sep) is reduced by 15% in the future period compared to historical conditions on domain average (Figure C2). The mean temperature change signal in the simulation is +3.4 K. Both values are within the range of the EURO-CORDEX ensemble projections (Jacob et al. 2014). The mean dew point temperature change is +3.0 K. The reduction of precipitation is strongest in the Southwest of the domain covering northeastern France and the Netherlands. In the eastern part of the domain, there is an increase in precipitation.

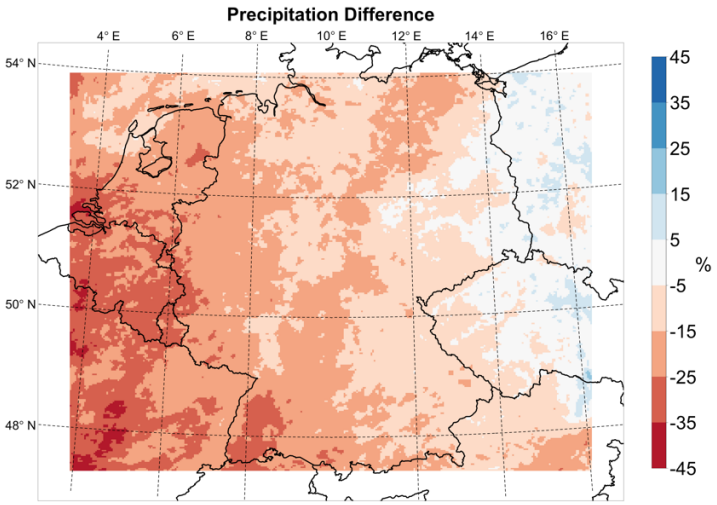

Figure C2: Relative change in mean summer (APR-SEP) precipitation from Historical to RCP8.

Despite the decrease in mean precipitation, the frequency of hourly precipitation intensities above 5 mm/h increases. The relative change is highest for the highest percentiles (Figure C3). Accordingly, mean convective precipitation (defined as spatial and temporal mean of precipitation classified by the tracking algorithm) increases from 0.25 mm/d to 0.29 mm/d, whereas non-classified precipitation decreases from 1.34 mm/d to 1.05 mm/d. This translates to an increase in the fraction of convective to total precipitation from 15.8% to 21.8%.

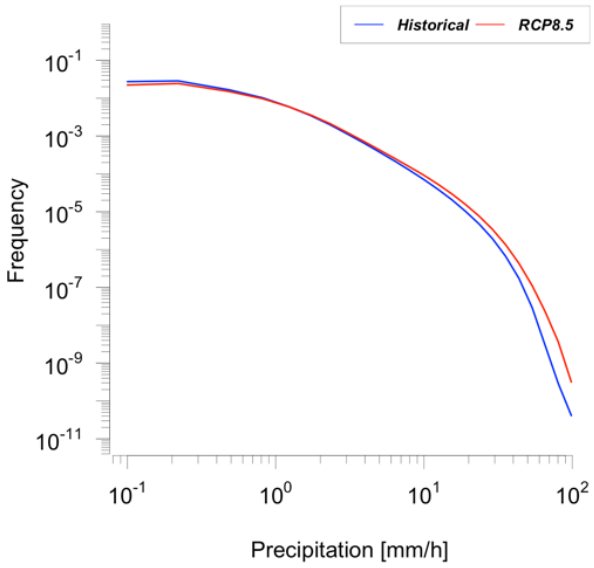

Figure C3: Frequency distribution of hourly precipitation intensity in Historical (blue) and RCP8.5 (red).

C.3.2 Cell characteristics

In this subsection, we investigate the frequency distributions of cell characteristics as well as the diurnal cycle and the spatial distribution of convective cells. The number of cells remains approximately constant. In the future simulation, ca. 5×10^5 cells are detected, which is a decrease of only 0.4% compared to the historical simulation. The frequency distribution of cell lifetime does not change either (Figure C4a). There is a decrease in frequency towards longer lifetimes in both simulations. The median and 99th percentile of cell lifetime are 35 min and 255 min respectively in both *Historical* and *RCP8.5*. There is

a shift towards higher mean (Figure C4b) and maximum intensity. Furthermore, maximum cell area is increasing (Figure C4c). The increase in mean intensity and area results in an increase in total precipitation sum per cell (Figure C4d).

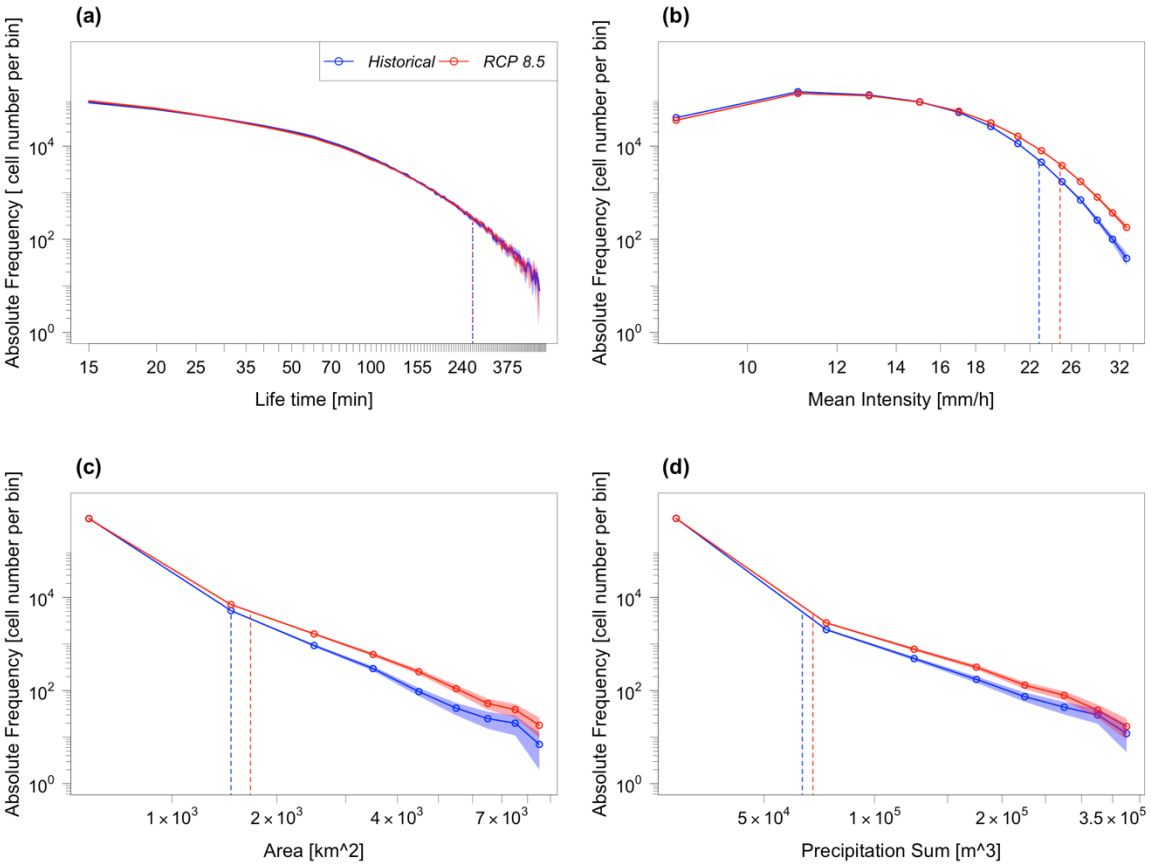

Figure C4: Frequency distribution of cell characteristics in the Historical (blue) and RCP8.5 (red) simulations: (a) lifetime, (b) mean intensity, (c) maximum area, (d) precipitation sum. Shaded areas denote the 95% confidence interval obtained from 1000 bootstrap samples of all cells. Dashed, vertical lines denote the 99th percentiles. Circles show the midpoints of bins.

The relative increase is strongest for the highest percentiles for all of these characteristics (mean and maximum intensity, area, and precipitation sum). However, caution should be taken when interpreting results related to the most severe cells since it has been shown that the precipitation intensity is underestimated by the model especially for long-lasting, organized convection (Purr et al. 2019). Table C1 summarizes the relative changes. The trend scaling (relative changes divided by the mean temperature change signal, Zhang et al., 2017) is slightly above the CC-rate for the highest percentiles of precipitation sum and maximum area and below the CC-rate for mean and maximum intensity.

Table C1: Relative changes in cell characteristics (from Historical to RCP8.5).

Change in %	Lifetime	Max. Area	Precipitation Sum	Mean Intensity	Max Intensity	Mean Speed
Mean	-2.1	+13.4	+18.3	+3.3	+8.3	+9.0
Median	0.0	+9.1	+3.2	+2.4	+5.8	+7.9
P95	0.0	+16.9	+16.9	+6.4	+12.6	+10.0
P99	0.0	+27.9	+27.0	+9.3	+15.8	+11.0
P99.9	+1.1	+32.0	+30.6	+11.3	+19.1	+13.4
Trend Scaling of P99 [%/K]	0.0	+8.2	+7.9	+2.7	+4.6	+3.2

The mean speed of convective cells increases in the future by 9%. The increase is approximately constant for all percentiles showing the highest value for the 99th percentile with +11%. Interestingly, the mean large-scale wind speed in the mid-troposphere, provided by the daily-mean wind speed in the 850 hPa, 700 hPa, and 500 hPa height levels of the driving intermediate simulation does not change accordingly. The overall mean changes in daily mean wind speed are between -0.7% and -3.9% for the 500 hPa and 850 hPa levels. The changes in the 99th percentile of daily mean wind speed are within ± 1% for all three levels. However, when only considering the large-scale wind speed in the presence of convective cells, there is an increase between 4.5% (850 hPa) and 7.7% (500 hPa) in mean wind speed.

Diurnal cycle

Deep convection has a pronounced maximum in the afternoon in mid-latitudes over land caused by solar insulation, which acts to destabilize the boundary layer. The model is capable of reproducing the timing of this maximum with a delay of about 40 min compared to observations (Purr et al. 2019). This characteristic convective maximum is damped in

the future, whereas the number of convective cells increases during the night and morning hours (Figure C5a). In contrast to the number of cells, the mean intensity per cell increases throughout the whole diurnal cycle in the future compared to present conditions (Figure C5b). This increase in precipitation per cell compensates for the drop in the number of cells resulting in only a slight decrease in total convective precipitation in the afternoon and an increase during the nighttime and early morning hours (Figure C5c). These results are in line with the findings of Meredith et al. (2019), who report a shift in the diurnal cycle of extreme precipitation from afternoon to early morning hours for future conditions under RCP8.5 using COSMO-CLM-simulations driven by MPI-ESM.

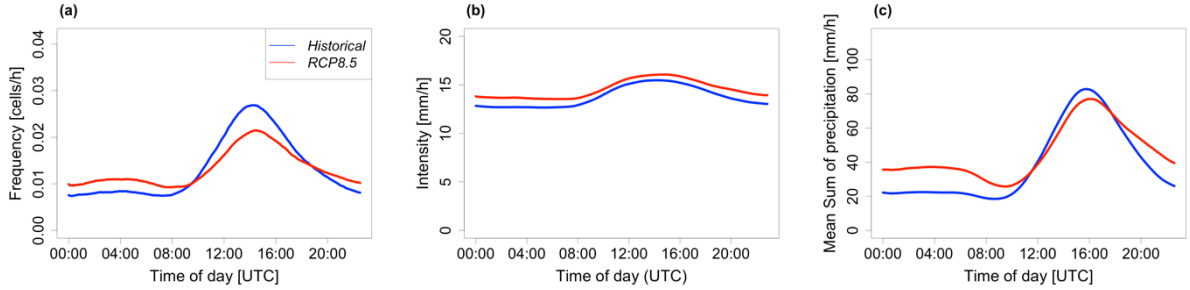

Figure C5: Diurnal cycle of (a) number of cells, (b) mean intensity per cell, and (c) mean sum of convective precipitation.

The increase in cell speed reported in the previous subsection is present during the whole diurnal cycle but is more pronounced at the time of increased convective activity. While the mean speed of cells initiated between 00:00 UTC and 09:00 UTC increases from 3.8 m/s to 4.0 m/s (i.e. 5.2%), this value increases from 3.2 m/s to 3.5 m/s (i.e. 8.8%) for cells initiated between 09:00 UTC and 18:00 UTC. This increase during the daytime is mainly caused by fewer slow-moving cells. Stratifying cells as slow-moving (< 3.3 m/s) and fast-moving (> 3.3 m/s) shows that the number of slow-moving cells decreases by 24%, whereas the number of fast-moving cells decreases by 5% during the daytime. This decrease in slow-moving cells is not present during nighttime, where slow-moving cells increase by 22%, and fast-moving cells increase by 34%.

Spatial distribution

The spatial distribution of convective cells is tightly coupled to the orography in Germany since mountains can initiate deep convection through various processes. The regions of highest convective activity in Germany are the alpine and pre-alpine area as well as the

Black forest with values up to 4 times as high as in the flatlands of Northern Germany (Figure C6a). The model is capable of reproducing the observed spatial distribution of convective cells in Germany with a tendency to overestimate convective activity in the mountains and to underestimate it slightly in the lowlands (Purr et al. 2019).

The total number of cells stays approximately constant in the future, but the change in cell number varies considerably in space (Figure C6b). In South-West Germany, the number of convective cells decreases while in the North-East increases prevail. However, these changes are not uniform, and changes between increases and decreases occur at small spatial scales of about 10-100 km. This pattern is not related to orography and likely caused by internal variability of the convective cells. Mean intensity increases throughout the domain. The sum of convective precipitation, which can be derived as cell number times mean intensity, therefore, shows a pattern similar to the number of convective cells (Figure C6c).

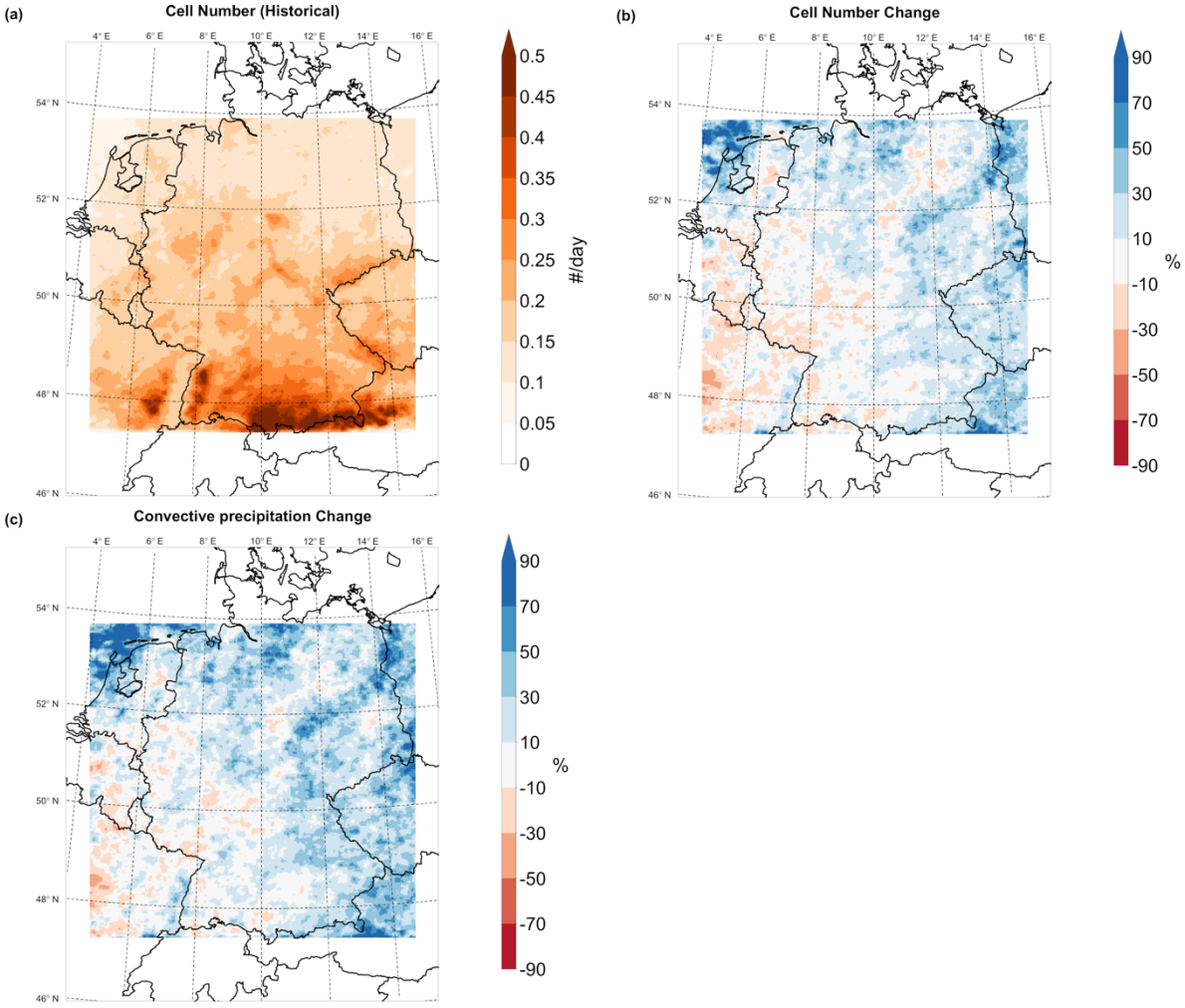

Figure C6: Spatial distribution of (a) cell number in the Historical simulation, (b) relative change in cell number in RCP8.5, and (c) relative change in convective precipitation sum.

C.3.3 Temperature and moisture scaling

In this subsection, we investigate the scaling of cell properties with temperature and dew point temperature as a measure for absolute humidity. The highest percentiles of cell area, mean intensity, maximum intensity, and precipitation sum increase with temperature. All of these characteristics follow a qualitatively similar increase up to a specific temperature. Above this temperature, the scaling curves level off. In contrast to this, lifetime does not increase with temperature. The scaling rates under historical conditions are in close agreement with the temperature scaling in a simulation using a similar setup with ERA-Interim reanalysis as driving data instead of the EC-Earth model (Purr et al. 2019). There

are two main differences between modelled and observed scaling of cell characteristics. Firstly, the lifetime of cells does not increase with temperature in the model, whereas it does in the observations. Secondly, mean intensity levels off in the simulations whereas it increases constantly, even at high temperatures, in the observations which can be attributed to the underestimation of intensity in long-lasting, severe cells mentioned previously.

While maximum intensity and area increase close to the Clausius-Clapeyron rate at the intermediate temperature range between 10 °C and 20 °C, mean intensity scales at considerably lower values (Figure C7a,c, and e). Precipitation sum shows super CC-scaling in the intermediate temperature range and a drop-off at high temperatures (Figure C7g). The peak values for all of these characteristics are higher in the future compared to historical values and occur at higher temperatures. Thus, the scaling curves show the same characteristic shift that is well known for extreme precipitation at fixed-locations (Prein et al. 2017a, Knist et al. 2018) and is also found in this study (Figure S1). Furthermore, the number of cells occurring at high temperatures which have a higher potential for large precipitation sums, areas, and intensity increases (Figure C7i).

To investigate the influence of limited moisture supply at high temperatures, which has been suggested as a cause for the drop off at high temperatures, we investigate the scaling of cell properties with dew point temperature. As expected, there is no drop off at high dew point temperatures, and the scaling rates are more continuous across the whole dew point range. The maximum area increases at rates slightly above the Clausius-Clapeyron rate (Figure C7b). The scaling rates for present and future conditions do not differ significantly. Also, the 99th and 95th percentile's absolute values of do not differ significantly in present and future conditions.

The scaling rates for the maximum intensity are remarkably close to the Clausius-Clapeyron rate (Figure C7d). Interestingly, the 90th (not shown) and the 95th percentile values are smaller in the future compared to present conditions; the values for the 99th percentile are closer. This also implies that the scaling rates under future conditions (7.4%/K for the 99th percentile) are a little higher than under historical conditions (6.1%/K).

Like for temperature, the mean intensity scales at values lower than the CC-rate (Figure C7f). Again, the absolute values for the 90th and 95th percentile under historical conditions are higher than the future values for a large part of the dew point temperature range up to 17 °C. This indicates that changes in other factors (like atmospheric instability) influence

the cell properties in the future. The precipitation sum scales at values of about 14%/K close to twice the CC-rate (Figure C7h).

More cells occur at high moisture levels in the future (Figure C7j). The increase in number at high dew point temperatures is compensated by a decrease at low dew point temperatures. While only 0.4% of all cells at present conditions occur at dew point temperatures above 18°C, in future conditions this ratio increases to 8.5 % Thus, the increase in the high percentiles of the overall frequency distribution of cell properties is largely caused by more cells occurring at higher moisture levels in the future. However, when looking at the relative number of cells per dew point bin (the number of cells per dew point bin divided by the number of occurrences of the dew point bin) as indicated by the lines in Figure C7j, we see apparent differences in present and future conditions. For dew point temperatures up to 18 °C, the relative number of cells is substantially lower in the future. For higher humidity levels, the relative number increases in the future while it decreases in the present. In contrast, the relative number of cells per temperature bin follows the same curve in the future with a maximum at 18 °C (Figure C7i).

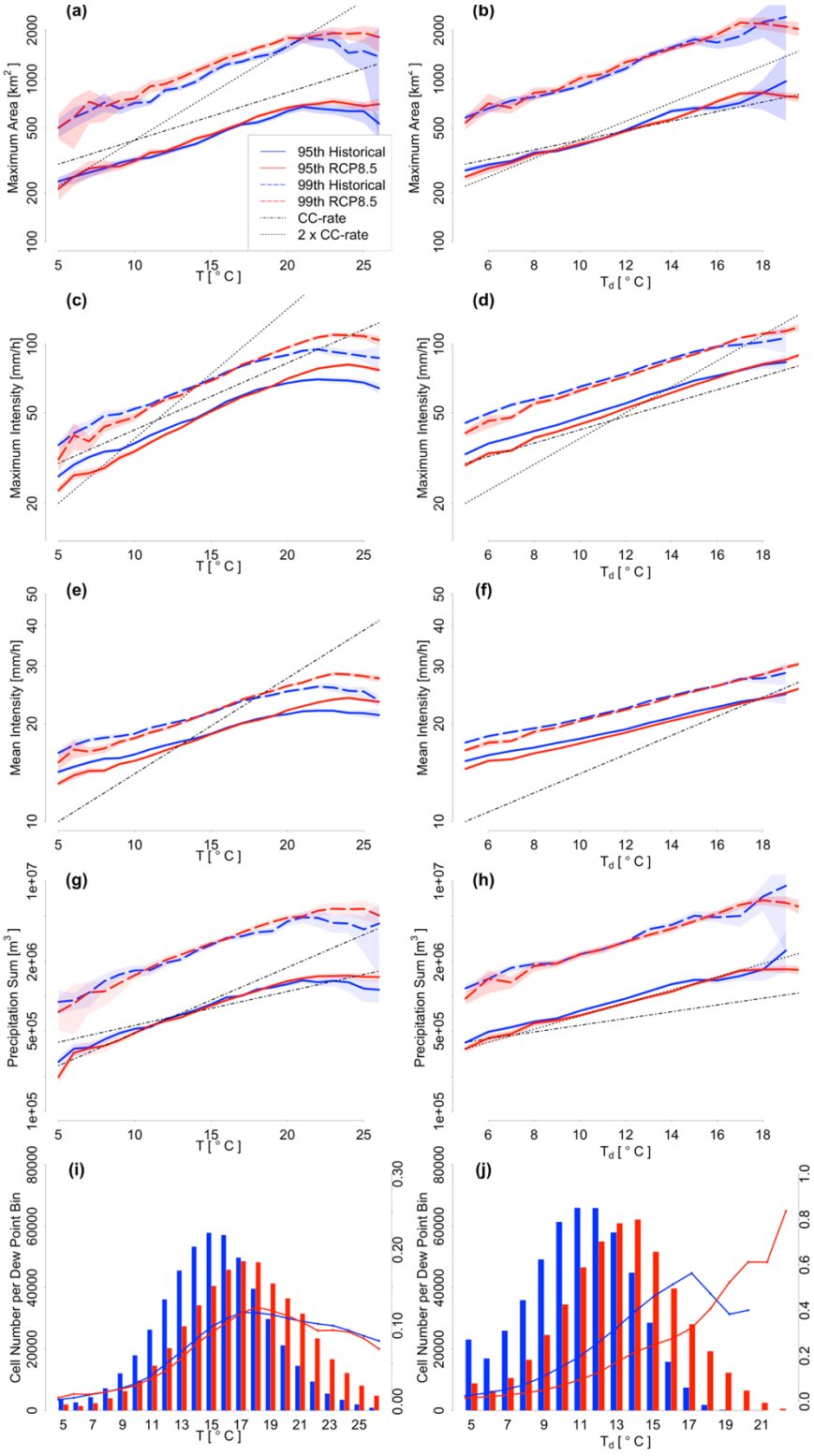

Figure C7: Temperature scaling (left column) and dew point temperature scaling (right column) of cell properties. (a) and (b): maximum area; (c) and (d): maximum intensity; (e) and (f): mean intensity; (g) and (h): precipitation sum. Shaded areas denote the uncertainty range caused by varying bin occupancy, obtained from bootstrapping cells in each bin. (i) and (j) show the frequency distribution of cells, where bars denote the absolute number of cells per temperature or dew point class (left y-axis) and lines denote the relative number of cells per occurrence of temperature or dew point temperature class (right y-axis).

C.3.4 Influence of static instability and wind shear

Since static instability plays a major role in determining the severity of atmospheric convection, we investigate the influence of CAPE on the moisture scaling of cell properties. In addition, the direct influence of CAPE and wind shear is investigated in Appendix S1.
From conceptual models, it can be shown that CAPE increases with warming. Specifically, peak CAPE in a continental environment which is characterized by not being in radiative-convective equilibrium scales with moisture at the CC-rate (Agard and Emanuel, 2017). These findings obtained from a simplified conceptual model are also supported by more complex regional climate models. Púčik et al. (2017) investigated the occurrence of storm environments and found an increase in static instability under warmer conditions.
In our simulations, the highest percentiles of daily maximum CAPE increase with dew point temperature at varying rates well above the CC-rate. Since high dew point values are much more abundant in the future, this leads to a strong increase in extreme CAPE values. As an example, the frequency of daily maximum CAPE exceeding 2000 J/kg increases from 0.8% to 2.2%. The connection between the increase in CAPE and high dew point temperature is not uniform but occurs mostly at high dew point levels. To investigate the effect of instability on the moisture scaling of cell properties, we stratify the convective cells according to environmental CAPE. Cells which occur at CAPE values below 200 J/kg are classified as low-CAPE cells while those above 200 J/kg are classified as high-CAPE cells. As expected, cells occurring at high CAPE are more extreme than low-CAPE cells, as illustrated by the 99th percentile of precipitation sum for high-CAPE cells and low-CAPE cells in Figure C8a. Despite the overall increase in CAPE, the scaling rates do not change from historical to future conditions. The scaling rate of precipitation sum per cell is below the 2xCC-rate found for all cells when considering only low-CAPE (historical: 5.9 %/K, RCP8.5: 9.2 %/K) cells or only high-CAPE cells (historical: 10.4 %/K, RCP8.5: 8.8 %/K). The reason for this is that more low-CAPE cells occur at low dew point temperatures and more high-CAPE cells occur at high dew point temperatures so that the overall scaling curve follows the lower values of the low-CAPE curve at low dew point temperature and shifts towards the high-CAPE curve at high dew point temperatures.

We now investigate the influence of wind shear on the scaling rates. We calculate wind shear as the difference between the wind in the 850 hPa and 500 hPa height levels. Higher wind shear leads to higher organization of convective cells. Thus, it is not surprising that higher wind shear leads to higher precipitation sum per cell (Figure C8b). The frequency distribution of wind shear does not change in the future. In contrast to CAPE, wind shear and dew point temperature are not correlated. As a result, an equal number of low- and high-wind shear cells occur at each dew point bin. The scaling rates are identical for low-wind shear and high wind shear cells.

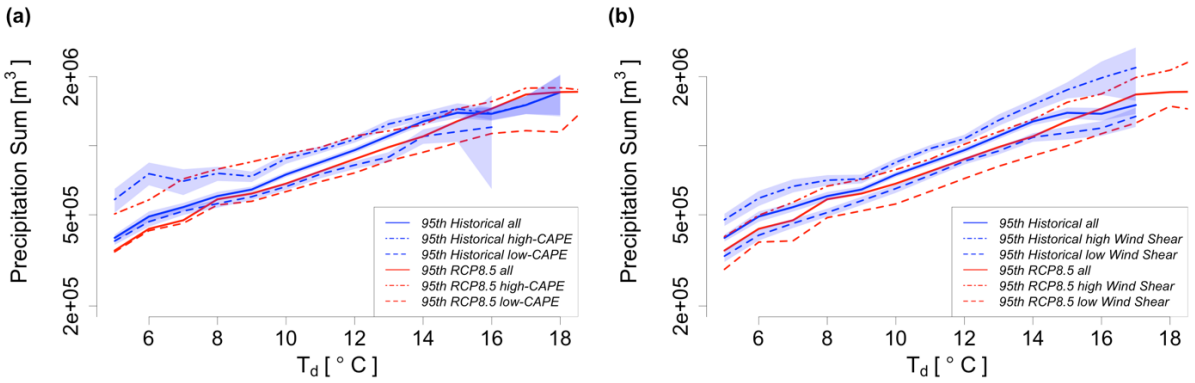

Figure C8: Dew point scaling of precipitation sum dependent on (a) environmental daily maximum CAPE, and (b) wind shear. Shaded areas denote the uncertainty range obtained from bootstrapping. The uncertainty range for the future period is omitted for readability.

C.4 Conclusions and outlook

We investigated how the characteristics of convective cells might change in a climate change scenario by applying a tracking algorithm to CPM precipitation with high temporal resolution. Changes in the frequency distribution of cell characteristics show a complex picture of the response of deep convection to climate warming. While the total number of cells and the lifetime does not change significantly in the future, as simulated for the end of the 21st century under RCP8.5, there is a shift towards larger and more intense events. In combination, this leads to higher precipitation sums per cell. We showed that the increase in extreme hourly precipitation is caused by an increase in the number of large, long-living convective cells occurring at high temperature and moisture levels.

The diurnal cycle of convective activity changes towards fewer convective cells during the afternoon maximum and more cells during the nighttime. In combination with the increase in mean precipitation intensity per cell this leads to up to 50% more convective precipitation during nighttime and a small decrease during the afternoon maximum. The afternoon decrease in cell number is primarily caused by fewer slow-moving cells despite the fact that there is no change in the large-scale wind speed. This suggests that there is less air mass convection in the future, which would be in line with the findings of Rasmussen et al. (2018), who report a shift towards more extreme and less moderate events because of increased CAPE and CIN values. The increase during evening and nighttime could be explained by the fact that once convection is initiated, the tendency towards more intense cells implies that these cells produce stronger cold pools which can trigger new cells.

The temperature scaling curves of cell properties peak at higher values in the future, which is caused by more abundant humidity at these high temperatures, resembling the scaling curves of extreme hourly precipitation at fixed locations. In contrast to the temperature scaling, dew point scaling curves in historical and future conditions are consistent across the whole dew point range.

The Clausius-Clapeyron scaling of cell area and maximum cell intensity in combination leads to super Clausius-Clapeyron scaling (ca. 14%/K) of the precipitation sum per cell. As a cause for super Clausius-Clapeyron scaling of extreme precipitation, a positive feedback of updraft strength with moisture supply has been discussed in the literature (Lenderink et al., 2017). While this may indeed contribute to super Clausius-Clapeyron scaling, we point out that the correlation of dew point temperature with CAPE may be a simple reason that can partially explain scaling above the Clausius-Clapeyron rate.

The scaling curves under historical and future conditions are most similar for the highest percentiles. The differences for the lower percentiles reflect the complex changes in the properties of convective cells related to, e.g., the change in diurnal cycle. The similar dew point scaling curves for the highest percentiles of cell characteristics facilitate inference of the upper limit of convective cell properties from large scale humidity values. However, the fact that the number of convective cells per dew point bin changes both in absolute and relative terms (number of cells per occurrence of dew point bin) prevents inference of extreme precipitation at fixed locations. This is also illustrated by the differences in the dew point temperature scaling curves of extreme precipitation at fixed locations.

While one CPM simulation is not sufficient to robustly estimate the increase in extreme precipitation, the Lagrangian approach adopted here can help to understand processes related to deep convection. More projections are necessary to determine the uncertainty related to large-scale changes in the general circulation because general circulation models vary in their representation of climate change in mid-latitudes. Common deficiencies that currently limit the skill of convection-permitting climate models at the kilometer scale include the representation of cold pools as a trigger mechanism (e.g. Hirt et al., 2020). Furthermore, the tracking algorithm could be enhanced to include the merging and splitting of convective cells. This would facilitate the investigation of convective organization, a topic mainly investigated in idealized simulations so far (Lochbihler et al., 2019; Moseley et al., 2016).

Acknowledgements

We thank the „Hessisches Landesamt für Naturschutz, Umwelt und Geologie“ and the „Rheinland-Pfalz Kompetenzzentrum für Klimawandelfolgen“ for funding the project „Konvektive Gefährdung über Hessen und Rheinland-Pfalz“ in the course of which the results of this paper were obtained. The simulations were performed on the LOEWE-CSC high-performance computer of Frankfurt University.

Supplementary Material

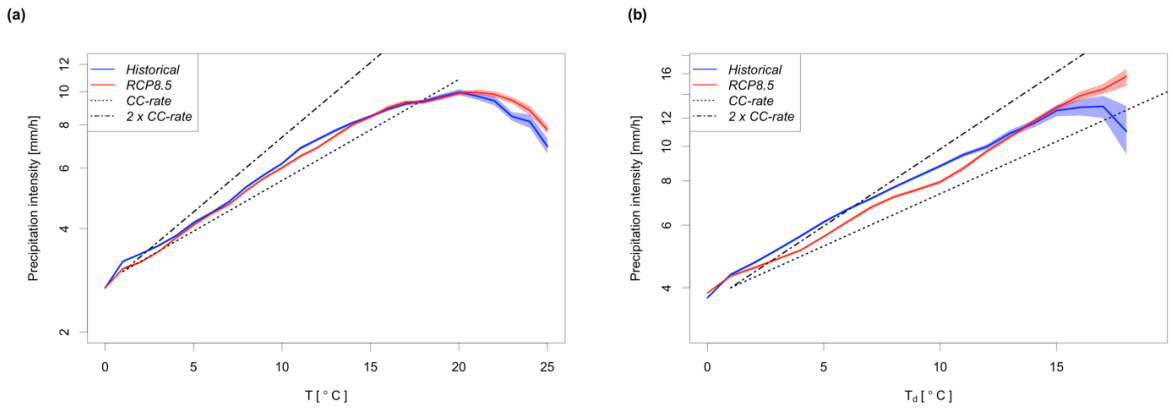

Figure S1: Temperature scaling (a) and dew point scaling (b) of hourly precipitation at fixed location.

The figure shows the scaling of hourly extreme precipitation at fixed location ("Eulerian" scaling). The scaling curves are calculated following Lenderink and van Meijgaard (2008) and Knist et al. (2018). The daily maximum of hourly precipitation is related to daily mean values of 2 m-temperature and 2 m-dew point temperature.

Appendix S1

Dependence of cell characteristics on CAPE and wind shear

In analogy to the temperature and dew point scaling in subsection 3.3, we investigate the changes in the highest percentiles of cell characteristics with CAPE and wind shear in this appendix. In contrast to dew point and temperature scaling, absolute values of the cell characteristics differ in present and future conditions. The future values are higher than the present values for all characteristics across the whole CAPE and wind shear range showing the effect of increased dew point temperature in the future. The maximum area of cells increases with CAPE and wind shear at approximately the CC-rate. In contrast, maximum intensity does not increase consistently with CAPE and even shows a decrease with wind shear. This decrease is surprising as one would expect an increasing degree of convective organization with increasing wind shear and thus higher maximum intensities. Maybe this effect is overcompensated by higher cell velocity, as higher wind shear implicates higher wind speeds steering the convective cells (and thus, distributing the extreme precipitation over multiple grid boxes). Changes in mean intensity are qualitatively similar to changes in maximum intensity. The precipitation sum of cells increases with both CAPE and wind shear at varying rates. Concerning the number of cells, in the future more cells occur in high-shear environments and fewer cells occur in low-shear environments. This supports the hypothesis that it is harder to initiate deep convection without dynamic trigger mechanisms like fronts or convergence lines associated with high shear in the future.

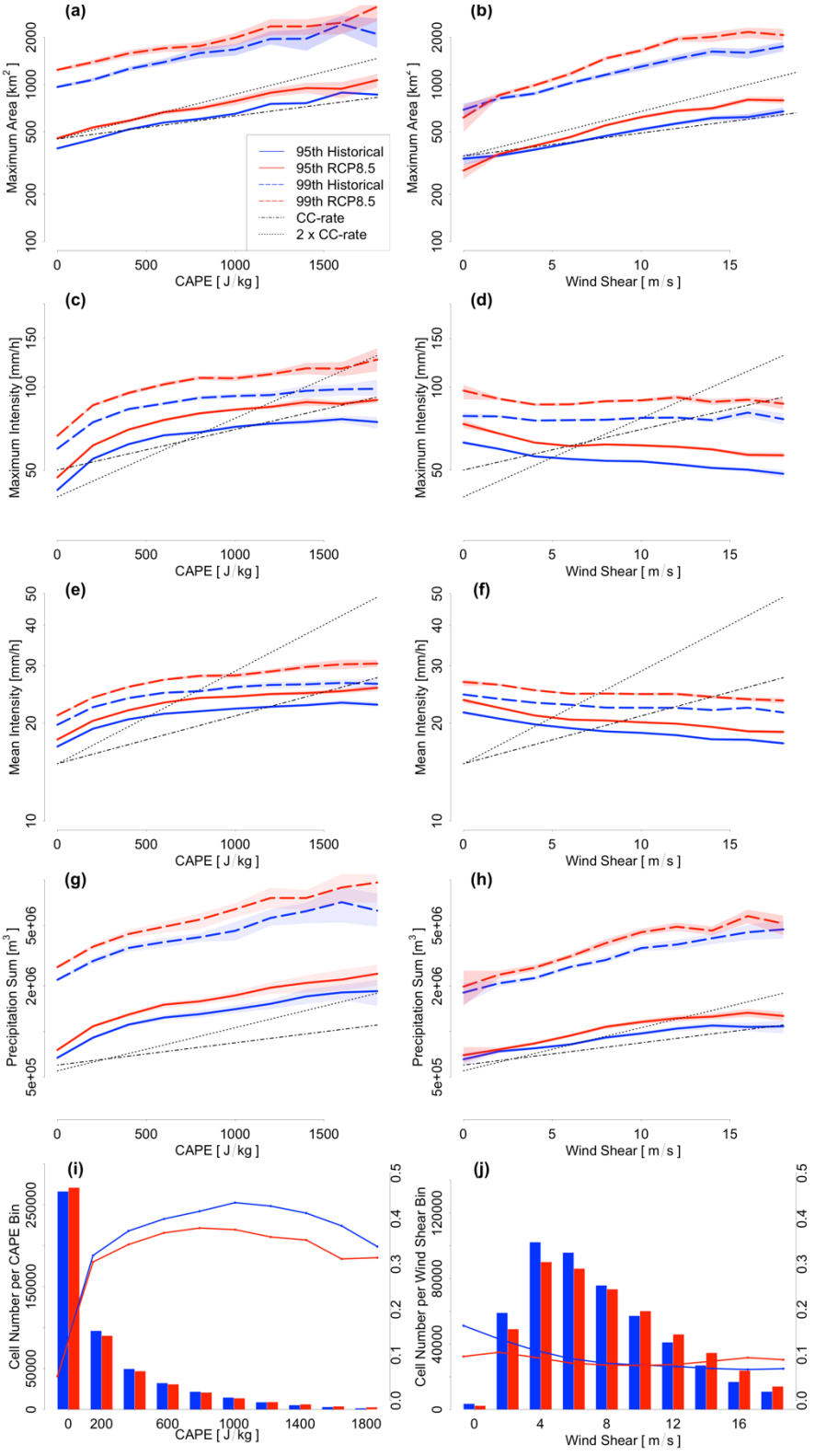

Figure S 2: Dependency of cell characteristics on CAPE and wind shear. Layout same as Figure 7.

D. Evaluation of Cell Characteristics in a CCLM Simulation Driven by ERA5

D.1. Motivation

While the evaluation of convective cell characteristics in COSMO-CLM conducted in paper 2 showed promising results, a few shortcomings were also noticeable.
To test if these shortcomings are inherent to the model or caused by simulation settings we evaluated another COSMO-CLM simulation. This simulation was conducted by Susanne Brienen at DWD in the framework of the research project *"Network of Experts - Adapting transport and infrastructure to climate change and extreme weather events".* While this is not a systematic sensitivity analysis of different model parameters, using this additional simulation can provide valuable insight as these are the first convection-permitting simulations with sub-hourly precipitation output for Germany.

D.2. Model Setup

The two simulations differ in a number of ways. Most notably, the driving reanalysis data is different, which is why we name the two simulations accordingly: CCLM-ERAi and CCLM-ERA5. As ERA5 is the newer reanalysis it has a number of advantages compared to ERA-Interim. It has a higher spatial resolution which enables the direct nesting of COSMO-CLM in the reanalysis. Furthermore, it provides a higher temporal resolution.
Another important difference is the simulation domain. The simulation domain of CCLM-ERA5 is bigger, including Austria and Switzerland in the South and Denmark in the North (Figure D1). Other important model parameters are summarized in Table D1.

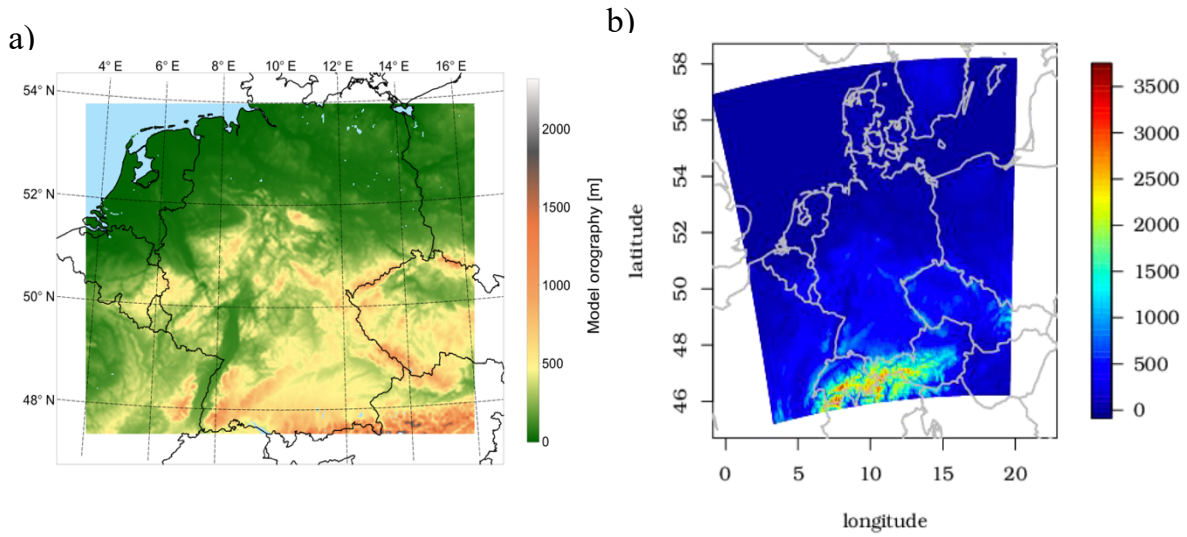

Figure D1: Simulation domains and orography of the two simulations. (a) CCLM-ERAi, (b) CCLM-ERA5.

Table D1: Model configurations of the two simulations.

Name	CCLM-ERAi	CCLM-ERA5
Model version	COSMO5.0_clm7	COSMO5.0_clm16
Frequency of boundary data	6h	1h
Intermediate nest	Yes	No
Grid spacing	0.0275°	0.0275°
Shallow-convection	On	On
Microphysics	1-moment with graupel	1-moment with graupel

D.3. Differences in applying the tracking algorithm

For the CCLM-ERAi simulation, the necessary wind information for using the tracking algorithm had to be taken from the intermediate nest as wind data was not stored for the inner nest. In contrast, the wind information for CCLM-ERA5 was taken directly from the inner nest. This leads to a better performance of the tracking algorithm, meaning the cells can be tracked for longer times, in CCLM-ERA5. However, this complicates the compari-

son to the observations where ERA-Interim wind data (interpolated in time to 5 min) is used for tracking.

D.4. Results

D.4.1. Mean Precipitation (for fixed location)

There is more precipitation in CCLM-ERA5 than in CCLM-ERAi in the evaluation period 2001-2015 (Figure D2). While total precipitation is overestimated by 6% in CCLM-ERA5 compared to the radar observations, it is underestimated by 14% in CCLM-ERAi. Both simulations overestimate precipitation in the mountain ranges, especially the Black forest. The CCLM-ERA5 simulation only underestimates precipitation along the North-Sea and parts of Schleswig-Holstein, whereas CCLM-ERAi underestimates precipitation in Northern Germany and parts of Hessen and Rheinland-Pfalz.
During the summer months (Apr-Sep) mean precipitation is well simulated in CCLM-ERA5 with overestimation in the mountain ranges which is compensated by underestimation in the low-land. CCLM-ERAi underestimates precipitation more strongly in the summer months (-34%). Again, the underestimation is focused on Western and Northern Germany.

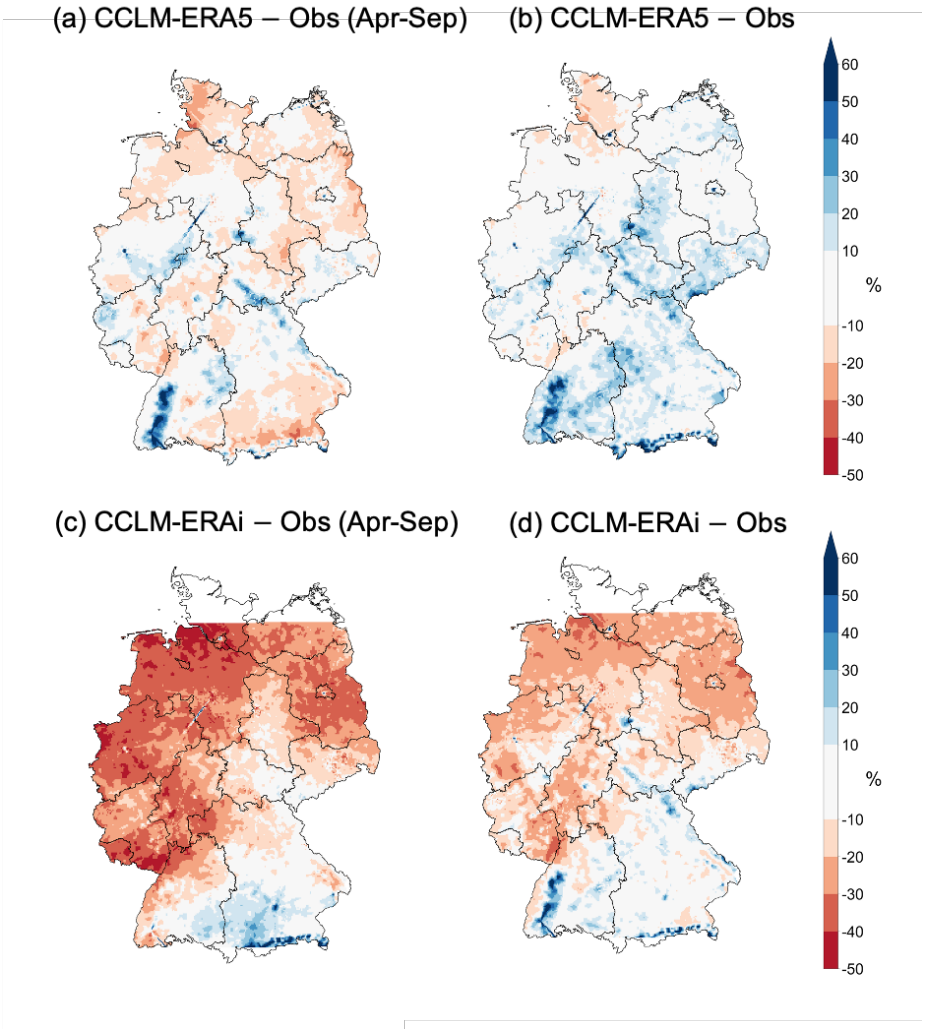

Figure D2: Mean precipitation bias in period 2001-2015. (a) CCLM-ERA5 summer months, (b) CCLM-ERA5 full year, (c) CCLM-ERAi summer months, (d) CCLM-ERAi full year.

D.4.2. Frequency distributions of convective cell characteristics

Both simulations match the frequency distributions of cell characteristics quite well compared to radar data (Figure D3). However, there are more long-living cells in CCLM-ERA5 which could be caused by the better performance of the tracking algorithm. Maximum cell intensity is better simulated in CCLM-ERA5. The Perkins Skill Scores for both simulations are summarized in Table D2.

Table D2: Perkin's Skill Scores for different cell characteristics.

	CCLM-ERAi	CCLM-ERA5
Lifetime	0.84	0.81
Precipitation Sum	0.98	0.99
Maximum Area	0.99	0.98
Maximum Intensity	0.84	0.87

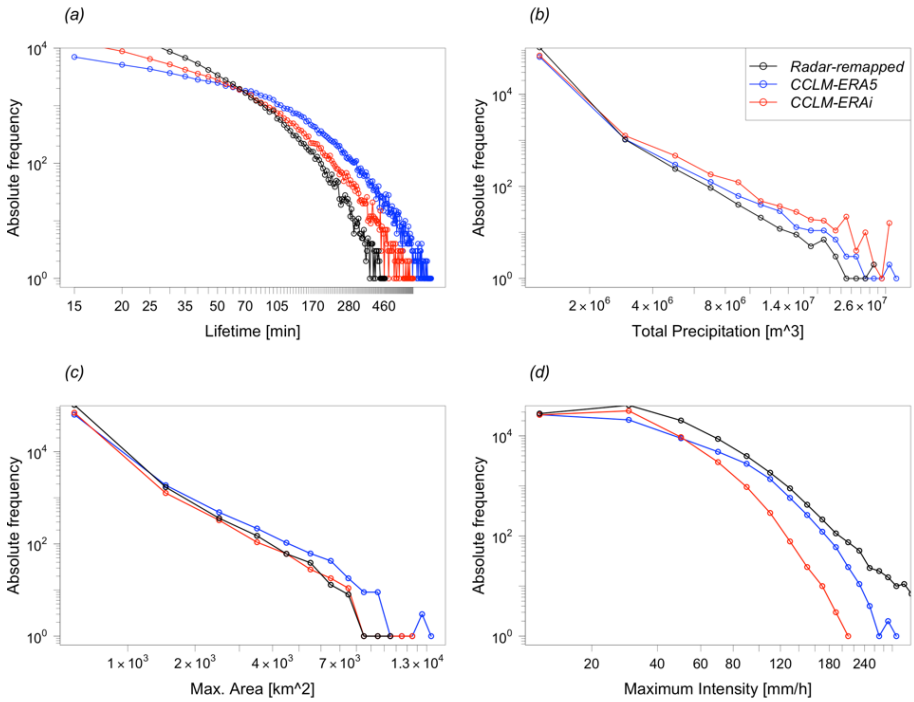

Figure D3: Frequency distributions of cell characteristics; (a) lifetime, (b) total precipitation, (c) maximum area, and (d) maximum intensity.

D.4.3. Diurnal cycle

The diurnal cycle of convective cells is better represented in CCLM-ERA5 (Figure D4). While the diurnal cycle of cell initiation is virtually similar with a slightly later peak in CCLM-ERAi (Figure D4a), the amplitude and phase of the diurnal cycle is more realistic in CCLM-ERA5 when counting cells multiple times according to their lifetime (Figure D4b). Furthermore, phase and amplitude of the diurnal cycles of mean and maximum intensity are much better represented in CCLM-ERA5 (Figure D4c and Figure D4d) as they do not underestimate the amplitude as strongly as CCLM-ERAi. For example, the diurnal

maximum of mean intensity is 18.7 mm/h in the observations, 17.8 mm/h in CCLM-ERA5, and 16.1 mm/h in CCLM-ERAi.

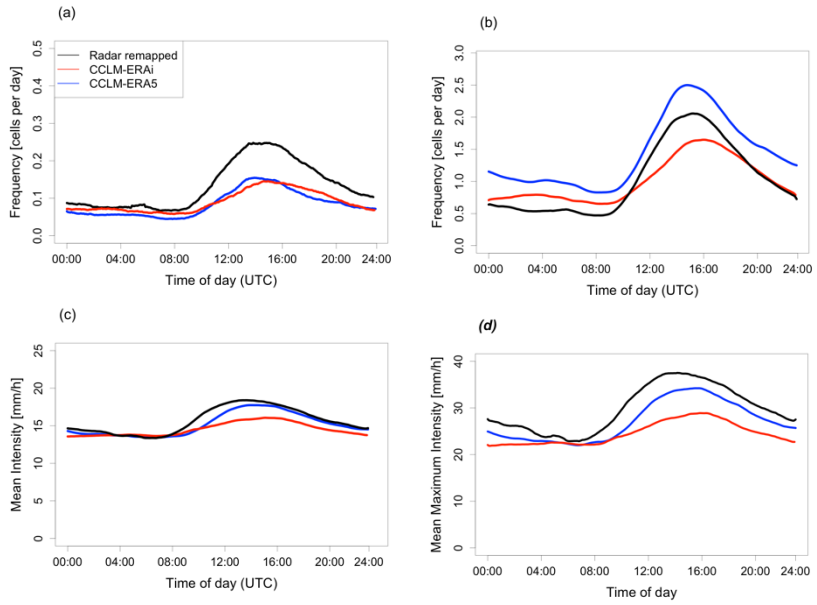

Figure D4: Diurnal cycle of (a) cell frequency with every cell counted once (at initiation), (b) cell frequency with every cell counted for every 5-min timestep, (c) mean intensity, and (d) maximum intensity.

D.4.4. Spatial distribution of convective cells

In this section, we first compare the spatial distribution of convective cells at initiation in the CCLM-ERAi and the CCLM-ERA5 simulation. Afterward, we use the method presented in paper 2, where every occurrence of a cell per 5-minute timestep is counted. Using the initiation of cells mitigates the effect of the more efficient tracking in CCLM-ERA5.

Both simulations can simulate the spatial distribution of increased initiation of convection in the alpine area and the lower mountain ranges (Figure D5) but generally underestimate the initiation of convection. CCLM-ERAi initiates more convection in the pre-alpine area than CCLM-ERA5. This could be explained by the larger domain of CCLM-ERA5 which allows for convection to be triggered over the entire alps. Assuming a southerly flow, this would mean that convective cells have already depleted when reaching the northern end of the Alps. The underestimation of convective activity in Northern Germany (North of 52°N) is stronger in CCLM-ERAi (-47%) than in CCLM-ERA5 (-40%).

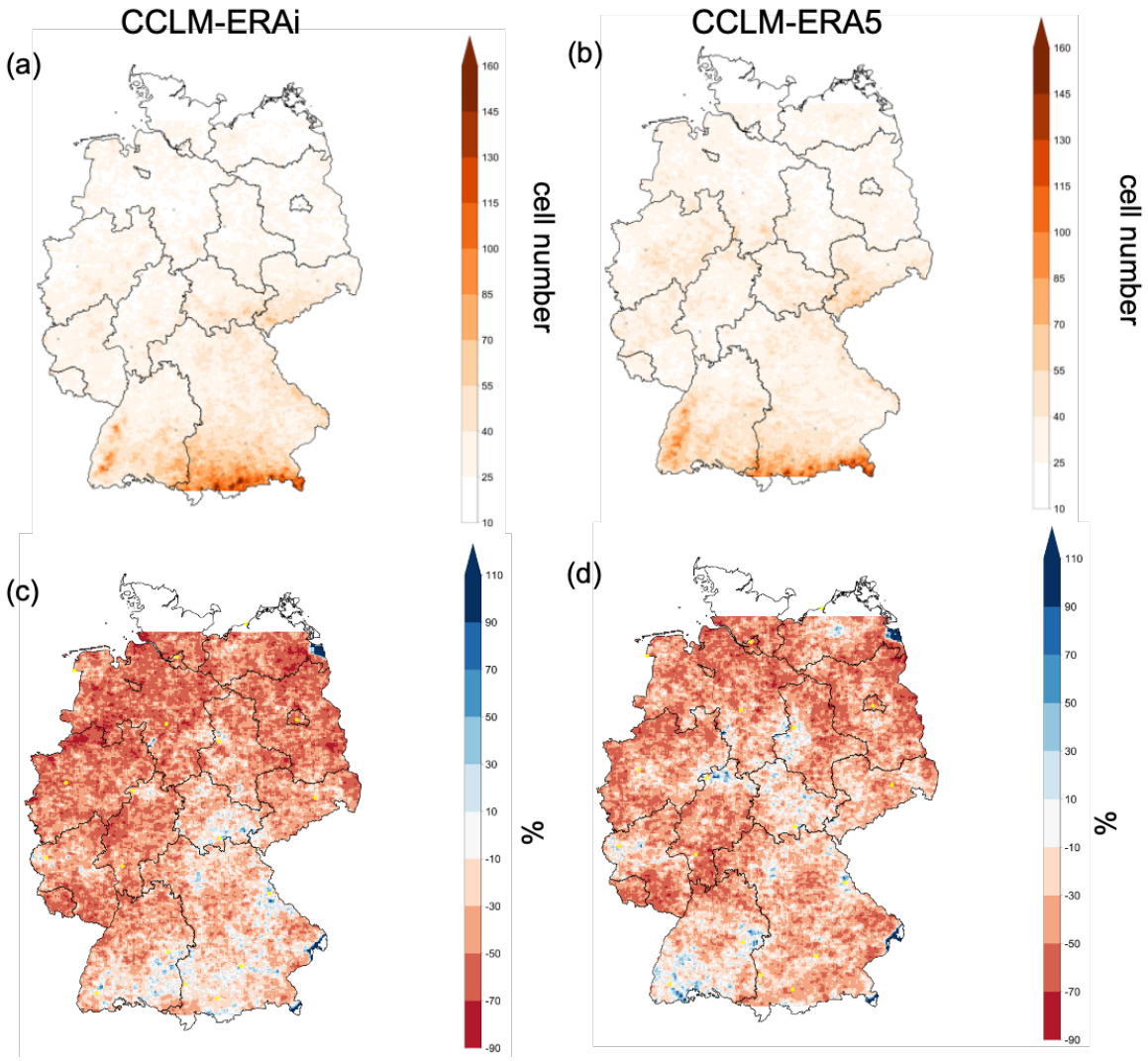

Figure D5: Spatial distribution of (a) convective cells at initiation in CCLM-ERAi, (b) convective cells at initiation in CCLM-ERA5, (c) relative Difference CCLM-ERAi to observations, and (d) relative difference CCLM-ERA5 to observations.

When counting every 5-min occurrence of cells according to their lifetime, CCLM-ERAi overestimates the number of convective cells in the South and underestimates it in the North. CCLM-ERA5 overestimates the number of cells everywhere. In both simulations, the cell number is overestimated near radar locations. Areas of underestimation tend to be located furthest away from the radar. Despite the general overestimation, the spatial distribution of cell is better captured in CCLM-ERA5. While cell number is underestimated predominantly in Northern Germany in CCLM-ERAi, the overestimation is more regularly distributed over Northern and Southern Germany in CCLM-ERA5.

D.5. Conclusions

Both simulations can represent the frequency distributions of cell characteristics showing the spectrum from short-living, unorganized convection to long-living, organized convection, as well as the North-South gradient and the elevation dependence of convective activity. CCLM-ERA5 has a number of advantages potentially caused by the larger simulation domain and more realistic boundary conditions. It can better represent the diurnal cycle of convection. Both the phase and amplitude of convective activity is closer to observations in CCLM-ERA5. Furthermore, the afternoon increase in the intensity of convective cells is much better represented. A drawback of CCLM-ERA5 is the higher overestimation of cell lifetime which is potentially caused by the better performance of the tracking algorithm. The spatial pattern of mean precipitation and convective cells is better represented in CCLM-ERA5 with a lower underestimation of precipitation in the Northern low-lands of Germany than CCLM-ERAi.

E. Convective Rain Cell Characteristics and Scaling in a CCLM Simulation Driven by MIROC5 for Germany

E.1. Motivation

As general circulation models vary in their representation of climate change in mid-latitudes, the results of paper 3 which are based on one GCM-CPM combination are subject to large uncertainty (see Outlook of paper 3). Because of this, it is very beneficial to reproduce the investigations using another simulation. Here, we use a CCLM simulation driven by MIROC5 conducted by Michael Haller at DWD.

E.2. Model setup

The MIROC5-driven simulation (MIROC5-CCLM) described here differs from the EC-Earth driven simulation (ECE-CCLM) in the following ways:

- nesting strategy: a downscaled CCLM simulation at 0.11° horizontal resolution taken from the EURO-CORDEX ensemble is used as intermediate nest instead of a 0.22° simulation
- simulation domain: the simulation domain is bigger, including Austria and Switzerland in the South and Denmark in the North similar to the ERA5-driven simulation (Figure D1b)
- parameterizations: similarly to ECE-CCLM a one-moment microphysics scheme including graupel is used and the parameterization of shallow convection is switched on

E.3. Results

E.3.1. Mean quantities

Total mean precipitation remains virtually constant in RCP8.5 compared to Hist at 2.1 mm/d. Precipitation increases mainly in Germany , Poland, Denmark and the Northern and Baltic Sea (Figure E1). It decreases in the Alps and the West of the simulation domain. Precipitation in the summer months (Apr-Sep) decreases by 9% from 2.0 mm/h in Hist to 1.8 mm/h in RCP8.5. Thus, this projection shows a smaller decrease than the EC-Earth driven simulation (-15%). Again, the decrease is strongest in the Alps and in the West of the simulation domain. In central Germany, summer precipitation is projected to increase slightly.

The mean temperature change is 4.4 K in the full simulation domain and 4.5 K in the ECE domain. It is higher than the temperature change in the EC-Earth simulation of 3.4 K. The spatial and temporal mean of convective inhibition (CIN) increases from present to future conditions in magnitude from -21.7 J/kg to -38.5 J/kg. CIN values at the starting point and starting time of convective cells change from -106.3 J/kg to -148.1 J/kg. Convective available potential energy (CAPE) increases from 30.4 J/kg to 55.3 J/kg in the spatial and temporal mean, and from 306.1 J/kg to 415 J/kg at the starting point and starting time of convective cells.

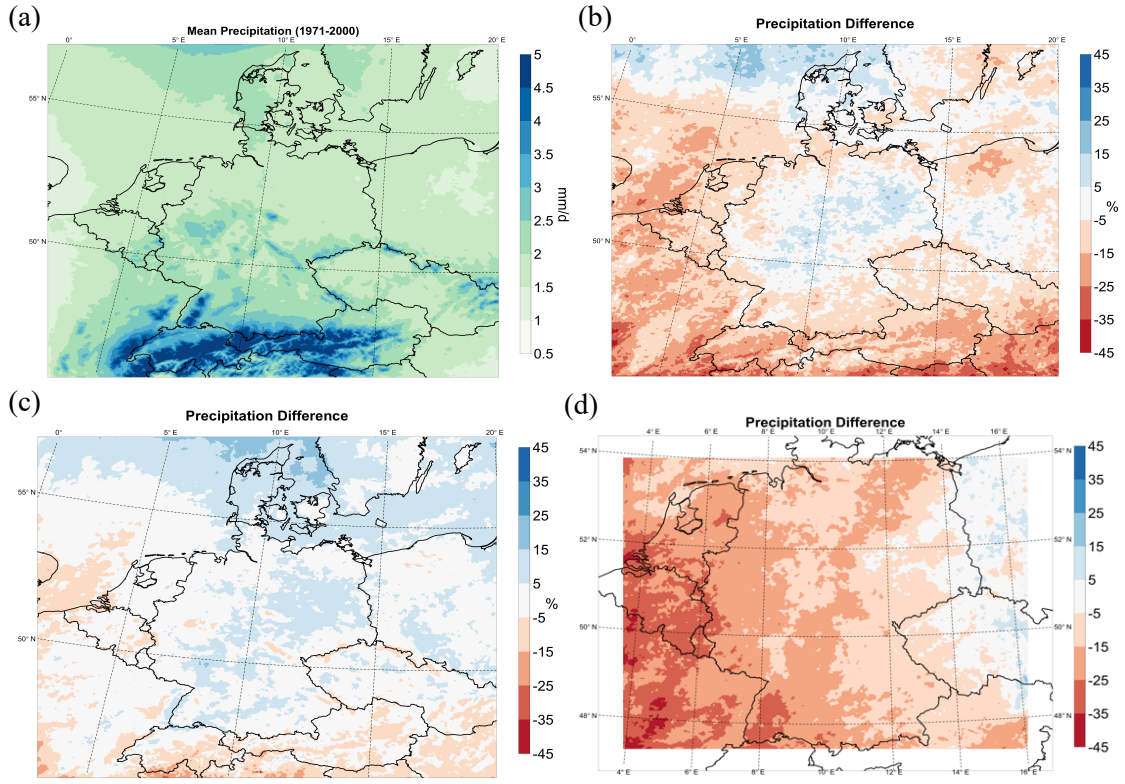

Figure E1: Mean precipitation. (a) historical, (b) difference RCP8.5 (2071-2100)-Hist (1971-2000) in Apr-Sep, (c) difference RCP8.5 (2071-2100)-Hist (1971-2000), (d) difference of EC-Earth driven simulation; RCP8.5 (2071-2100)-Hist (1976-2005) in Apr-Sep.

E.3.2. Cell characteristics

The frequency distributions of the cell characteristics lifetime, area, precipitation sum, and intensity are qualitatively similar to the EC-Earth simulation but differ quantitatively in a number of ways. First of all, cells are longer living in MIROC5-CCLM (Figure E2a). This might be related to the fact that in ECE-CCLM we had to use wind data from the intermediate nest for tracking whereas in MIROC5-CCLM wind data from the inner nest was used. Furthermore, there are more cells with high maximum intensity and fewer cell with low maximum intensity in MIROC5-CCLM compared to ECE-CCLM (Figure E2b). Cell area is quite similar in both simulations (Figure E2c). In combination this leads to higher precipitation sums per cell in MIROC5-CCLM (Figure E2d).

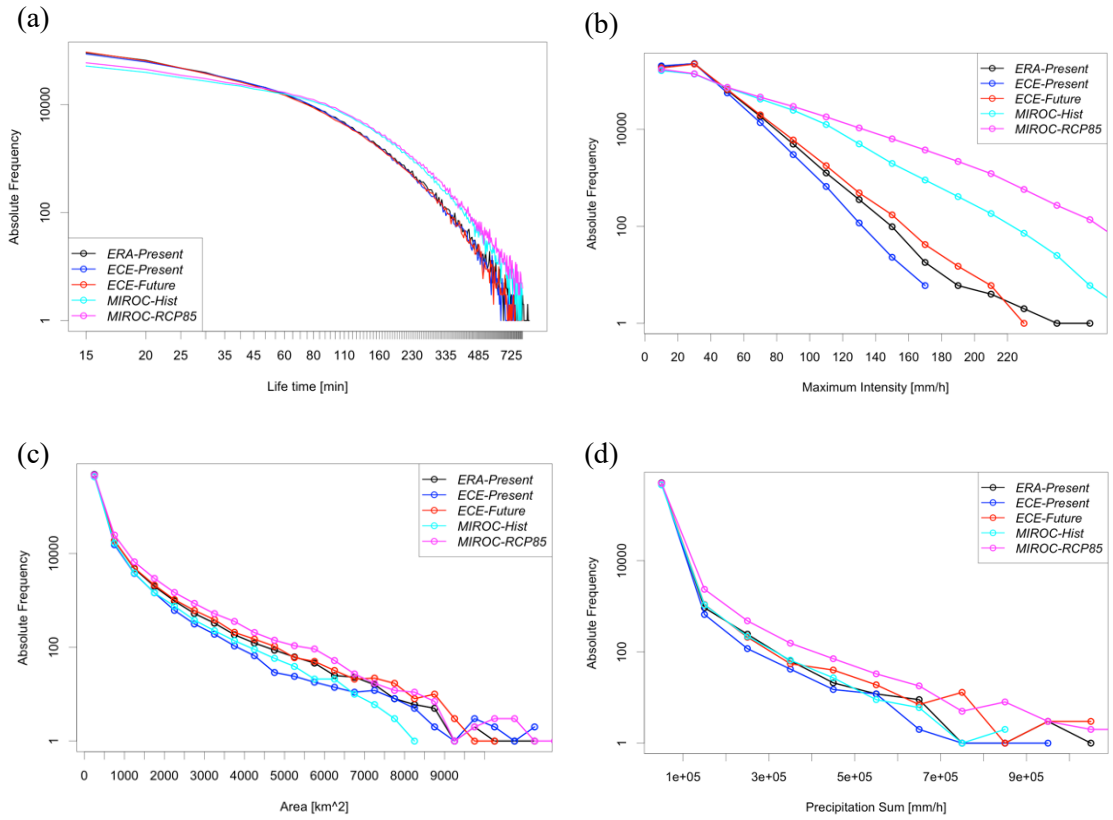

Figure E2: Frequency distribution of cell characteristics in the Historical (blue) and RCP8.5 (red) simulations: (a) lifetime, (b) mean intensity, (c) maximum area, (d) precipitation sum. Shaded areas denote the 95% confidence interval obtained from 1000 bootstrap samples of all cells. Dashed, vertical lines denote the 99th percentiles. Circles show the midpoints of bins.

To quantify the changes in cell characteristics in the future, we calculate the relative changes in cell characteristics for different percentiles of the frequency distributions.

These changes are then compared to the ECE-simulation (see Table C1 in Appendix C). For comparison the changes are calculated for the full domain and for the ECE domain separately; the results do not differ much but the changes are a little higher for the ECE domain (compare Table E1 and Table E2). As in ECE-CCLM, the relative changes are highest for the highest percentiles. The relative changes of all cell characteristics are higher in MIROC5-CCLM than in ECE-CCLM for the high percentiles (Table E1) and about the same for the median (except for precipitation sum which is 3,2% and thus lower in ECE-CCLM). This higher increase in extreme cells seems to be caused by the higher temperature change signal as can be seen from the trend scaling. Trend scaling of P99 is very similar in ECE-CCLM and MIROC5-CCLM. For maximum area, precipitation sum, and mean and maximum intensity the scaling rate does not differ more than 1% between

the two simulations. As in ECE-CCLM, the scaling rates for maximum area and precipitation sum are very close to the CC-rate.

Table E1: Relative changes in cell characteristics (from Historical to RCP8.5) for the ECE domain.

Change in %	Lifetime	Max. Area	Precip. Sum	Mean Intensity	Max. Intensity	Mean Speed
Median	-10,00	16,70	11,60	2,00	5,10	8,10
Mean	0,20	22,5	30,25	4,95	13,1	9,38
P75	0,00	18,20	18,70	5,30	12,20	10,80
P90	0,00	23,80	26,00	9,00	18,20	12,00
P99	4,50	40,60	44,70	15,70	31,60	11,90
Trend scaling of P99 (%/K)	1,0	7,60	8,20	3,2	6,1	2,50

Table E2: Relative changes in cell characteristics (from Historical to RCP8.5) for the full domain.

Change in %	Lifetime	Max. Area	Precip. Sum	Mean Intensity	Max. Intensity	Mean Speed
Median	0,00	8,30	12,50	2,20	5,20	4,50
Mean	1,90	21,00	29,80	3,25	8,32	8,99
P75	5,50	13,60	18,40	4,90	10,80	11,00
P90	3,20	22,00	24,70	7,90	15,70	10,50
P99	5,60	39,20	40,00	14,00	28,50	11,1
Trend scaling of P99 (%/K)	1,2	7,5	7,6	3,0	5,6	2,3

E.3.3. Yearly and diurnal cycle

In general, the diurnal cycle of convective activity is simulated very similar in MIROC5-CCLM compared to ECE-CCLM. The afternoon maximum is damped in the future compared to present conditions. The main difference in the MIROC5-CCLM simulations is that in the future convective activity declines more slowly in the afternoon after reaching

its peak at around 15 UTC (Figure E3a). Furthermore, mean intensity of cells does not increase in the morning between 10 and 12 UTC (Figure E3b). In combination this leads to an increase of convective precipitation during the whole day except for the time between 12 UTC and 15 UTC (Figure E3c).

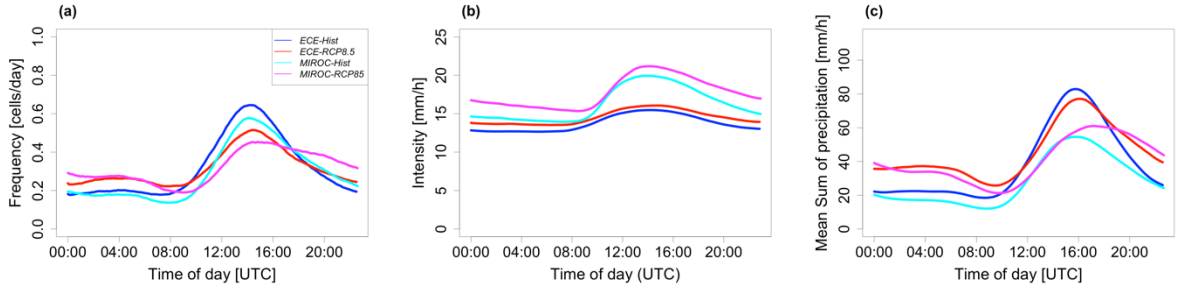

Figure E3: Diurnal cycle of (a) number of cells, (b) mean intensity per cell, and (c) mean sum of convective precipitation.

While the tracking could only be carried out for the summer months (Apr-Sep) for the ECE-CCLM simulation, the MIRCO5-CCLM simulations provide data for the whole year. The maximum of convective activity occurs in July for both historical and future periods in MIROC5-CCLM (Figure E4a), whereas in ECE-CCLM it occurs earlier (June for hist and May for RCP8.5). The mean intensity is higher in MIROC5-CCLM during the whole summer season (Figure E4b). In sum, the yearly cycle of convective precipitation is shifted by about 1-2 months in MIROC5-CCLM compared to ECE-CCLM (Figure E4c). The relative increase per month in the future is quite constant, meaning that the total increase in convective precipitation is strongest in the wettest months of June and July.

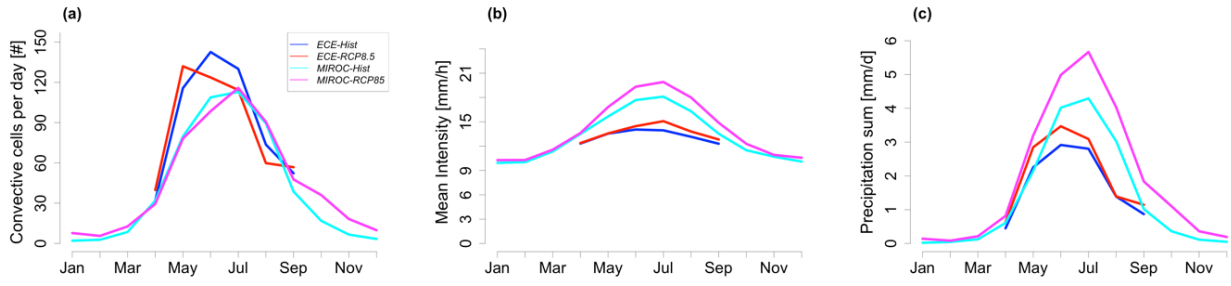

Figure E4: Yearly cycle of (a) number of cells, (b) mean intensity per cell, and (c) mean sum of convective precipitation.

E.3.4. Spatial distribution

Convective activity as measured by the occurrence of convective cells increases by 38% (compared to virtually no change in the ECE simulation). The increase is strongest in the Alps and Northern and Baltic Sea (Figure E5). In the Alps, convective activity increases especially in an area which experiences little convective activity in the present, on the main Alpine ridge.

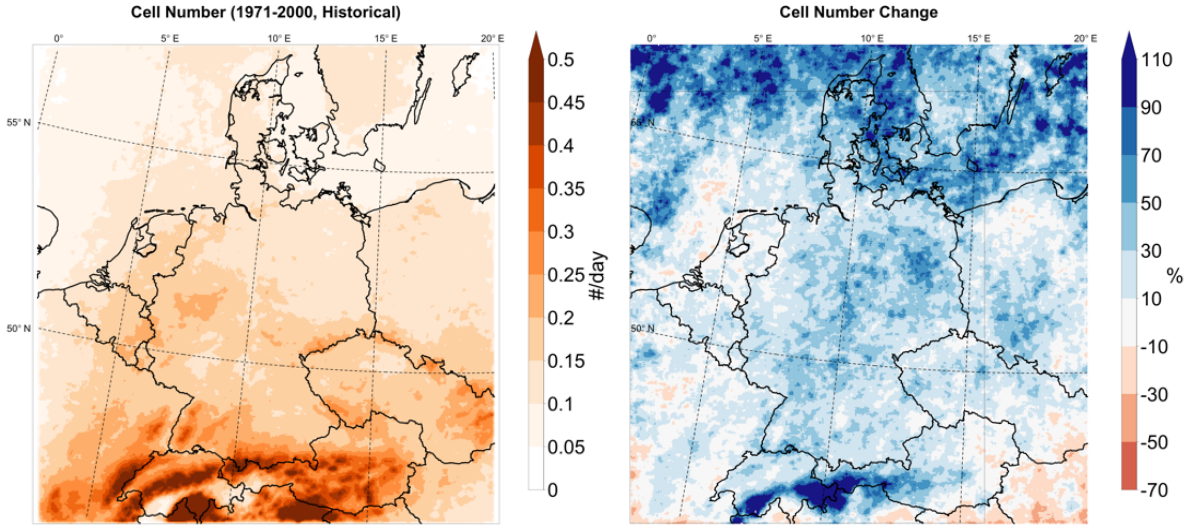

Figure E5: Spatial distribution of (a) cell number in the historical simulation, (b) relative change in cell number in RCP8.5.

E.3.5. Temperature and dew point scaling of cell characteristics

One of the main conclusions in Purr et al. (2021) was that near-surface T_d is a good predictor of the upper limit of cell characteristics because the scaling curves for the highest percentiles (99th perc.) were similar in present and future conditions. To assess the robustness of this result, we repeat the same analysis using the MIROC5-CCLM simulation.
In contrast to the ECE-CCLM simulations, the scaling rates differ for present and future conditions in MIROC5-CCLM (Figure E6). Concerning the temperature scaling, the scaling rates are higher in future conditions for all cell characteristics over the whole temperature range (Figure E6, left column). Again, this is in contrast to the ECE-CCLM simulation where temperature-scaling is similar in the intermediate temperature range and the difference between present and future are higher peak values in the future. Concerning

dew point scaling, the differences are not as large as for temperature scaling but still larger than in the ECE-CCLM simulation. For maximum area and precipitation sum, the extreme values are higher in the future but the mean scaling rate across the whole dew point range are almost identical (Figure E6b and h). For maximum and mean intensity the scaling rate for future conditions is higher than for present conditions meaning that extreme values are higher at high T_d values and lower at low T_d values (Figure E6d and f).

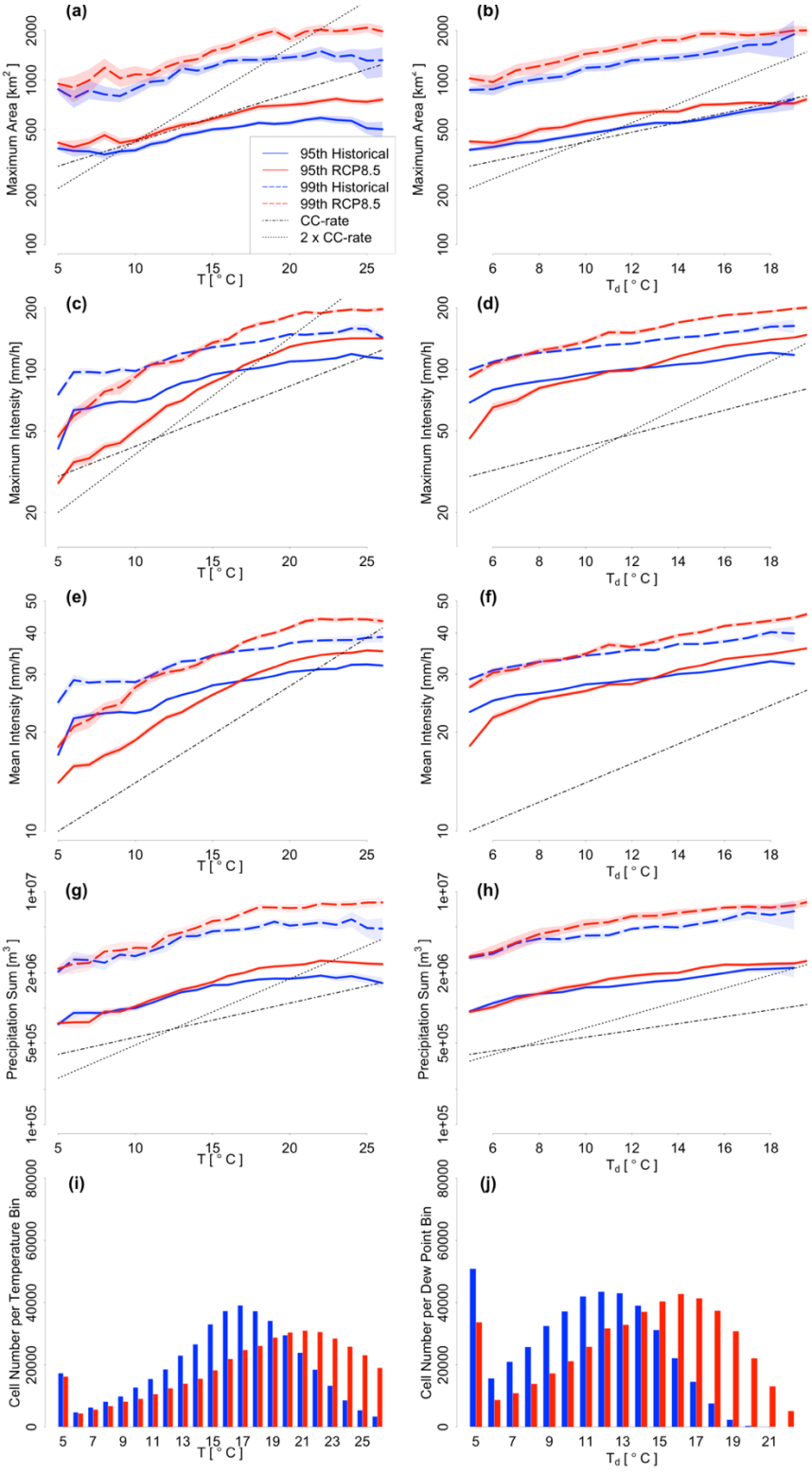

Figure E6: Temperature scaling (left column) and dew point temperature scaling (right column) of cell properties. (a) and (b): Maximum area; (c) and (d): Maximum intensity; (e) and (f): Mean intensity; (g) and (h): Precipitation sum. Shaded areas denote the uncertainty range caused by varying bin occupancy, obtained from bootstrapping cells in each bin. (i) and (j) show the frequency distribution of cells, where bars denote the absolute number of cells per temperature or dew point class (left y-axis).

These results question the conclusion that near-surface T_d is a good predictor of the upper limit of cell characteristics. A potential reason for this deviation could the difference in the large scale circulation. Hypothetically, the higher extreme values at high T_d values in the future could be caused by more instability or more wind shear in these cases. Further investigations are required to clarify these contrasting results.

F. Deutsche Zusammenfassung

Über die Intensivierung konvektiver Starkregenereignisse bei steigenden Temperaturen in Deutschland

Konvektive Starkregenereignisse gehören zu den verheerendsten Naturkatastrophen in Mitteleuropa. Speziell in Deutschland traten in den letzten Jahren einige markante Starkregenereignisse auf, die sehr hohe Niederschlagssummen brachten und große Schäden verursachten, z.B. 2016 (Piper et al. 2016) und 2021[4]. Allerdings konnte eine Zunahme von Niederschlagsextremen in der Gegenwart für Dauerstufen unter einem Tag auf Basis von Beobachtungsdaten bisher nicht belegt werden (Rauthe et al. 2020). Dies liegt vor allem an der geringen räumlichen Ausdehnung von konvektiven Niederschlagsgebieten, wodurch die Erfassung von Starkniederschlägen erschwert wird. Seit einigen Jahren stehen allerdings Fernerkundungstechniken, wie z.B. Regenradare zur Verfügung, die eine kontinuierliche Beobachtung konvektiver Stürme erlauben. Diese werden in zunehmendem Maße für klimatologische Untersuchungen eingesetzt (Lengfeld et al. 2020). Im ersten Teil dieser Arbeit wird solch ein Radardatensatz benutzt, um mithilfe eines Zellverfolgungsalgorithmus konvektive Regengebiete über ihren Lebenszyklus zu verfolgen.
Für die zukünftige Entwicklung stimmen theoretische Überlegungen und komplexe Klimamodelle darin überein, dass sich der Wasserkreislauf und somit Extremniederschläge im globalen Mittel intensivieren werden (Trenberth et al. 2003, Fischer & Knutti 2016). Um diese Änderung zu quantifizieren, wird als erste Näherung oft die Clausius-Clapeyron Beziehung benutzt (Lenderink et al. 2008, Zhang et al. 2017). Sie besagt, dass der Sättigungsdampfdruck für Wasserdampf in Luft exponentiell mit der Temperatur ansteigt, und zwar um 7 %/K. Allerdings können verschiedene Faktoren zu Abweichungen von dieser Rate führen. Zunächst basiert diese Näherung auf der Annahme, dass sich die relative Feuchte im Klimawandel nicht ändert. Diese Annahme kann auf regionaler Skala verletzt werden, wenn eine Änderung der großskaligen Zirkulation zu regionalen Klimaänderungen führt. Typischerweise haben Skalierungskurven ein Maximum bei der Temperatur, über welcher geringere Feuchte dazu führt, dass Niederschlag begrenzt ist

[4] Hydro-klimatologische Einordnung der Stark- und Dauerniederschläge in Teilen Deutschlands im Zusammenhang mit dem Tiefdruckgebiet „Bernd“ vom 12. bis 19. Juli 2021. https://www.dwd.de/DE/leistungen/besondereereignisse/niederschlag/20210721_bericht_starkniederschlaege_tief_bernd.pdf?__blob=publicationFile&v=6. Letzter Zugriff: 21.11.2021

(Drobinski et al. 2016). Verschiedene Studien, z.B. Prein et al. 2017a, haben anhand von Klimasimulationen gezeigt, dass dieses Maximum in der Zukunft bei höheren Temperaturen auftritt. Um dieses Problem zu umgehen, wurde vorgeschlagen, den Taupunkt als abhängige Variable für das Niederschlagsscaling zu verwenden (Lenderink et al. 2008). Während der beobachtete Anstieg von täglichen Niederschlagsextremen mit der Temperatur in mittleren Breiten gut mit der Clausius-Clapeyron-Rate übereinstimmt, wurden für kurzzeitige Starkniederschläge, also auf einer Zeitskala von Minuten bis Stunden, Anstiege oberhalb der Clausius-Clapeyron-Rate in bestimmten Regionen beobachtet (siehe Fowler et al. 2021 für eine Übersicht). Für Deutschland fanden Berg et al. (2013) Skalierungsraten von bis zu 14%/K, also der doppelten Clausius-Clapeyron-Rate.

Als Erklärung für dieses super-Clausius-Clapeyron-Scaling werden in der Literatur mehrere Hypothesen diskutiert, die sich gegenseitig nicht ausschließen. Erstens wird der statistische Effekt angeführt, dass der Anteil konvektiver Niederschläge bei zunehmender Temperatur ansteigt. Zweitens wird ein positiver Rückkopplungsmechanismus diskutiert, der die Dynamik konvektiver Stürme bei hohen Temperaturen überproportional verstärkt. Diese Hypothese besagt, dass mit höheren Temperaturen das Feuchteangebot in der Grenzschicht, also am Wolkenunterrand, ansteigt. Ist mehr Feuchte vorhanden, kann im Aufwindbereich von konvektiven Zellen durch Kondensation auch mehr latente Wärme freigesetzt werden, was wiederum zu einer Erhöhung der Auftriebskraft führt. Der so verstärkte Aufwindbereich kann wiederum mehr Feuchte aus einem größeren Gebiet der Grenzschicht ansaugen. Als weiterer Einflussfaktor wird der Organisationsgrad der konvektiven Stürme diskutiert. Der Einfluss von steigenden Temperaturen auf den Organisationsgrad wird in der Literatur hauptsächlich im Zusammenhang mit tropischer Konvektion diskutiert (Wing et al. 2017). Nichtsdestotrotz untersuchen auch einige Studien anhand von idealisierten Simulationen die Temperaturabhängigkeit des Organisationsgrads von Konvektion in mittleren Breiten (Moseley et al. 2016, Lochbihler et al. 2019).

Aufgrund dieser komplexen, nicht-linearen Prozesse sind Klimamodelle mit einer hohen zeitlichen und räumlichen Auflösung nötig, um hochreichende Konvektion und deren Veränderungen im Klimawandel realistisch zu simulieren. Solche, häufig als „konvektionserlaubend“ bezeichneten Modelle sind gekennzeichnet durch eine Gitterweite kleiner als 4 km und werden seit einigen Jahren erfolgreich zur Simulation hochreichender Konvektion eingesetzt (eine Übersicht bietet z.B. Prein et al. 2015). Aufgrund des hohen Berechnungsaufwands sind die Zeiträume und Simulationsgebiete allerdings begrenzt, sodass bisher nur wenige Simulationen über Jahrzehnte existieren, die meist einzelne Län-

der oder in einigen Fällen Kontinente abdecken. Eine Übersicht über alle wesentlichen, bisher durchgeführten konvektionserlaubenden Simulationen bieten Lucas-Picher et al. (2021).Welche Prozesse zu einer Intensivierung konvektiver Starkniederschläge führen und wie sich diese Prozesse in der Zukunft verändern werden, sind die Leitfragen dieser Arbeit. Das Ziel ist es, die Abhängigkeit von Eigenschaften konvektiver Stürme, wie deren Lebenszeit, Größe und Niederschlagsintensität, von großskaligen Umgebungsvariablen wie Taupunkt, Schichtungsstabilität und vertikaler Windscherung in Beobachtungen und Klimasimulationen besser zu verstehen.

Zunächst wurden Eigenschaften konvektiver Stürme mittels eines Zellverfolgungsalgorithmus aus einem an ortsfeste Niederschlagsmessungen angeeichten Radardatensatz gewonnen und untersucht, wie diese von großskaligen, atmosphärischen Variablen abhängen, um zu verstehen, welche Prozesse für das beobachtete super-Clausius-Clapeyron-Scaling von konvektiven Niederschlägen verantwortlich sein könnten. Insbesondere wurde der Frage nachgegangen, welche Rolle die vertikale Windscherung spielt, da sie zum einen den Organisationsgrad und somit die Intensität konvektiver Stürme erhöht, zum anderen aber dafür sorgt, dass sich diese Stürme schneller verlagern, was die Niederschlagsdauer und somit die Niederschlagsmenge für einen ortsfesten Beobachter senkt.

Die Niederschlagssumme konvektiver Zellen steigt mit der Taupunkttemperatur weit über der Clausius-Clapeyron-Rate an, wobei der Anstieg mit steigender Taupunkttemperatur zunimmt. Dieser starke Anstieg wird durch eine Zunahme der Convective Available Potential Energy (CAPE) mit der Taupunkttemperatur verursacht, sowie durch den Effekt, dass vertikale Windscherung die Fläche der konvektiven Zellen und somit auch die Niederschlagssumme erhöht. Gleichzeitig sorgt hohe vertikale Windscherung dafür, dass die konvektiven Zellen sich schneller verlagern, sodass die ortsfesten Skalierungsraten unter denen der mitbewegten Niederschlagssumme, aber immer noch über der Clausius-Clapeyron-Rate liegen. Der Anstieg der Zellfläche mit größerer Windscherung wird also durch die erhöhte Zuggeschwindigkeit überkompensiert was ortsfeste Niederschläge angeht. Dies führt dazu, dass konvektive Zellen, die ortsfeste Starkniederschläge (>25 mm/h) auslösen im Mittel langsamer ziehen als die Gesamtheit aller beobachteten Zellen. Die Tatsache, dass CAPE und Windscherung die Skalierungsraten beeinflussen, macht es unwahrscheinlich, dass die gegenwärtigen Skalierungsraten für ortsfeste Niederschläge in die Zukunft übertragen werden können.

Im zweiten Teil der Arbeit wurde evaluiert, inwieweit das regionale Klimamodell COSMO-CLM die Eigenschaften konvektiver Zellen abbilden kann. Hierzu wurden Si-

mulationen, die mit den Reanalysen ERA-Interim und ERA5 angetrieben wurden, mit Beobachtungsdaten verglichen. Insgesamt kann das Modell die Eigenschaften konvektiver Zellen mit einigen Abstrichen gut darstellen. Die beobachteten Häufigkeitsverteilungen der Zelleigenschaften Lebensdauer, mittlere und maximale Intensität, Fläche und Niederschlagssumme werden vom Modell gut wiedergegeben. Weiterhin kann auch der Anstieg von Intensität und Fläche mit der Lebensdauer korrekt simuliert werden, was nahelegt, dass auch das Spektrum von wenig intensiven Einzelzellengewittern bis hin zu intensiveren, organisierten Formen von Konvektion wie Superzellen oder mesoskaligen Komplexen im klimatologischen Mittel gut dargestellt wird. Allerdings wird die Niederschlagsintensität vor allem bei den langlebigen, intensiven Ereignissen systematisch unterschätzt. Das Modell kann den Anstieg der hohen Perzentile von Intensität, Fläche und Niederschlagssumme mit der Temperatur wiedergeben, aber nicht den Anstieg der Lebensdauer. Hinsichtlich der räumlichen Verteilung können beide Simulationen die erhöhte konvektive Aktivität im Bergland gut wiedergeben. Allerdings zeigt die mit ERA-Interim angetriebene Simulation eine Unterschätzung (Überschätzung) des konvektiven Niederschlags in Norddeutschland (Süddeutschland), was in der ERA5-angetriebenen Simulation schwächer ausgeprägt ist. Der Tagesgang der konvektiven Aktivität mit seinem typischen Maximum am Nachmittag wird von beiden Simulationen realistisch wiedergegeben. Allerdings wird der Tagesgang der mittleren und maximalen Intensität der konvektiven Zellen von der ERA-Interim angetriebenen Simulation unterschätzt, wohingegen die ERA5-angetriebene Simulation einen ausgeprägteren Anstieg am Nachmittag und somit realistischere Werte dieser Größen simuliert. Zusammenfassend lässt sich sagen, dass das Modell die wesentlichen Eigenschaften und die raum-zeitliche Variabilität konvektiver Regenzellen hinreichend gut abbilden kann. Die hier verwendete Art der Evaluation erlaubt es, Modelldefizite zu identifizieren, die durch die klassische Evaluation ortsfester Niederschläge nicht erkennbar sind.

Um herauszufinden, wie sich die Eigenschaften konvektiver Zellen und der Einfluss großskaliger Umgebungsvariablen in Zukunft verändern könnten, wurden kontinuierliche Klimasimulationen für Gegenwart (1976-2005) und Zukunft (2071-2100) unter dem repräsentativen Konzentrationspfad RCP8.5 durchgeführt. Die Antriebsdaten stammen vom Globalmodell EC-Earth. Zusätzlich wurde die Analyse mit einer weiteren Simulation mit anderen Antriebsdaten (MIROC5) und leicht verändertem Simulationsgebiet wiederholt, um die Unsicherheit der Ergebnisse, die von Unterschieden in der großskaligen Zirkulation verursacht werden, grob abschätzen zu können.

In der Zukunftsprojektion zeigen beide Simulationen einen Anstieg der ortsfesten, stündlichen Starkniederschläge im Sommer bei gleichzeitiger Abnahme des mittleren Sommerniederschlags, was mit den Ergebnisses größerer Ensembles regionaler Klimamodelle übereinstimmt (Jacob et al. 2014). Die Intensität und Fläche der konvektiven Zellen steigt in der Zukunft im Vergleich zur Gegenwart stark an, wohingegen Anzahl und Lebenszeit der Zellen gleich bleiben. Der relative Anstieg von Intensität und Fläche ist am größten für die hohen Perzentile, was bedeutet, dass sich extreme konvektive Ereignisse am stärksten intensivieren. In der von MIROC5 angetriebenen Simulation sind die Anstiege deutlich höher als in der von EC-Earth angetriebenen Simulation, z.B. für das 99. Perzentil der Niederschlagssume mit 44,7% im Vergleich zu 27%. Allerdings sind die Skalierungsraten für das *trend-scaling*, also der Änderungsrate pro K Temperaturänderungssignal, nahezu identisch mit 8,2% bzw. 7,9%. Dies deutet darauf hin, dass die stärkere Zunahme hauptsächlich durch stärkere Erwärmung verursacht ist.
Für den Tagesgang zeigen beide Simulationen eine Abnahme des nachmittäglichen Maximums und eine Verlagerung des konvektiven Niederschlags zu späteren Tageszeiten. Grund hierfür sind eine Zunahme der Convective Inhibition (CIN), wodurch es schwieriger wird, Konvektion auszulösen. Die Abnahme der Anzahl konvektiver Zellen am Nachmittag wird vor allem durch eine Abnahme langsam ziehender Zellen verursacht. Diese Abnahme ist bemerkenswert, da sich die großskalige Windgeschwindigkeit in den Simulationen nicht ändert, was darauf hindeutet, dass es weniger Luftmassengewitter gibt und stattdessen öfters ein dynamischer Auslösemechanismus nötig ist. Gleichzeitig steigen die CAPE und die bodennahe, absolute Luftfeuchte in der Zukunft an, sodass die konvektiven Ereignisse intensiver werden, wenn sie einmal ausgelöst sind. Dieses Ergebnis deckt sich z.B. mit Ergebnissen aus den USA, wo in der Zukunft ebenfalls höhere CAPE und CIN Werte simuliert werden und eine Verschiebung von moderaten hin zu extremen konvektiven Ereignissen projiziert wird (Rasmussen et al. 2018). Um zu untersuchen, ob und wie sich die Beziehung von den Eigenschaften konvektiver Zellen zu den großskaligen Umgebungsvariablen in Zukunft ändert, berechnen wir das *binning scaling* der Zelleigenschaften mit Temperatur und Taupunktstemperatur. Wie bei ortsfesten Niederschlägen verschieben sich die Skalierungskurven in der Zukunft hin zu höheren Temperaturen. Im Gegensatz dazu sind die Skalierungsraten der Zelleigenschaften mit dem Taupunkt in Gegenwart und Zukunft laut der EC-Earth angetriebenen Simulation nahezu identisch, was bedeutet, dass die bodennahe Taupunkttemperatur einen guten Prädiktor für die Obergrenze der Intensität, der Fläche, und der Niederschlagssumme von konvekti-

ven Zellen darstellt. Dies gilt allerdings nicht für ortsfeste Starkniederschläge, da sich die Häufigkeitsverteilung von konvektiven Zellen pro Taupunktsklasse ändert. In der von MIROC5 angetriebenen Simulation konnten die identischen Skalierungsraten für die Taupunktstemperatur nicht reproduziert werden. Hier sind die Skalierungsraten in der Zukunft höher als in der Gegenwart. Weitere Untersuchungen sind nötig, um die Gründe hierfür heraus zu finden.

Bibliography

Agard, V.; Emanuel, K. (2017). Clausius–Clapeyron Scaling of Peak CAPE in Continental Convective Storm Environments. Journal of the Atmospheric Sciences, 74, 3043–3054. https://doi.org/10.1175/JAS-D-16-0352.1.

Allen, M.; Ingram, W. (2002). Constraints on future changes in climate and the hydrologic cycle. Nature 419, 228–232. https://doi.org/10.1038/nature01092.

Ali, H.; Fowler, H. J.; Lenderink, G.; Lewis, E.; Pritchard, D. (2021). Consistent large-scale response of hourly extreme precipitation to temperature variation over land. Geophysical Research Letters, 48, e2020GL090317. https://doi.org/10.1029/2020GL090317.

Ban, N.; Schmidli, J.; Schär C. (2014). Evaluation of the convection-resolving regional climate modeling approach in decade-long simulations. Journal of Geophysical Research Atmospheres, 119, 7889–7907. https://doi.org/10.1002/2014JD021478.

Barbero, R.; Westra, S.; Lenderink, G.; Fowler, H.J. (2018). Temperature-extreme precipitation scaling: A two-way causality? International Journal of Climatology, 38, e1274–e1279. https://doi.org/10.1002/joc.5370.

Berg, P.; Moseley, C.; Haerter, J. (2013). Strong increase in convective precipitation in response to higher temperatures. Nature Geosciences, 6, 181–185. https://doi.org/10.1038/ngeo1731.

Berthou, S.; Kendon, E. J.; Chan, S. C.; Ban, N.; Leutwyler, D.; Schär, C.; Fosser, G. (2020). Pan-european climate at convection-permitting scale: A model intercomparison study. Climate Dynamics, 55, 35–59. https://doi.org/10.1007/s00382-018-4114-6.

Böhm, U.; Kücken, M.; Ahrens, W.; Block, A.; Hauffe, D.; Keuler, K.; Rockel, B.; Will. A. (2003). CLM - The Climate Version of LM: Brief Description and Long-Term Applications. COSMO Newsletter, 6, 225–235.

Bohnenstengel, S.I; Schlünzen, K.H.; Beyrich, F. (2011). Representativity of in-situ precipitation measurements – a case study for the LITFASS area in North-Eastern Germany. Journal of Hydrology, 400 (3–4), 387–395. https://doi.org/10.1016/j.jhydrol.2011.01.052.

Brisson, E.; Demuzere, M.; van Lipzig, N.P.M. (2015). Modelling strategies for performing convective permitting climate simulations. Meteorologische Zeitschrift, 25,149–163, https://doi.org/10.1127/metz/2015/0598.

Brisson, E.; van Weverberg, K.; Demuzere, M.; Devis, A.; Saeed, S.; Stengel, M.; van Lipzig, N.P.M. (2016). How well can a convection-permitting climate model reproduce decadal statistics of precipitation, temperature and cloud characteristics? Climate Dynamics, 47, 3043–3061, https://doi.org/10.1007/s00382-016-3012-z.

Brisson, E.; Brendel, C.; Herzog, S.; Ahrens, B. (2017). Lagrangian evaluation of convective shower characteristics in a convection-permitting model. Meteorologische Zeitschrift, 27, 59 – 66. https://doi.org/10.1127/metz/2017/0817.

Brisson, E.; Blahak, U.; Lucas-Picher, P.; Purr, C.; Ahrens, B. (2021). Contrasting lightning projection using the lightning potential index adapted in a convection-permitting regional climate model. Climate Dynamics, 57(7), 2037–2051. https://doi.org/10.1007/s00382-021-05791-z.

Brune, S.; Kapp, F.; Friederichs, P. (2018). A wavelet-based analysis of convective organization in ICON large-eddy simulations. Quarterly Journal of the Royal Meteorological Society, 144, 2812–2829, https://doi.org/10.1002/qj.3409.

Byrne, M. P.; O'Gorman P.A. (2018). Trends in continental temperature and humidity directly linked to ocean warming. Proceedings of the National Academy of Science of the United States of America. USA, 115, 4863–4868. https://doi.org/10.1073/pnas.1722312115.

Chan, S.C.; Kendon, E.J.; Roberts, N.M.; Fowler, H.J.; Blenkinskop, S. (2016). Downturn in scaling of UK extreme rainfall with temperature for future hottest days. Nature Geosciences, 9, 24–28. https://doi.org/10.1038/ngeo2596.

Chen, Q.; Fan, J.; Hagos, S.; Gustafson, W. I. Jr.; Berg, L. K. (2015). Roles of wind shear at different vertical levels: Cloud system organization and properties. Journal of Geophysical Research Atmospheres, 120, 6551–6574. https://doi.org/10.1002/2015JD023253.

Chow, F. K.; Schär, C.; Ban, N.; Lundquist, K. A.; Schlemmer, L.; Shi, X. (2019). Crossing multiple gray zones in the transition from mesoscale to microscale simulation over complex terrain. Atmosphere, 10(5), 274. https://doi.org/10.3390/atmos10050274.

Collins, M.; Knutti, R.; Arblaster, J et al. (2013). Climate Change 2013 - The Physical Science Basis: Contribution of Working Group I to the Fifth Assessment Report of the Intergovernmental Panel on Climate Change (pp. 1029-1136). (Intergovernmental Panel on Climate Change). Cambridge University Press.

Coppola, E.; Sobolowski, S.; Pichelli, E. et al. (2020). A first-of-its-kind multi-model convection permitting ensemble for investigating convective phenomena over Europe and the Mediterranean. Climate Dynamics 55, 3–34. https://doi.org/10.1007/s00382-018-4521-8

Cornes, R.; van der Schrier, G.; van den Besselaar, E.J.M.; Jones, P.D. (2018). An Ensemble Version of the E-OBS Temperature and Precipitation Datasets. Journal of Geophysical Research Atmospheres. https://doi.org/10.1029/2017JD028200.

Davies, H.C. (1976). A lateral boundary formulation for multi-level prediction models. Quarterly Journal of the Royal Meteorological Society, 102, 405–418. https://doi.org/10.1002/qj.49710243210.

Dobler, A.; Ahrens, B. (2008). Precipitation by a regional climate model and bias correction in Europe and South Asia. Meteorologische Zeitschrift, 17, 499–509, https://doi.org/10.1127/0941-2948/2008/0306.

Doms, G.; Forstner, J.; Heis E.; Herzog H.J.; Raschendorfer M.; Reinhardt T.; Ritter B.; Schrodin, R.; Schulz, J.P.; Vogel, G. (2018). A description of the nonhydrostatic regional COSMO model part II: physical parameterization. Technical report.

Donat, M.; Lowry, A.; Alexander, L. (2016). More extreme precipitation in the world's dry and wet regions. Nature Climate Change 6, 508–513. https://doi.org/10.1038/nclimate2941.

Drobinski, P.; Alonzo, B.; Bastin, S.; Da Silva, N.; Muller, C. (2016). Scaling of precipitation extremes with temperature in the French Mediterranean region: What explains the hook shape? Journal of Geophysical Research, 121(7), 3100–3119. https://doi.org/10.1002/2015JD023497.

Fischer, E.M.; Knutti, R. (2016). Observed heavy precipitation increase confirms theory and early models, Nature Climate Change, 6. https://doi.org/10.1038/NCLIMATE3110.

Fosser, G.; Khodayar, S.; Berg, P. (2017). Climate change in the next 30 years: What can a convection-permitting model tell us that we did not already know? Climate Dynamics, 48, 1987–2003. https://doi.org/10.1007/s00382-016-3186-4.

Fowler, H.J.; Lenderink, G.; Prein, A.F.; Westra, S.; Allan, R.P.; Ban, N.; Barbero, R.; Berg, P.; Blenkinsop S.; Do, H.X.; Guerreiro, S.; Haerter, J.O.; Kendon, E.J.; Lewis, E.; Schaer, C.; Sharma, A.; Villarini, G.; Wasko, C.; Zhang X. (2021). Anthropogenic intensification of short-duration rainfall extremes. Nature Reviews Earth & Environment, 2, 107–122. https://doi.org/10.1038/s43017-020-00128-6

Gelaro, R.; McCarty, W.; Suárez, M. J.; Todling, R.; Molod, A.; Takacs, L.; Randles, C. A.; Darmenov, A.; Bosilovich, M. G.; Reichle, R.; Wargan, K.; Coy, L.; Cullather, R.; Draper, C.; Akella, S.; Buchard, V.; Conaty, A.; da Silva, A. M.; Gu, W.; Kim, G.; Koster, R.; Lucchesi, R.; Merkova, D.; Nielsen, J. E.; Partyka, G.; Pawson, S.; Putman, W.; Rienecker, M.; Schubert, S. D.; Sienkiewicz, M.; Zhao, B. (2017). The Modern-Era Retrospective Analysis for Research and Applications, Version 2 (MERRA-2), Journal of Climate, 30(14), 5419-5454. https://doi.org/10.1175/JCLI-D-16-0758.1.

Gordon, H.B.; Whetton, P.H.; Pittock, A.B.; Fowler, A.M.; Haylock, M.R. (1992). Simulated changes in daily rainfall intensity due to the enhanced greenhouse effect: implications for extreme rainfall events. Climate Dynamics 8, 83–102. https://doi.org/10.1007/BF00209165

Groisman, P. Y.; Knight, R. W.; Easterling, D. R.; Karl, T. R.; Hegerl, G. C.; Razuvaev, V. N. (2005). Trends in Intense Precipitation in the Climate Record, Journal of Climate, 18(9), 1326–1350. https://doi.org/10.1175/JCLI3339.1.

Haerter, J. O.; Berg, P.; Moseley, C. (2017). Precipitation onset as the temporal reference in convective self-organization, Geophysical Research Letters, 44, 6450–6459, https://doi:10.1002/2017GL073342.

Hardwick Jones, R.; Westra, S.; Sharma, A. (2010). Observed relationships between extreme sub-daily precipitation, surface temperature,and relative humidity. Geophysical Research Letters, 37, 1–5, https://doi.org/10.1029/2010GL045081.

Hazeleger, W.; Wang, X.; Severijns, C. (2012). EC-Earth V2.2: description and validation of a new seamless earth system prediction model. Climate Dynamics, 39, 2611–2629. https://doi.org/10.1007/s00382-011-1228-5.

Hersbach, H. et al. (2020). The ERA5 global reanalysis. Quarterly Journal of the Royal Meteorological Society, 810 1–51, https://doi.org/10.1002/qj.3803.

Hirt, M; Craig, GC; Schäfer, SAK; Savre, J; Heinze, R. (2020). Cold-pool-driven convective initiation: using causal graph analysis to determine what convection-permitting models are missing. Quarterly Journal of the Royal Meteorological Society; 146: 2205–2227. https://doi.org/10.1002/qj.3788.

Houze, R. A., Jr. (2014). Cloud Dynamics, Chapter 8.4 Environmental Conditions Favoring Different Types of Deep Convective Storms. 2nd ed. Elsevier/Academic Press.

Jacob, D.; Petersen, J.; Eggert, B.; et al. (2014). EURO-CORDEX: new high-resolution climate change projections for European impact research. Regional Environmental Change, 14, 563–578. https://doi.org/10.1007/s10113-013-0499-2.

Kaltenboeck, R.; Steinheimer, M. (2015). Radar-based severe storm climatology for Austrian complex orography related to vertical wind shear and atmospheric instability, Atmospheric Research, 158–159, 216–230. https://doi.org/10.1016/j.atmosres.2014.08.006.

Kendon, E.J.; Roberts, N.M.; Fowler, H.J.; Roberts, M.J.; Chan, S.C.; Senior, C.A. (2014). Heavier summer downpours with climate change revealed by weather forecast resolution model. Nature Climate Change, 4, 570–576, https://doi.org/10.1038/nclimate2258.

Kirshbaum, D.J.; Adler, B.; Kalthoff, N.; Barthlott, C.; Serafin, S. (2018). Moist Orographic Convection: Physical Mechanisms and Links to Surface-Exchange Processes. Atmosphere, 9, 80. https://doi.org/10.3390/atmos9030080.

Knist, S.; Goergen, K.; Simmer, C. (2018). Evaluation and projected changes of precipitation statistics in convection-permitting WRF climate simulations over Central Europe. Climate Dynamics, https://doi.org/10.1007/s00382-018-4147-x.

Kotlarski, S.; Keuler, K.; Christensen, O. B.; Colette, A.; Déqué, M.; Gobiet, A.; Goergen, K.; Jacob, D.; Lüthi, D.; van Meijgaard, E.; Nikulin, G.; Schär, C.; Teichmann, C.; Vautard, R.; Warrach-Sagi, K.; and Wulfmeyer, V. (2014). Regional climate modeling on European scales: a joint standard evaluation of the EURO-CORDEX RCM ensemble, Geoscientific Model Development, 7, 1297–1333, https://doi.org/10.5194/gmd-7-1297-2014.

Kreklow, J.; Tetzlaff, B.; Burkhard, B.; Kuhnt, G. (2020). Radar-Based Precipitation Climatology in Germany—Developments, Uncertainties and Potentials. Atmosphere 11, 2: 217. https://doi.org/10.3390/atmos11020217.

Kunz, M.: Wandel, J.; Fluck, E.; Baumstark, S.; Mohr, S.; Schemm, S. (2020). Ambient conditions prevailing during hail events in central Europe. Natural Hazards and Earth System Sciences, 20(6), 1867–1887. https://doi.org/10.5194/nhess-20-1867-2020.

Laprise, R.; de Elía, R.; Caya, D.; Biner, S.; Lucas-Picher, P.; Diaconescu E.; Leduc, M.; Alexandru, A.; Separovic L. (2008). Challenging some tenets of Regional Climate Modelling. Meteorology and Atmospheric Physics, 100**,** 3–22. https://doi.org/10.1007/s00703-008-0292-9.

Lenderink, G.; van Meijgaard, E. (2008). Increase in hourly precipitation extremes beyond expectations from temperature changes. Nature Geosciences, 1(8), 511–514. https://doi.org/10.1038/ngeo262.

Lenderink, G.; Mok, H.; Lee, T.; Van Oldenborgh G. (2011). Scaling and trends of hourly precipitation extremes in two different climate zones—Hong Kong and the Netherlands, Hydrology and Earth System Sciences, 15(9), 3033–3041, https://doi.org/10.5194/hessd-8-4701-2011.

Lenderink, G.; Barbero, R.; Loriaux, J.M.; Fowler H.J. (2017). Super-Clausius–Clapeyron Scaling of Extreme Hourly Convective Precipitation and Its Relation to Large-Scale Atmospheric Conditions. Journal of Climate, 30, 6037–6052, https://doi.org/10.1175/JCLI-D-16-0808.1.

Lengfeld, K.; Winterrath, T.; Junghänel, T.; Hafer, M. (2019). Characteristic spatial extent of hourly and daily precipitation events in Germany derived from 16 years of radar data. Meteorologische Zeitschrift, 28(5), 363–378.
https://doi.org/10.1127/metz/2019/0964.

Lengfeld, K.; Kirstetter, P. E.; Fowler, H. J.; Yu, J.; Becker, A.; Flamig, Z.; Gourley, J. (2020). Use of radar data for characterizing extreme precipitation at fine scales and short durations. Environmental Research Letters, 15(8). https://doi.org/10.1088/1748-9326/ab98b4.

Lengfeld, K.; Walawender, K.; Winterrath, T.; Becker, A. (2021). CatRaRE: A Catalogue of Radar-based Heavy Rainfall Events in Germany Derived from 20 Years of Data. Meteorologische Zeitschrift, 30(6), 469–487.
https://doi.org/10.1127/metz/2021/1088, 2021.

Lepore, C.; Veneziano, D.; Molini, A. (2015). Temperature and CAPE dependence of rainfall extremes in the eastern United States. Geophysical Research Letters, 42, 74–83, https://doi.org/10.1002/2014GL062247.

Lepore, C.; Allen, J.T.; Tippett, M.K. (2016). Relationships between Hourly Rainfall Intensity and Atmospheric Variables over the Contiguous United States, Journal of Climate 29, 9: 3181–3197, https://doi.org/10.1175/JCLI-D-15-0331.1.

Lochbihler, K.; Lenderink, G.; Siebesma, A.P. (2017). The spatial extent of rainfall events and its relation to precipitation scaling. Geophysical Research Letters, 44, 8629–8636, https://doi.org/10.1002/2017GL074857.

Lochbihler, K.; Lenderink, G.; Siebesma, A. P. (2019). Response of extreme precipitating cell structures to atmospheric warming. Journal of Geophysical Research: Atmospheres, 124, 6904–6918. https://doi.org/10.1029/2018JD029954.

Lucas-Picher, P.; Argüeso, D.; Brisson, E.; Tramblay, Y.; Berg, P.; Lemonsu, A.; Kotlarski, S.; Caillaud, C. (2021). Convection-permitting modeling with regional climate

models: Latest developments and next steps. Wiley Interdisciplinary Reviews: Climate Change, 12(6), e731. https://doi.org/10.1002/wcc.731.

Market, P.; Allen, S.; Scofield, R.; Kuligowski, R.; Gruber, A. (2003). Precipitation Efficiency of Warm-Season Midwestern Mesoscale Convective Systems. Weather and Forecasting 18, 6, 1273–1285, https://doi.org/10.1175/1520-0434(2003)018<1273:PEOWMM>2.0.CO;2.

Markowski, P.; Richardson, Y. (2010). Mesoscale Meteorology in Midlatitudes, Wiley-Blackwell, Chichester.

Meredith, E. P.; Ulbrich, U.; Rust, H. W. (2019). The diurnal nature of future extreme precipitation intensification. Geophysical Research Letters, 46, 7680–7689. https://doi.org/10.1029/2019GL082385.

Moseley, C.; Berg, P.; Haerter, J. O. (2013). Probing the precipitation life cycle by iterative rain cell tracking, Journal of Geophysical Research Atmosphere, 118, 13,361–13,370, https://doi.org/10.1002/2013JD020868.

Moseley, C.; Hohenegger, C.; Berg, P.; Haerter J.O. (2016). Intensification of convective extremes driven by cloud–cloud interaction. Nature Geoscience 9**,** 748–752. https://doi.org/10.1038/ngeo2789.

Noda, A.; Tokioka, T. (1989). The Effect of Doubling the CO2 Concentration on Convective and Non-convective Precipitation in a General Circulation Model Coupled with a Simple Mixed Layer Ocean Model, Journal of the Meteorological Society of Japan. Ser. 67, 6, 1057-1069. https://doi.org/10.2151/jmsj1965.67.6_1057

O'Gorman, P. A.; Muller, C. J. (2010). How closely do changes in surface and column water vapor follow Clausius–Clapeyron scaling in climate change simulations? Environmental Research Letters 5, 025207. https://doi.org/10.1088/1748-9326/5/2/025207

O'Gorman, P.A. (2015). Precipitation Extremes Under Climate Change. Current Climate Change Reports, 1, 49–59 (2015). https://doi.org/10.1007/s40641-015-0009-3.

Orr, A.; Listowski, C.; Couttet, M.; Collier, E.; Immerzeel, W.; Deb, P.; Bannister, D. (2017). Sensitivity of simulated summer monsoonal precipitation in Langtang Valley, Himalaya, to cloud microphysics schemes in WRF. Journal of Geophysical Research: Atmospheres, 122, 6298–6318. https://doi.org/10.1002/2016JD025801.

Peleg, N.; Marra, F.; Fatichi, S.; Molnar, P.; Morin, E.; Sharma, A.; Burlando, P. (2018). Intensification of Convective Rain Cells at Warmer Temperatures Observed from High-Resolution Weather Radar Data. Journal of Hydrometeorology, 19, 715–726, https://doi.org/10.1175/JHM-D-17-0158.1.

Perkins, S.E.; Pitman, A.J.; Holbrook, N.J.; McAneney, J. (2007). Evaluation of the AR4 Climate Models' Simulated Daily Maximum Temperature, Minimum Temperature, and Precipitation over Australia Using Probability Density Functions. Journal of Climate, 20, 4356–4376, https://doi.org/10.1175/JCLI4253.1.

Pfeifroth, U.; Hollmann, R.; Ahrens, B. (2012). Cloud Cover Diurnal Cycles in Satellite Data and Regional Climate Model Simulations. Meteorologische Zeitschrift, 21, 551–560. https://doi.org/ 10.1127/0941-2948/2012/0423.

Piper, D.; Kunz, M.; Ehmele, F.; Mohr, S.; Mühr, B.; Kron, A.; Daniell, J. (2016). Exceptional sequence of severe thunderstorms and related flash floods in May and June 2016 in

Germany – Part 1: Meteorological background. Natural Hazards and Earth System Sciences, 16, 2835–2850, https://doi.org/10.5194/nhess-16-2835-2016.

Prein, A.F.; Langhans, W.; Fosser, G.; Ferrone, A.; Ban, N.; Görgen, K.; Keller, M.; Tölle, M.; Gutjahr, O.; Feser, F.; Brisson, E.; Kollet, S.; Schmidli, J.; van Lipzig, N.P.M.; Leung R. (2015). A review on regional convection-permitting climate modeling: Demonstrations, prospects, and challenges. Reviews in Geophysics, 53, 323–361, https://doi.org/10.1002/2014RG000475.

Prein, A.F.; Gobiet, A. (2017). Impacts of uncertainties in European gridded precipitation observations on regional climate analysis. International Journal of Climatology, 37, 305–327, https://doi.org/10.1002/joc.4706.

Prein, A., Rasmussen, R., Ikeda, K.; Liu, C.; Clark, M.P.; Holland, G.J. (2017a). The future intensification of hourly precipitation extremes. Nature Climate Change, 7, 48–52. https://doi.org/10.1038/nclimate3168.

Prein, A.F.; Liu, C.; Ikeda, K.; Trier, S.B.; Rasmussen, R.M.; Holland, G.J.; Clark, M.P.(2017b). Increased rainfall volume from future convective storms in the US. Nature Climate Change, 7, 880–884. https://doi.org/10.1038/s41558-017-0007-7.

Prein, A.F.; Liu, C.; Ikeda, K.; Bullock, R.; Rasmussen, R.M.; Holland, G.J.; Clark, M. (2020). Simulating North American mesoscale convective systems with a convection-permitting climate model. Climate Dynamics. https://doi.org/10.1007/s00382-017-3993-2.

Púčik, T.; Groenemeijer, P.; Rädler, A.T.; Tijssen, L.; Nikulin, G.; Prein, A.F.; van Meijgaard, E.; Fealy, R. ; Jacob, D.; Teichmann C. (2017). Future Changes in European Severe Convection Environments in a Regional Climate Model Ensemble. Journal of Climate, 30, 6771–6794, https://doi.org/10.1175/JCLI-D-16-0777.1.

Purr, C.; Brisson, E.; Ahrens B. (2019). Convective Shower Characteristics Simulated with the Convection-Permitting Climate Model COSMO-CLM. Atmosphere, 10(12):810. https://doi.org/10.3390/atmos10120810.

Purr, C.; Brisson, E.; Ahrens, B. (2021). Convective rain cell characteristics and scaling in climate projections for Germany. International Journal of Climatology, 41: 3174– 3185. https://doi.org/10.1002/joc.7012.

Rasmussen, K.L.; Prein, A.F.; Rasmussen, R.M.; Ikeda, K.; Liu C. (2020). Changes in the convective population and thermodynamic environments in convection-permitting regional climate simulations over the United States. Climate Dynamics, 55, 383–408. https://doi.org/10.1007/s00382-017-4000-7.

Rauthe, M.; Brendel C.; Helms.; Lohrengel, A.-F.; Meine, L.; Nilson, E.; Norpoth, M.; Rasquin, C.; Rudolph, E.; Schade, N. H.; Deutschländer, T.; Forbriger, M.; Fleischer, C.; Ganske, A.; Herrmann, C., Kirsten, J.; Möller, J.; Seiffert, R. (2020): Klimawirkungsanalyse des Bundesverkehrssystems im Kontext Hochwasser: Schlussbericht des Schwerpunktthemas Hochwassergefahren (SP-103) im Themenfeld 1 des BMVI-Expertennetzwerks. https://doi.org/10.5675/ExpNRM2020.2020.04.

Rio, C.; Del Genio, A.D.; Hourdin, F. (2019). Ongoing Breakthroughs in Convective Parameterization. Current Climate Change Reports, 5, 95–111.
https://doi.org/10.1007/s40641-019-00127-w.

Ritter, B.; Geleyn, J. (1992). A Comprehensive Radiation Scheme for Numerical Weather Prediction Models with Potential Applications in Climate Simulations. Monthly Weather Review, 120, 303–325.
https://doi.org/10.1175/1520-0493(1992)120<0303:ACRSFN>2.0.CO;2.

Rockel, B.; Will, A.; Hense, A. (2008). The Regional Climate Model COSMO-CLM (CCLM). Meteorologische Zeitschrift, 17 (4), 347–348. https://doi.org/10.1127/0941-2948/2008/0309.

Schroeer, K.; Kirchengast, G.; O, S. (2018a). Strong dependence of extreme convective precipitation intensities on gauge network density. Geophysical Research Letters, 45, 8253–8263. https://doi.org/10.1029/2018GL077994.

Schroeer, K.; Kirchengast, G. (2018b). Sensitivity of extreme precipitation to temperature: the variability of scaling factors from a regional to local perspective. Climate Dynamics, 50, 3981–3994. https://doi.org/10.1007/s00382-017-3857-9.

Schumacher, R. S.; Johnson, R. H. (2005). Organization and environmental properties of extreme-rain-producing mesoscale convective systems. Monthly Weather Review, 133(4), 961–976. https://doi.org/10.1175/MWR2899.1.

Seeley, J. T.; D. M. Romps (2015). The Effect of Global Warming on Severe Thunderstorms in the United States. Journal of Climate, 28, 2443–2458. https://doi.org/10.1175/JCLI-D-14-00382.1.

Shepherd, T. (2014). Atmospheric circulation as a source of uncertainty in climate change projections. Nature Geoscience, 7, 703–708. https://doi.org/10.1038/ngeo2253.

Sherburn, K. D.; Parker, M.D.; King, J.R.; Lackmann G.M. (2016). Composite Environments of Severe and Nonsevere High-Shear, Low-CAPE Convective Events. Weather and Forecasting 31, 6: 1899–1927. https://doi.org/10.1175/WAF-D-16-0086.1.

Steppeler, J.; Doms, G.; Schaettler, U.; Bitzer, H.W.; Gassmann, A.; Damrath, U.; Gregoric, G. (2003). Meso-gamma scale forecasts using the nonhydrostatic model LM. Meteorology and Atmospheric Physics, 82, 75–96. https://doi.org/10.1007/s00703-001-0592-9.

Sun, Q.; Zwiers, F.; Zhang, X.; Li, G. (2020). A Comparison of Intra-Annual and Long-Term Trend Scaling of Extreme Precipitation with Temperature in a Large-Ensemble Regional Climate Simulation, Journal of Climate, 33(21), 9233–9245. https://doi.org/10.1175/JCLI-D-19-0920.1.

Taszarek, M.; Pilguj, N.; Allen, J. T.; Gensini, V.; Brooks, H. E.; Szuster, P. (2020). Comparison of convective parameters derived from ERA5 and MERRA2 with rawinsonde data over Europe and North America. Journal of Climate, 1–55. https://doi.org/10.1175/JCLI-D-20-0484.1.

Tiedtke, M. (1989). Comprehensive Mass Flux Scheme for Cumulus Parameterization in Large-Scale Models. Monthly Weather Review, 117, 1779–1800, https://doi.org/10.1175/1520-0493(1989)117<1779:ACMFSF>2.0.CO;2.

Trenberth, K.E. (1999). Conceptual Framework For Changes Of Extremes Of The Hydrological Cycle With Climate Change. Climatic Change, 42, 327–339, https://doi.org/10.1023/A:1005488920935.

Trenberth, K.E.; Dai, A.; Rasmussen, R.M.; Parsons, D.B. (2003). The changing character of precipitation. Bulletin of the American Meteorological Society, 84, 1205–12017, https://doi.org/10.1175/BAMS-84-9-1205.

Van Weverberg, K.; Goudenhoofdt, E.; Blahak, U.; Brisson, E.; Demuzere, M.; Marbaix, P.; van Ypersele, J. P. (2014). Comparison of one moment and two-moment bulk micro-

physics for high-resolution climate simulations of intense precipitation. Atmospheric Research, 147, 145–161. https://doi.org/10.1016/j.atmosres.2014.05.012.

Vergara-Temprado, J.; Ban, N.; Panosetti, D.; Schlemmer, L.; Schär, C. (2020). Climate models permit convection at much coarser resolutions than previously considered. Journal of Climate, 33, 1915–1933. https://doi.org/10.1175/JCLI-D-19-0286.1.

Visser, J. B.; Wasko, C.; Sharma, A.; Nathan, R. (2020). Resolving inconsistencies in extreme precipitation-temperature sensitivities. Geophysical Research Letters, 47, e2020GL089723. https://doi.org/10.1029/2020GL089723.

Wapler, K.; James, P. (2013). High-resolution climatology of lightning characteristics within Central Europe. Meteorology and Atmospheric Physics, 122, 175–184, https://doi.org/10.1007/s00703-013-0285-1.

Wapler, K.; James, P. (2015). Thunderstorm occurence and characteristics in Central Europe under different synoptic conditions. Atmospheric Research, 158–159, 231–244, https://doi.org/10.1016/j.atmosres.2014.07.011.

Weisman, M.L.; Klemp, J.B. (1982). The Dependence of Numerically Simulated Convective Storms on Vertical Wind Shear and Buoyancy. Monthly Weather Review, 110, 504–520. https://doi.org/10.1175/1520-0493(1982)110<0504:TDONSC>2.0.CO;2.

Westra, S.; Fowler, H. J.; Evans, J. P.; Alexander, L. V. ; Berg, P. ; Johnson, F.; Kendon, E. J.; Lenderink, G.; Roberts N. M. (2014). Future changes to the intensity and frequency of shortduration extreme rainfall, Reviews of Geophysics., 52, 522–555, https://doi.org/10.1002/2014RG000464.

Wing, A.A.; Emanuel, K.; Holloway, C.E.; Muller, C. (2017). Convective Self-Aggregation in Numerical Simulations: A Review. Surveys in Geophysics, 38**,** 1173–1197. https://doi.org/10.1007/s10712-017-9408-4.

Winterrath, T.; Brendel, C.; Hafer, M.; Junghänel, T.; Klameth, A.; Lengfeld, K.; Walawender, E.; Weigl, E.; Becker, A. (2017). Erstellung einer radargestützten Niederschlagsklimatologie. Berichte des Deutschen Wetterdienst, 251, Available online: http://nbn-resolving.de/urn:nbn:de:101:1-20170908911.

Winterrath, T.; Brendel, C.; Hafer, M.; Junghänel, T.; Klameth, A.; Lengfeld, K.; Walawender, E.; Weigl, E.; Becker, A. (2018a). RADKLIM Version 2017.002: Reprocessed quasi gauge-adjusted radar data, 5-minute precipitation sums (YW), doi:10.5676/DWD/RADKLIM_YW_V2017.002.

Winterrath, T.; Brendel, C.; Hafer, M.; Junghänel, T.; Klameth, A.; Lengfeld, K.; Walawender, E.; Weigl, E.; Becker, A. (2018b). RADKLIM Version 2017.002: Reprocessed gauge-adjusted radar data, one-hour precipitation sums (RW). doi:10.5676/DWD/RADKLIM_RW_V2017.002.

Yano, J.; Moncrieff, M. W. (2016). Numerical Archetypal Parameterization for Mesoscale Convective Systems, Journal of the Atmospheric Sciences, 73(7), 2585–2602. https://doi.org/10.1175/JAS-D-15-0207.1.

Zhang, X.; Zwiers, F.; Li, G.; Wan, H.; Cannon A.J. (2017). Complexity in estimating past and future extreme short-duration rainfall. Nature Geoscience, 10, 255–259. https://doi.org/10.1038/ngeo2911